The persistent cosmic web and its filamentary structure - I. Theory and implementation

T. Sousbie

Monthly Notices
of the
ROYAL ASTRONOMICAL SOCIETY

Mon. Not. R. Astron. Soc. **414,** 350–383 (2011) doi:10.1111/j.1365-2966.2011.18394.x

The persistent cosmic web and its filamentary structure – I. Theory and implementation

T. Sousbie[1,2]★

[1]*Department of Physics, The University of Tokyo, Tokyo 113-0033, Japan*
[2]*Institut d'astrophysique de Paris & UPMC (UMR 7095), 98, bis boulevard Arago 75 014, Paris*

Accepted 2011 January 19. Received 2011 January 14; in original form 2010 September 20

ABSTRACT

We present DisPerSE, a novel approach to the coherent multiscale identification of all types of astrophysical structures, in particular the filaments, in the large-scale distribution of the matter in the Universe. This method and the corresponding piece of software allows for a genuinely scale-free and parameter-free identification of the voids, walls, filaments, clusters and their configuration within the cosmic web, directly from the discrete distribution of particles in N-body simulations or galaxies in sparse observational catalogues. To achieve that goal, the method works directly over the Delaunay tessellation of the discrete sample and uses the Delaunay tessellation field estimator density computed at each tracer particle; no further sampling, smoothing or processing of the density field is required.

The idea is based on recent advances in distinct subdomains of the computational topology, namely the *discrete* Morse theory which allows for a rigorous application of topological principles to astrophysical data sets, and the theory of persistence, which allows us to consistently account for the intrinsic uncertainty and Poisson noise within data sets. Practically, the user can define a given persistence level in terms of robustness with respect to noise (defined as a 'number of σ') and the algorithm returns the structures with the corresponding significance as sets of critical points, lines, surfaces and volumes corresponding to the clusters, filaments, walls and voids – filaments, connected at cluster nodes, crawling along the edges of walls bounding the voids. From a geometrical point of view, the method is also interesting as it allows for a robust quantification of the topological properties of a discrete distribution in terms of Betti numbers or Euler characteristics, without having to resort to smoothing or having to define a particular scale.

In this paper, we introduce the necessary mathematical background and describe the method and implementation, while we address the application to 3D simulated and observed data sets in the companion paper (Sousbie, Pichon & Kawahara, Paper II).

Key words: methods: data analysis – methods: numerical – galaxies: formation – galaxies: kinematics and dynamics – cosmology: observations – large-scale structure of Universe.

1 INTRODUCTION

The existence of an intricate network of filaments in the large-scale distribution of matter is now considered an established fact. Its was first observed by de Lapparent, Geller & Huchra (1986) (see also e.g. Colless et al. 2003) and later theorized (see e.g. Bond, Kofman & Pogosyan 1996; Pogosyan et al. 1996): underdense void regions bounded by sheet-like walls embedded in a web-like filamentary network branching on high-density dark matter haloes and galaxy clusters form the so-called cosmic web (Bond et al. 1996) that spans over a wide range of scales larger than the megaparsec. Dark matter haloes and galaxy clusters have arguably been the most-studied component and there exist a wide range of methods to identify them in simulations or observational catalogues such as the classical friends-of-friends (FOF) (Huchra & Geller 1982), hierarchical FOF and 6D minimal spanning tree (Gottloeber 1998), SUBFIND (Springel et al. 2001), VOBOZ (Neyrinck, Gnedin & Hamilton 2005) and ADAPTAHOP (Aubert, Pichon & Colombi 2004; Tweed et al. 2009) (the list is not exhaustive). Cosmological voids were first observed by Kirshner et al. (1981) and theoretical models were later developed (see e.g. Hoffman & Shaham 1982; Icke 1984; Bertschinger 1985). Although they have been the subject of less attention, there still exist a large number of references describing their features and introducing numerical void finders, such as, for instance, Neyrinck (2008), Platen, van de Weygaert & Jones (2007) and Aragón-Calvo et al. (2010a) (see also the references therein). Because of the intrinsic difficulty of even defining the concepts of

★E-mail: tsousbie@gmail.com, sousbie@utap.phys.s.u-tokyo.ac.jp

walls and filaments, not to mention designing consistent identification algorithms (especially in the case of observational data), their generic properties still remain relatively uncertain. One can, for instance, refer to Aragón-Calvo, van de Weygaert & Jones (2010c) for a nice review of the different identification techniques and a study of the filament properties in dark matter N-body simulations (see also e.g. Gay et al. 2010), and Stoica, Martínez & Saar (2010) and Sousbie et al. (2008a) for recent attempts at identifying filaments properties in the SDSS and 2dFGRS galaxy catalogues, using the Candy model (Stoica et al. 2005) and skeleton formalism (Sousbie et al. 2008b), respectively. In this paper, we present a general framework within which the physically meaningful objects that are the voids, walls, filaments and haloes are rigorously and consistently defined and we also detail the corresponding numerical method that allows for their direct identification in simulated as well as observational data sets. We focus in particular on what is probably the most-striking feature of the matter distribution on large scales in the Universe, its filamentary structure.

During the last few years, the Morse theory (e.g. Milnor 1963; Jost 2008) has been recognized as a very promising approach to the global identification of all types of astrophysically significant features of the large-scale galaxy distribution in the universe (see e.g. Novikov, Colombi & Doré 2006; Hahn et al. 2007; Sousbie et al. 2008a,b; Forero-Romero et al. 2009; Sousbie, Colombi & Pichon 2009; Aragón-Calvo et al. 2010b). The main reason for this strong interest comes from the fact that all the salient features of the web-like pattern of galaxies have a direct, mathematically well-defined equivalent in the Morse theory. In fact, the Morse theory mainly relies on the definition of the so-called ascending and descending k-manifolds, which *partition* space into a series of k-dimensional domains defined by the gradient of a function (in the present case, the density field), and the network whose branches are formed by their intersections and whose nodes are the critical points, the so-called the Morse complex (see Section 2). As illustrated in Fig. 1, each of those can be directly associated to an astrophysical object of interest: an ascending 3-manifold defines a void, an ascending 2-manifold defines a wall and an ascending 1-manifold defines a filament, a descending 3-manifold defines a peak patch of the peak theory (Bardeen et al. 1986) and the Morse complex defines some sort of hierarchy and a notion of neighbourhood between them (see Section 2 for more details).

Nevertheless, and as promising as it may seem, all the efforts towards applying the Morse theory to astrophysical data sets such as galaxy catalogues have so far been plagued by major difficulties. Those difficulties are a direct consequence of the fact that the Morse theory, although very attractive, is fundamentally a mathematical theory defined for idealized, well-defined and properly behaved smooth functions, which of course is not generally the case with any physical data set resulting from actual measurements. At least two critical issues can be identified in the case of the large-scale structure identification problem. The first results from the presence of the Poisson noise and large observational biases in galaxy catalogues, which should be dealt with from the start, especially when the data set is relatively sparse as it becomes even more difficult in that case to distinguish between noise features and the actual features of the sampled data set. The second issue arises from the fact that the Morse theory applies to the so-called Morse functions (see Definition 2.2), which are sufficiently smooth twice-differentiable *continuous* functions (whose critical points are non-degenerate), whereas the galaxy distribution is discrete by nature. This incompatibility is fundamental, as it means that the theoretical notions of the Morse theory may actually not apply to any practical data set. A more detailed discussion of this problem is presented in Appendix A as well as an example of the consequences of neglecting this inconsistency in the case of watershed-based methods, such as Sousbie et al. (2009) and Aragón-Calvo et al. (2010b).

In this paper, we focus on presenting DisPerSE, a formalism, and the corresponding software specifically designed for analysing the cosmic web and its filamentary network. This formalism is based on the Morse theory, while the aforementioned incompatibilities with astrophysical data sets are overcome by relying on relatively recent advances in distinct subdomains of the computational topology. These domains are the discrete Morse theory [a distinct though related theory developed by Forman, see Forman (1998b, 2002), and references therein] and persistent homology, first introduced in Edelsbrunner, Letscher & Zomorodian (2000, 2002). We therefore start by introducing the corresponding necessary notions of the computational topology in Sections 2–4. Note that no previous knowledge in the field of computational topology is assumed here, the goal of those sections being mainly to introduce the required mathematical vocabulary that we use extensively in the following sections and give a glimpse at how those theories can help deepen our understanding of the structure of the cosmic web. The reader interested in pursuing this investigation further should refer to the aforementioned references for a more detailed and involved introduction. In particular, we strongly recommend the reading of Gyulassy (2008) and especially Zomorodian (2009) for a very didactic presentation of these concepts. Indeed, the particular method and implementation presented in this paper are inspired by the work presented in those two references.

We then proceed by showing in Section 5 how it is possible, relying on the previously mentioned theories, to design an algorithm that rigorously computes the *discrete* Morse complex of a discrete density field, obtained using the Delaunay tessellation field estimator (DTFE) technique (Schaap & van de Weygaert 2000; van de Weygaert & Schaap 2009) from the Delaunay tessellation of a given discretely sampled data set, such as the distribution of galaxies in the universe. Within our approach, the Morse complex is directly computed from the Delaunay tessellation which means it is scale adaptive and parameter free. The problem of dealing with the Poisson noise and measurement errors is addressed in Section 6, where we make use of the persistence theory to remove spurious topological features from the Morse complex. Practically, the filamentary network (and associated voids, walls, etc.) computed from the initial distribution is simplified by cancelling pairs of critical points according to a persistence criterion that can be restated in terms of the significance relative to shot noise. Finally, in Section 7, we address technical questions such as dealing with boundary conditions, smoothing the identified voids, walls and filaments, and important implementation problems before concluding in Section 8.

Importantly, let us emphasize that within this framework, the mathematical theories that we use are fundamentally discrete and readily apply to the measured raw data; the unique supplementary but critical step consists in defining heuristically a consistent labelling of the segments, triangle and tetrahedron of the Delaunay tessellation with regards to the DTFE densities computed at the sampling points (see Section 5.1). This warrants that all the well-known and extensively studied mathematical properties of the Morse complex are ensured *by construction* at the mesh level and that the corresponding cosmological structures therefore correspond to well-defined mathematical objects with known mathematical properties. It also provides a consistent way of reconnecting the corresponding network after the removal of insignificant (non-persistent) pairs of critical points.

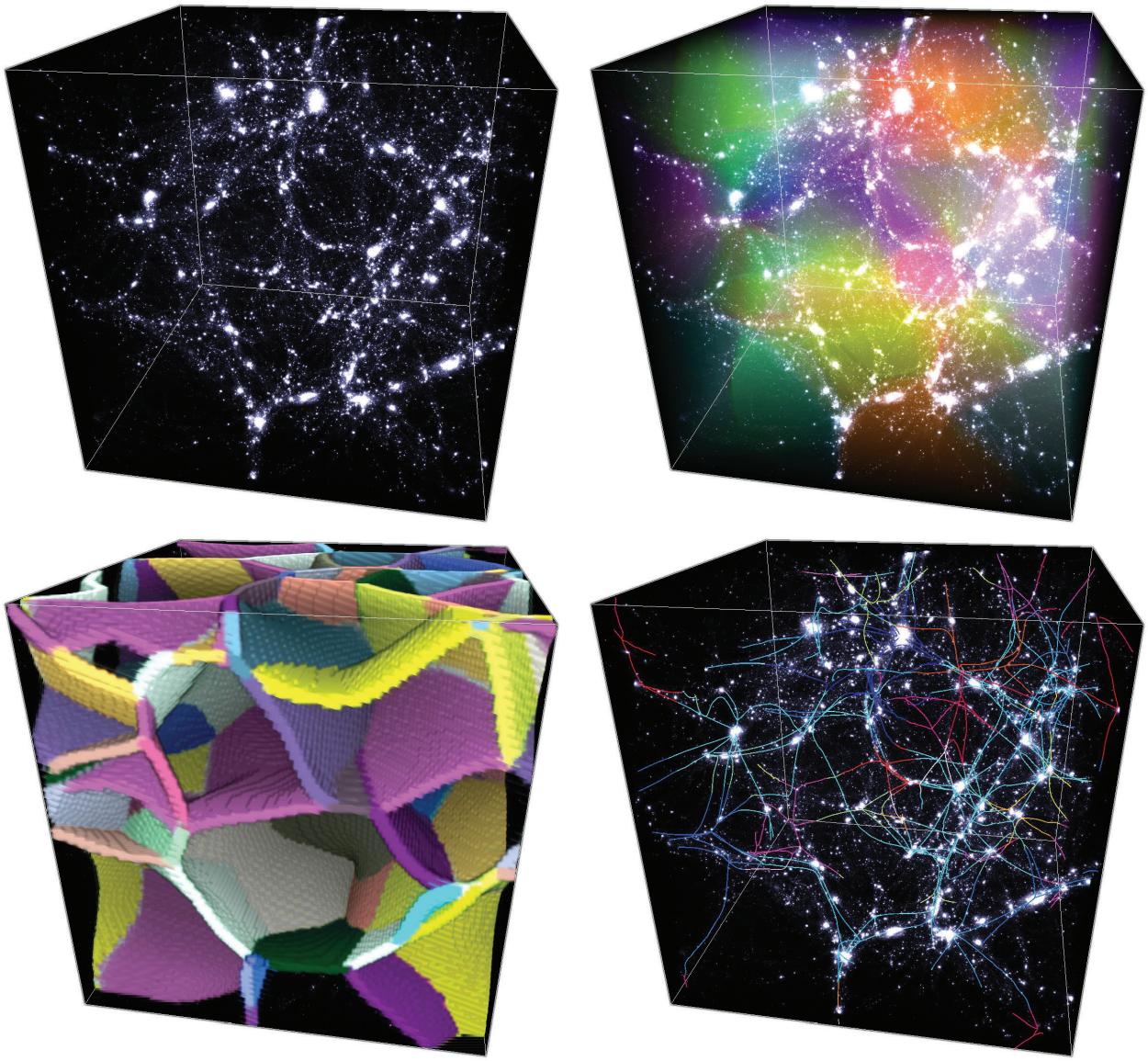

Figure 1. The dark matter density distribution in a $50\,h^{-1}$ Mpc large cosmological simulation (top left-hand panel), with its ascending 3-manifolds (i.e. the voids, top right-hand panel), ascending 2-manifolds (i.e. the walls, bottom left-hand panel) and ascending 1-manifolds (i.e. the filaments, bottom right-hand panel). The manifolds were computed using the method introduced in Sousbie et al. (2009).

Note that a reference is given in the last two pages, in which most mathematical terminologies introduced in Sections 2–4 is defined in relatively simple terms. As we only aim here to introduce the necessary mathematical notions and give a detailed description of the computation pipeline, extensively illustrating each step, the application to actual data sets is presented in a less-technical companion paper, Sousbie, Pichon & Kawahara (2010) (hereinafter Paper II). In that paper, we show the potential of this approach by applying it to typical cosmological data sets: a large-scale dark matter cosmological *N*-body simulation and the 7th Data Release (DR7) of the SDSS galaxy catalogue (Abazajian et al. 2009).

2 MORSE THEORY FOR SMOOTH MANIFOLDS

Mathematically speaking, the Morse theory is concerned with smooth scalar functions (say, height of a mountain or the temperature in a room) defined over generic manifolds. In the present case, we are mainly interested in density fields: real-valued functions defined over d-dimensional Euclidean spaces[1] $\mathbb{R}^d$. We will therefore restrict the present discussion to such geometries for the sake of simplicity. The Morse theory provides a way to capture the intricate relation between the geometrical and topological properties of a function. What one means by the geometrical property is basically any property unaffected by rigid motions such as translations or rotations. If h is the altitude function of a mountain landscape, for instance, the altitude of the highest peak or its total surface are geometrical properties. Topology, on the other hand, captures how points are connected to each other with notions such as that of neighbourhood. Topological properties are invariant under smooth

[1] This is actually not generally true. Numerical simulations, for instance, often use periodic boundary conditions, which amount to defining the density on a torus $\mathbb{T}^d \subset \mathbb{R}^d$.

continuous transformations. Sometimes topology is coined to be rubber geometry. If we stick to the landscape analogy and define a mountain as a set of points that can be reached from its summit by going down the slope (i.e. following the gradient of h), then the mountain itself is in some sense a topological property of the altitude function. Indeed, in winter, when covered with snow, or during summer, after the snow melted, the altitude map slightly changes, but the underlying mountain can still be easily identified as the same mountain. For the same reasons, a crest linking two mountains or a valley, for instance, are also topological properties of the landscape. When it comes to characterizing a function such as the matter density ρ on large scales in the universe, both topological and geometrical properties are interesting. While topological properties such as the number of galaxy clusters or dark matter haloes in a given volume are robust with respect to changes in the precise measured value of ρ, geometrical properties, such as the density profile and precise location of a halo or a filament, are more specific and characterize better the properties of ρ.

The relation between geometry and topology is intricate and while modifying the topology certainly requires a modification of the geometry, the reverse is not generally true. For instance, the shape of a mountain may only slightly change with season, but more drastic events such as the explosion of a volcano (i.e. a drastic change in the geometry) could actually erase it. The Morse theory captures this relation for a generic function f by relying on the gradient $\nabla_{\boldsymbol{x}} f(\boldsymbol{x}) = \mathrm{d}f/\mathrm{d}\boldsymbol{x}(\boldsymbol{x})$ and its flow. The gradient defines a preferential direction at every point (the direction of the steepest ascent) except where it vanishes (i.e. where $\nabla_{\boldsymbol{x}} f = 0$). Those particular points are called critical points and can be classified according to the sign of the Hessian matrix, the $d \times d$ matrix of the second derivatives $\mathcal{H}_f(\boldsymbol{x}) = \mathrm{d}^2 f/\mathrm{d}x_i \mathrm{d}x_j(\boldsymbol{x})$:

Definition 2.1. (Critical point of order k) Let f be a function defined over $\mathbb{R}^d$ and P a point with the coordinate $\boldsymbol{p} \in \mathbb{R}^d$. Then P is a critical point of f if $\nabla_{\boldsymbol{x}} f(\boldsymbol{p}) = 0$. It is said to be of order k if the Hessian matrix $\mathcal{H}_f(\boldsymbol{p})$ has exactly k negative eigenvalues.

Intuitively, in 2D, the top of a mountain is the maximum (order 2), a pass is a saddle point (order 1) and the bottom of a valley is the minimum (order 0). The top left-hand panel of Fig. 2 shows the gradient and critical points of a function defined over $\mathbb{R}^2$. On this picture, the blue, green and red circles stand for the critical points of order 0 (minima), 1 (saddle points) and 2 (maxima), respectively. Note that according to Definition 2.1, the order of a critical point is defined by the sign of the eigenvalues of the Hessian, which must therefore be non-null. This condition is essential to the Morse theory: a function f which obeys the Morse theory must necessarily satisfy this constraint. Conversely, such functions are called Morse functions.

Definition 2.2. (Morse function) A Morse function is a smooth function whose critical points are non-degenerate. This means that for any P such that $\nabla_{\boldsymbol{x}} f(\boldsymbol{p}) = 0$, $\det \mathcal{H}_f(\boldsymbol{p}) \neq 0$.

We will assume from now on that f is a Morse function.[2] At the location of any non-critical point, the gradient indicates a preferred direction and one can therefore define specific lines, the integral lines, by following the gradient flow.

Definition 2.3. (Integral line or field line) An integral line (also called the field line) is a curve $\boldsymbol{L}(t) \in \mathbb{R}^d$ such that

$$\frac{\mathrm{d}\boldsymbol{L}(t)}{\mathrm{d}t} = \nabla_{\boldsymbol{x}} f \,. \tag{1}$$

Its origin and destination are defined as $\lim_{t\to-\infty} \boldsymbol{L}(t)$ and $\lim_{t\to+\infty} \boldsymbol{L}(t)$, respectively.

The pink curves in the top left-hand panel of Fig. 2 show examples of integral lines: the lower order critical point at their extremity is their origin and the higher one their destination. The integral lines of a Morse function actually always have critical points as the origin and destination. Let us consider the case of an integral line passing through a base point P. One can show that such integral line obeys certain properties:

Property 2.3.1. (Integral lines of a Morse function) The integral lines of a Morse function f defined over $\mathbb{R}^d$ and passing through a given point P is obtained by following the gradient and minus the gradient from P. It obeys the following properties:

(i) The origin and destination of an integral line are critical points.

(ii) Two integral lines passing through the points P and P' may only be identical or fully distinct: two integral lines cannot intersect (they can share their origin and/or destination though).

(iii) The set of all the integral lines covers all of $\mathbb{R}^d$ and each point P of space belongs to exactly one integral line. It may be the origin/destination of several integral lines if it is a critical point though.

(iv) An integral line with the base point a critical point P is reduced to that point P.

The combination of the first and second properties is particularly interesting, as it allows to classify each point of space according to the origin *or* destination of its (unique) integral line. Such classification defines distinct regions of space called ascending and descending manifolds.

Definition 2.4. (Ascending/descending n-manifold) Let P be a critical point of order k of the Morse function f defined over $\mathbb{R}^d$. The ascending $(d-k)$-manifold defines a region of space with dimension $(d-k)$: the set of points reached by integral lines with origin P. The descending k-manifold defines a region of space with dimension k, the set of points reached by integral lines with destination P.

There exist exactly d different classes of ascending and descending manifolds, classified according to the order of the critical point at their origin or destination. Note that an ascending or descending d-manifold of a Morse function always spans a domain of dimension d [i.e. a 0-manifold is a (critical) point, a 1-manifold a line, a 2-manifold a surface, a 3-manifold a volume, etc.]. The middle panels of Fig. 2 show the ascending and descending 2-manifolds of the 2D function in the upper panel. The notions of ascending and descending manifolds are actually at the core of the Morse theory and the set of the descending or ascending manifolds is usually called the Morse complex.[3]

Definition 2.5. (Morse complex) The Morse complex of a Morse function f is the set of its ascending (or descending) manifolds.

[2] This is a strong requirement in practice, as shown in Appendix A.

[3] Whether one chooses to use the ascending or the descending manifolds is only a matter of convention, as the descending n-manifolds of f are the ascending n-manifolds of $-f$.

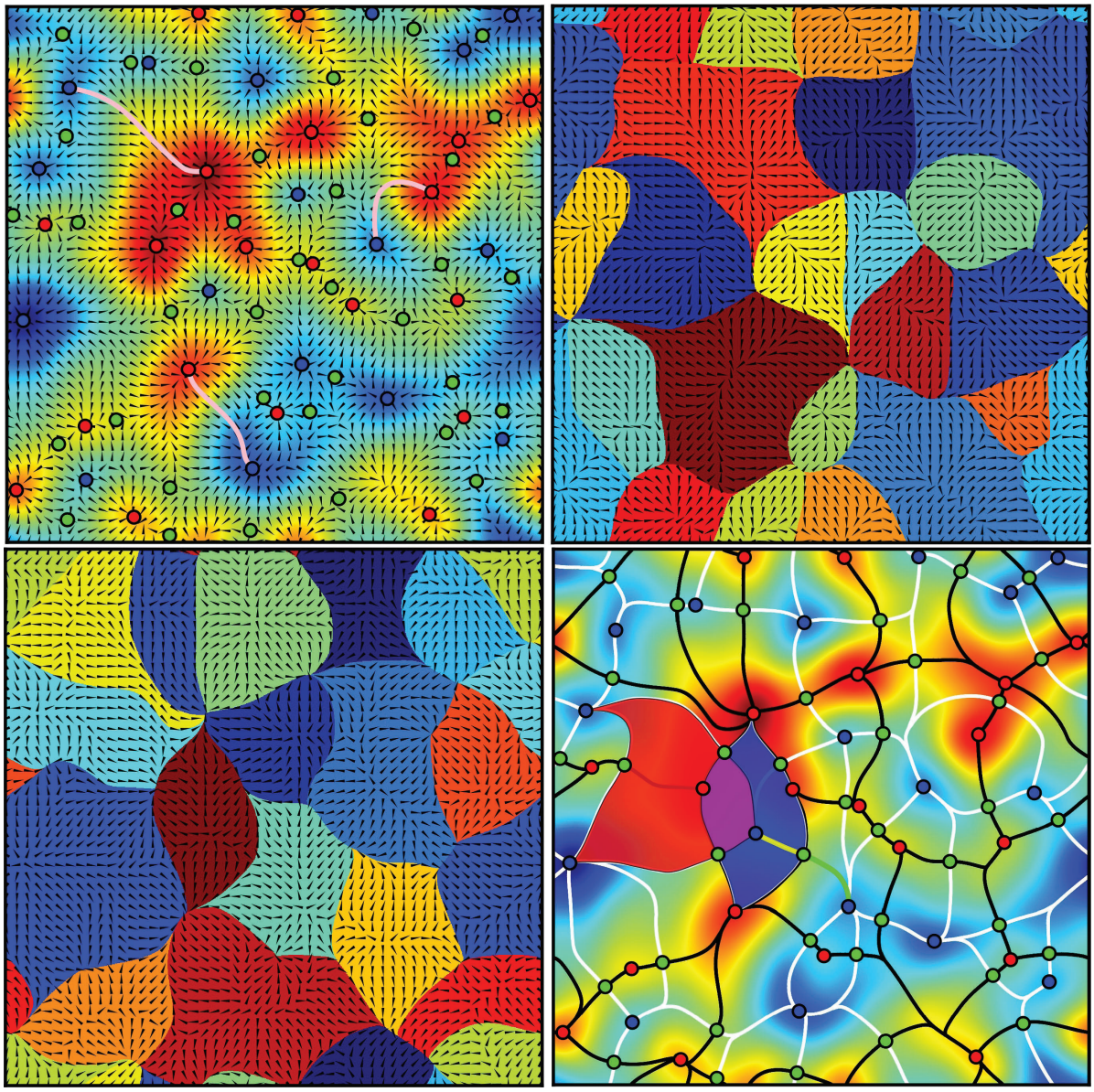

Figure 2. A 2D density field with its gradient (top left-hand panel), its descending 2-manifolds (top right-hand panel), its ascending 2-manifolds (bottom left-hand panel) and its Morse–Smale complex (bottom right-hand panel, see the black and white network). The maxima/saddle points/minima are represented as the red/green/blue circled discs, respectively, and three integral lines are drawn in pink in the top left-hand panel. On the central left-hand part of the bottom right-hand panel, an arc (i.e. a 1-cell) is represented in yellow (intersection of a green ascending 1-manifold and a blue descending 2-manifold) and a quad (i.e. a 2-cell) in purple (intersection of a red descending 2-manifold and a blue ascending 2-manifold).

The notion of the Morse complex can actually be extended by following Smale and adding one more condition to a Morse function.

Definition 2.6. (Morse–Smale function) A Morse–Smale function is a Morse function whose ascending and descending manifolds intersect only transversely,

where the word 'transverse' can be understood as the opposite of 'tangent', in the sense that there exists no point where two transverse manifolds are tangent. In other words, two ascending and descending manifolds should not be tangent and they should always penetrate each other where they cross (i.e. they should 'distinctly' intersect where they do). This additional condition ensures that the intersection of the ascending and descending manifolds is properly defined everywhere, so that the intersection of a p-ascending manifold and a q-ascending manifold may only have dimension $n = \min(p, q)$ or be void. Such a non-null intersection is called a Morse–Smale n-cell:

Definition 2.7. (Morse–Smale n-cell) A Morse–Smale n-cell is the non-void intersection of a p-ascending and a q-ascending manifold of a Morse–Smale function such that $n = \min(p, q)$. A 1-cell is generally called an arc, a 2-cell is a quad and a 3-cell a crystal.

An n-cell is a refinement of the concept of an ascending/descending manifold, whereas the descending and ascending manifolds are defined by the sets of integral lines having a common origin *or* common destination, respectively; a n-cell is defined by the sets of

integral lines with a common origin *and* destination. The bottom right-hand panel of Fig. 2 displays examples of n-cells in 2D. The purple region, for instance, is the quad defined by the intersection of the red descending 2-manifold and the blue ascending 2-manifold: all integral lines within this region have the minimum on its boundary as the origin and the maximum as the destination (see also the upper right-hand and lower left-hand panels). Similarly, the yellow curve defines an arc at the intersection of the blue ascending 2-manifold and the green descending 1-manifold, as only one integral line has the minimum and saddle point at its extremities as the origin and destination. The set of all n-cells defines the Morse–Smale complex.

Definition 2.8. (Morse–Smale complex) The Morse–Smale complex of a Morse–Smale function f is the set of all the n-cells of f.

In the same figure, the Morse–Smale complex is described by the critical points and the black and white curves. Basically, the critical points are its 0-cells, the set of black or white curves linking two critical points are its arcs (1-cells), and the regions bounded by a black and a white border are its quads (2-cells). In the 3D case we will consider in the next sections, the Morse–Smale complex is also composed of 3-cells (the so-called crystals). Note that the notion of an n-cell is very interesting as it defines a natural partition of space induced by the flow of the gradient, literally dividing it into a so-called cell complex (a generalization of the concept of a simplicial complex presented in Section 3). We do not give further details here though as only the concept of the arc is really needed for our purpose; the arcs really define how critical points are connected to each other by integral lines. Actually, and although this is not formally correct, the reader may find it simpler to only consider the nodes (critical points) and arcs of the Morse–Smale complex, each arc connecting the critical points at their extremities, two critical points being potentially connected only if their orders differ by 1 (i.e. a minimum and a 1-saddle, a 1-saddle and a 2-saddle or a 2-saddle and a maximum). For instance, the arcs connecting maxima to saddle points are subsets of the ascending 1-manifolds and they enclose the information on how each filament (represented by its saddle point) connects exactly two maxima. Note that the geometry of an arc is determined by the integral lines whose origin and destination are the two critical points the arc connects. The Morse–Smale complex obeys the following 'combinatorial'[4] properties:

Property 2.8.1. (Morse–Smale complex arcs) The arcs (i.e. 1-cells) in the Morse–Smale complex connect critical points in such a way that

(i) two arcs may only intersect at a critical point;
(ii) an arc in the Morse–Smale complex links two critical points with an index difference 1;
(iii) there are exactly two descending arcs reaching a given critical point of order 1 (each departing from not necessarily distinct minima); and
(iv) there are exactly two ascending arcs departing from a given critical point of order $d - 1$ (each reaching not necessarily distinct maxima).

[4] In this context, the term *combinatorial* is used to signify the discrete properties of the network formed by the Morse–Smale complex: its number of nodes, their types, the number of branches and cycles, etc. (see below).

Fig. 1 illustrates how the theoretical concepts of the Morse theory apply to cosmology. In this figure, the dark matter density distribution in a cosmological simulation is displayed in the top panel, together with its ascensing 3-, 2- and 1-manifolds on the second, third and fourth panels from the top, respectively. The ascending 3-manifolds associated to minima clearly trace the underdense regions, usually denominated voids. The type 1 critical points trace the geometry of the walls through their ascending 2-manifolds and the filaments are traced by the ascending 1-manifolds, associated to critical points of type 1. As stated as the beginning of this section, a Morse complex actually establishes the link between the geometrical (where are the critical points? what path does each arc follow?) and topological (how are critical points connected? how many of each type are there?) properties of the cosmic web. If the large-scale matter density distribution ρ were a Morse function, then each critical point of ρ could in fact be associated to a topological feature of the cosmic web whose geometry would then be described by an ascending or descending manifold, the arcs defining a hierarchical neighbourhood relation between them (the so-called combinatorial property). The purpose of this paper is to construct, from the particles, a discrete Morse function which closely resembles[5] the sampled density (which in fact matches it at the vertex of the tessellation) and which will therefore warrant all the corresponding discrete topological features.

3 DISCRETE MORSE THEORY

Even though the idea of applying the Morse theory directly to the analysis of the cosmic web is quite appealing a priori, the task is actually not straightforward in practice. Indeed, the Morse theory is defined for a Morse function, which is basically a smooth and at least twice differentiable real-valued function satisfying the Morse criterion (Definition 2.2). Whether it is because they result from fundamentally discrete processes, as in the case of the galaxy distribution, or obtained through sampling, as for numerical simulation or observational data, typical astrophysical data sets typically do not comply with those criteria in general. In contrast, the discrete Morse theory, first introduced by Forman (1998b, 2002), is a very powerful theory which manages to capture the essence of the smooth Morse theory while still being readily applicable to discrete or sampled data commonly available to scientists. It is basically a combinatorial adaptation of the Morse theory that applies to intrinsically discrete functions defined over simplicial complexes.[6]

Let us start by defining the basic building block of such spaces, the simplex. A k-simplex is the simplest possible geometrical figure of dimension k or simply speaking the k-dimensional analogue of a triangle: a 0-simplex, for instance, is a point, a 1-simplex a segment, a 2-simplex a triangle, a 3-simplex a tetrahedron, etc. More formally:

Definition 3.1. (k-simplex) A k-simplex σ_k is the convex hull of $k + 1$ affinely independent points $S = \{p_0, \ldots, p_k\}$. In other words, it is the set of points within the smallest possible solid with vertices (i.e. its summits) the $k + 1$ points in S. It may be noted $\sigma_k = \{p_0, \ldots, p_k\}$.

[5] Conversely, this construction would bias the reconstructed Morse–Smale complex if the underlying density was far from being a Morse function.
[6] Actually, the discrete Morse theory applies to the broader class of topological spaces called CW-complexes, which also include functions sampled over a regular cubic grid, for instance.

A simplex may have faces and cofaces.

Definition 3.2. (Face/coface of a k-simplex) A face of a k-simplex σ_k with vertices $S = \{p_0, \ldots, p_k\}$ is any l-simplex γ_l with $l \leq k$, such that its vertices $P = \{p_0, \ldots, p_l\} \subset S$. If γ_l is a face of σ_k, then σ_k is a coface of γ_l. In general, when k and l only differ by 1, a face is called a facet and a coface is called a cofacet.

Simply speaking, considering a tetrahedron in 3D (i.e. a 3-simplex) with four vertices, its 2-faces are four triangles (i.e. its facets, any possible combination of three vertices), its 1-faces are six segments (i.e. any possible combination of two vertices) and its 0-faces are fours points (i.e. any possible combination of one vertex). Reciprocally, the tetrahedron is a coface of any of those triangles, segments or points, and in particular it is a cofacet of any of the triangles. In general, a k-simplex has C_{l+1}^{k+1} faces of dimension l. Finally, a simplicial complex is a set of k-simplexes that comply with specific criteria:

Definition 3.3. (Simplicial complex) A simplicial complex K is a finite union of simplexes such that

(i) any face of a simplex in K also belongs to K; and
(ii) the intersection of two simplexes in K is empty or a simplex of dimension lower than or equal to the highest-dimension simplex they share.

Fig. 3 shows an example of a combination of simplexes that form a simplicial complex (left-hand panel) and a different combination that do not (right-hand panel). A common example of a simplicial complex in astrophysics is the Delaunay tessellation (see e.g. Okabe 2000; Schaap & van de Weygaert 2000; van de Weygaert & Schaap 2009) of a set of discretely sampled points.

As stated previously, the discrete Morse theory directly applies to functions defined over a simplicial complex. Those particular functions are called discrete functions and for the discrete Morse theory to apply, they also need to comply with certain criteria:

Definition 3.4. (Discrete Morse function) A discrete function f defined over a simplicial complex K associates a real value $f(\sigma_k)$ to each simplex $\sigma_k \in K$. The discrete function f is a discrete Morse function if and only if, for each $\sigma_k \in K$,

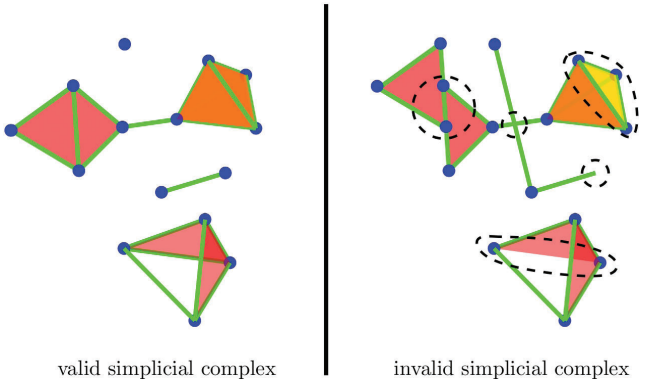

Figure 3. Illustration of two sets of 3D simplexes, K and K', forming a valid (left-hand panel) and an invalid (right-hand panel) simplicial complex. It is invalid because, from the left-hand to right-hand side and top to bottom, the intersection of the two 2-simplexes is not a simplex in K', two 1-simplexes intersect, a 3-simplex (light yellow, mostly hidden tetrahedron), a 1-simplex and a 2-simplex each lacks one of their facets.

(i) there exists *at most* one facet α_{k-1} of σ_k such that $f(\sigma_k) \leq f(\alpha_{k-1})$; and
(ii) there exists *at most* one cofacet β_{k+1} of σ_k such that $f(\sigma_k) \geq f(\beta_{k+1})$.

In other words, the Hessian non-degeneracy condition of the smooth Morse theory (Definition 2.2) becomes a condition on the value of the functions in the discrete theory: locally, a simplex has a higher value than its facets and a lower value than its cofacets, and there can only be one exception at most in each case. The reason for such a condition is not obvious at first sight, but it is actually essential to the existence of a discrete gradient, the counterpart of the gradient in the smooth theory. In fact, if conditions (i) and (ii) of Definition 2.2 of a discrete Morse function are satisfied, then, locally, the discrete gradient of f (see below) can only define at most one preferential direction, as does the gradient of the corresponding smooth theory. Following this line of thought, the analogue of a critical point of order k (see Definition 2.1), a critical k-simplex of f, is a simplex for which f does *not* have any preferential relationship with one of its direct neighbourhood (i.e. its facets and cofacets).

Definition 3.5. (Critical k-simplex) A k-simplex σ_k is critical for the discrete Morse function f if

(i) there exists *no* facet α_{k-1} of σ_k such that $f(\sigma_k) \leq f(\alpha_{k-1})$; and
(ii) there exists *no* cofacet β_{k+1} of σ_k such that $f(\sigma_k) \geq f(\beta_{k+1})$.

It is important here to realize that the equivalent in the discrete Morse theory of a critical point of order k is a critical k-simplex: in 2D, a minimum is a critical vertex (0-simplex), a saddle point is a critical segment (1-simplex) and a maximum is a critical triangle (2-simplex). This actually introduces an asymmetry in the discrete theory that does not exist in its smooth counterpart: while a minimum and a maximum are both points in space, critical points of order 0 and 3 are a vertex and a tetrahedron, respectively.[7]

We now proceed with the definition of a the discrete gradient. If Definition 3.4 is satisfied, then at least one of the two conditions of Definition 3.5 is verified, which leaves us with only two possible configurations for a simplex σ_k: exactly one of its cofacets and all its facets have a lower value or exactly one of its facets and all its cofacets have a higher value. In both cases, a preferential relation is established between σ_k and one of its facets or cofacets, which also defines a preferential direction, and leads to the following definition:

Definition 3.6. (Discrete gradient vector field) A discrete gradient vector field can be defined for a discrete Morse function f over K by coupling simplexes in gradient arrows (also called gradient pairs):

(i) If a simplex σ_k has exactly one lower valued cofacet α_{k+1}, then $[\sigma_k, \alpha_{k+1}]$ form a gradient arrow.
(ii) If a simplex σ_k has exactly one higher valued facet β_{k-1}, then $[\sigma_k, \beta_{k-1}]$ form a gradient arrow.

[7] A direct consequence is that f being a discrete Morse function does not imply that $-f$ also is. This apparent contradiction is solved by defining the opposite of a discrete Morse function over the dual complex (i.e. the Voronoi tessellation for the Delaunay tessellation). Indeed, each k-simplex has a $D-k$ dimensional dual counterpart and one can show that the discrete function $-f$ that attributes the value $-f(\sigma)$ to the dual cell of each simplex σ is Morse. Note that it also defines the same topology, the critical index of critical cells being simply reversed.

(iii) If a simplex σ_k satisfies Definition 3.5, it is critical and does not belong to a gradient arrow.

Note that other configurations are impossible precisely because f is a discrete Morse function. Also, within a gradient arrow, the lowest-valued simplex is the tail and the highest-valued one is the head (i.e. the discrete gradient actually points in the opposite direction of its smooth counterpart).

Fig. 4 shows a discrete Morse function defined over a 2D simplicial complex (upper left-hand panel) and its corresponding discrete gradient vector field and critical simplexes (upper right-hand panel). One can note the similarity in the relation between the discrete gradient flow and the critical simplexes and that between the gradient and critical points in the top panel of Fig. 2. Finally, one last important definition is that of the discrete integral line. In the terminology of Forman (1998a), it is called a V-path.

Definition 3.7. (V-path) A V-path is a strictly decreasing alternating sequence of k-simplexes α_k^i and $(\mathrm{k}+1)$-simplexes β_{k+1}^j

$$\alpha_k^0, \beta_{k+1}^0, \alpha_k^1, \beta_{k+1}^1, \ldots, \alpha_k^n, \beta_{k+1}^n,$$

where each pair $\{\alpha_k^i, \beta_{k+1}^i\}$ forms a gradient pair and α_k^{i+1} is a facet of β_{k+1}^i.

Tracing a V-path basically consists in intuitively following the direction of the gradient pairs, as one can see in the lower left-hand panel of Fig. 4 where two V-paths are highlighted in purple.

Using the previously introduced concepts, it becomes relatively straightforward to define a discrete Morse–Smale complex (DMC) and contrary to the smooth case, no manifold transversality condition (Definition 2.6) needs to be enforced, as this is naturally achieved by the tessellation itself. In fact, following Definition 2.4:

Definition 3.8. (Discrete A./D. *n*-manifold) Let σ_k be a critical simplex of order k of the discrete Morse function f defined over a simplicial complex K. The discrete ascending $(d-k)$-manifold is the set of k-simplexes that belong to at least one V-path with origin σ_k. The discrete descending k-manifold is the set of k-simplexes reached by field lines with destination σ_k.

Note that according to that definition, a discrete k-manifold only contains k-simplexes (those in the V-paths of σ_k). This makes it difficult to define discrete n-cells (see Definition 2.7) by intersecting manifolds, as they are made of simplexes with different dimensions. Following Gyulassy (2008), this definition is therefore extended to:

Definition 3.9. (Extended discrete A./D. *n*-manifold) An extended discrete ascending (descending) n-manifolds is a discrete ascending (descending) n-manifold, together with its cofacets (facets) and their extended discrete ascending (descending) n-manifolds.

This literally fills lower dimensional 'holes' in the manifold, making the intersection of two extended manifolds a very simple operation. In the lower right-hand panel of Fig. 4, for instance, the discrete ascending 2-manifold is represented by the blue dots only. Their cofacets, the green segments, are included in the extended manifold, as well as their extended ascending manifolds (red triangles). The definition of the discrete Morse complex is therefore similar to the one in the smooth case:

Definition 3.10. (Discrete morse complex) The discrete Morse complex of a Morse function f is the set of its extended ascending (or descending) manifolds.

Similarly, a discrete n-cell is the intersection of two extended ascending and descending discrete manifolds (Definition 2.7), and the DMC remains the set of the discrete n-cells (Definition 2.8). As in the smooth case, the DMC is really a combinatorial object as it describes a particular way of grouping critical simplexes in pairs, quads, crystals, etc., associating to each of those combinations the geometry spanned by intersections of ascending and descending manifolds. We conclude by noting that neglecting the effect of boundary conditions, the arcs of the DMC (i.e. the V-paths linking critical simplexes) obey the same properties as those of the Morse–Smale complex (Definition 2.8.1).

4 TOPOLOGICAL PERSISTENCE

The concept of the persistence was first formalized in Edelsbrunner et al. (2002) (see also Robins (2000)). It is basically a method to quantify the importance of the topological features of a space and was initially developed as a way to robustly measure topological properties when the noise is present and to enable the topological simplification (i.e. the modification of a function or a space so that its less-significant *topological* features are removed). The theory was originally described in the context of simplicial homology (for functions defined over a simplicial complex, see Appendix B) and was very nicely exposed in Edelsbrunner et al. (2002). We would like to stress here that the concept of the persistence itself is largely independent of the fact that a function is smooth or not, as it only quantifies the robustness of its topological properties, given one can measure them, whatever be the nature of the function itself.

Persistence itself is a relatively simple concept. To study the topology of a given function, one measures how the topology of its excursion sets (i.e. the set of points with values higher than a given threshold) evolves with the threshold. Whenever the threshold crosses the value of a critical point, a component of the excursion set gets created or destroyed, connected or disconnected, etc., each critical point therefore contributing positively or negatively to the Euler number of the set. The persistence is the measure of how long a given positive critical point was contributing to the result before being cancelled by the appearance of a given negatively indexed critical point. In other words, a specific pair of positive and negative critical points corresponds to the creation and destruction of a given topological feature in the excursion set. The difference between the values of the points in the pair is usually called its persistence (although other ways of measuring persistence exist) and it basically measures the lifetime of the corresponding feature in the excursion set or equivalently its robustness with respect to changes in the function.

More formally, for smooth functions, the persistence theory is based on the evolving properties of the so-called sublevel sets or equivalently of the excursion sets of a function ρ, as they change with the value of the level ρ_0. A sublevel set (an excursion set) is basically a set of points where $\rho(\boldsymbol{x} = (x_1, \ldots, x_n))$ is lower (higher) than or equal to a certain value ρ_0:

Definition 4.1. (Level set, sublevel set) A level set (also called an isocontour) of a function $\rho(\boldsymbol{x})$ of n variables x_i at level ρ_0 is defined as

$$(x_1, \ldots, x_n) \,|\, \rho(x_1, \ldots, x_n) = \rho_0.$$

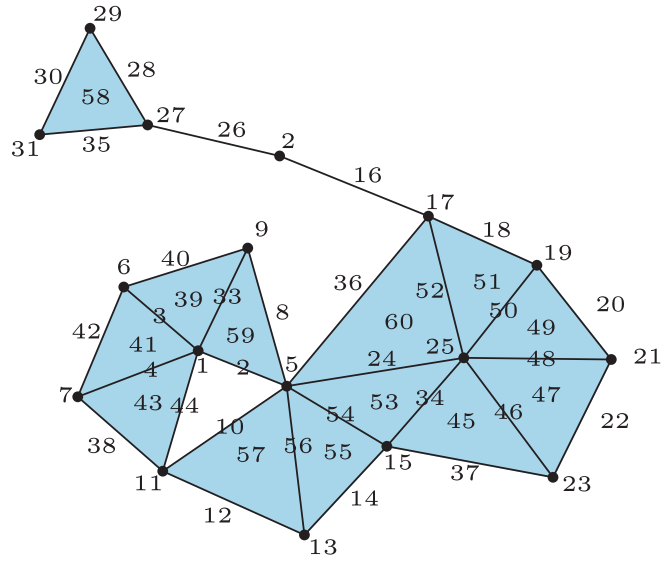

(a) A discrete Morse function over a 2D simplicial complex

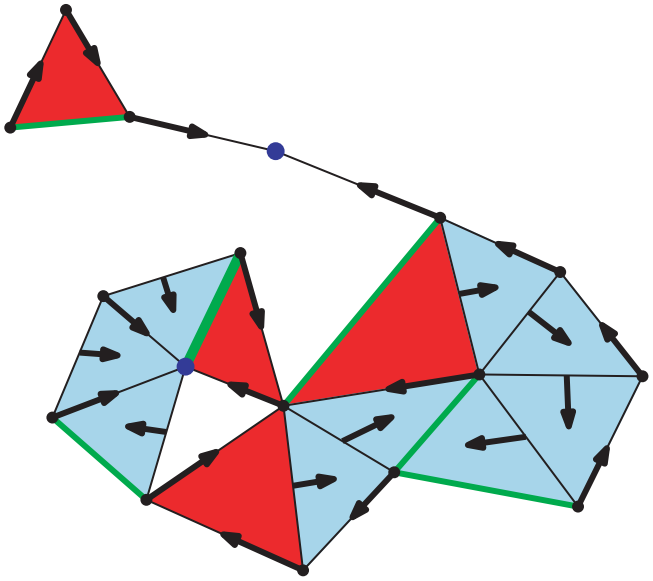

(b) The corresponding discrete gradient and critical simplexes (red triangles, green segments, and blue vertices)

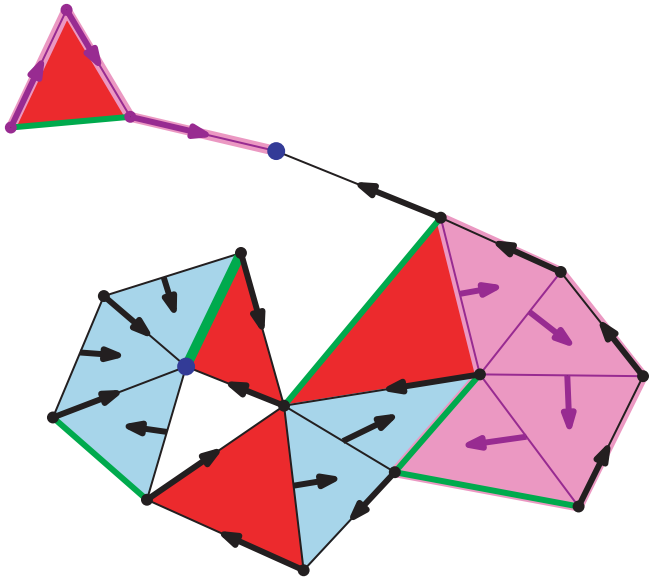

(c) Example of two V-pathes (purple shade)

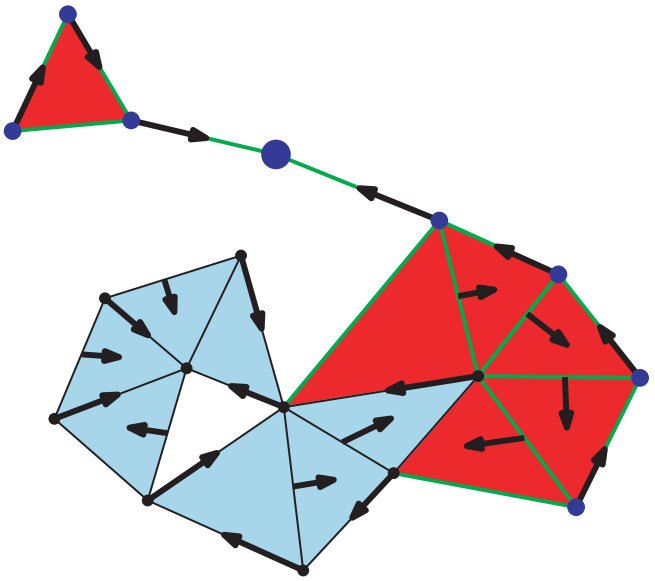

(d) Example of an ascending 2-manifold (union of the blue vertices, green segments and red triangles)

Figure 4. Illustration of the notions introduced by the discrete Morse theory. In the upper left-hand panel [panel (a)], the numbers associated to each k-simplex (i.e. vertices, segments and triangles) of the underlying simplicial complex define a discrete Morse function. Note that a discrete Morse function must comply with Definition 3.4, which is relatively restrictive, and in the present case, the function has been designed to illustrate notions of the discrete Morse theory on a relatively small complex. We show in Section 5.1 how a discrete Morse function can be defined to mimic the properties of a smooth function (such as the density or an altitude field, for instance). The corresponding discrete gradient (see Definition 3.6) is represented by the arrows in the upper right-hand panel [panel (b)], each arrow associating a $k-1$-simplex (the tail) to a k-simplex (the head). In the same panel [see also panel (c)], the red, green and blue shaded simplexes are the critical 2-, 1- and 0-simplexes of the discrete function, respectively (i.e. the equivalent of the maxima, saddle points and minima of the smooth theory). In the lower left-hand panel [panel (c)], the two purple-shaded sets of simplexes correspond to two V-paths of the discrete Morse function (the discrete analogue of an integral line, see Definition 3.7). Intuitively, a V-path is a set of simplexes linked by discrete gradient arrows, similarly to the integral lines of the smooth theory. Finally, the extended ascending manifold (see Definition 3.9) of the minimum with value 2 (the large blue disc) is shown in the lower right-hand panel [panel (d)]. Similarly to the smooth theory, the corresponding ascending 0-manifold (Definition 3.8) is defined by the set of simplexes that one can reach by following the gradient arrows from the minimum (i.e. all the blue vertices and green segments that belong to a gradient pair – i.e. an arrow). For the sake of consistency, one needs to define discrete extended manifolds (Definition 3.8), which also include recursively the cofacets of any simplex in the discrete manifold, as well as the ascending manifolds of those cofacets that are critical. The resulting discrete extended ascending 0-manifolds is the set of blue vertices, green segments and red triangles in the bottom right-hand panel.

A sublevel set is defined as

$$(x_1, \ldots, x_n) | \rho\,(x_1, \ldots, x_n) \leq \rho_0.$$

A notion equivalent to that of a sublevel set, which astrophysicists are familiar with, is that of an excursion set:

Definition 4.2. (Excursion set) An excursion set is the set of points such that

$$(x_1, \ldots, x_n) | \rho\,(x_1, \ldots, x_n) \geq \rho_0.$$

We would like to emphasize here that using sublevel sets or excursion sets to define persistence is only a matter of convention: while it is most common to find the former in mathematical papers (e.g. Forman 2002), the latter is more common in astrophysics, density peaks corresponding to isolated components.

As previously mentioned and whatever be the convention, the persistence can be interpreted as a measure of the 'lifetime' of topological features, the so-called k-cycles, in the sublevel sets. For instance, when the threshold value, ρ_0, skims through the image of ρ [i.e. the set of values $\rho\,(\boldsymbol{x})$ may take] from the top to bottom, the corresponding excursion set grows and the way it is connected evolves. In 3D, isolated islands (also called components or 0-cycles) first appear around the maxima. Those islands later merge into each other at saddle points of type 1 to finally form rings bordering holes (the 1-cycles). For lower values of ρ_0, those holes get filled at saddle points of type 2, destroying the corresponding 1-cycles, to later form spherical shells around minima (the 2-cycles), when a sufficient number of holes have been filled and those spherical shells also end up being filled at minima, therefore destroying the corresponding 2-cycles. The persistence relates the importance of a given k-cycle to the length of the interval of values ρ_0 can take and for which a given k-cycle exists within the growing excursion sets.

Fig. 5 illustrates how the persistence works in 1D. In this figure, the upper part displays four different functions, where the two on the right-hand side (labelled A' and B') were obtained by discretely sampling the two on the left-hand side (labelled A and B), adding random noise and linearly interpolating between the sample points. The lower part of the figure shows the different excursion sets of these functions for values corresponding to their critical points. In the bottom left-hand panel, for instance, the excursion sets of $\rho\,(x)$ are empty for levels $\rho_0 > 22$. At level $\rho_0 = 22$ though, a new component (i.e. a 0-cycle) appears, which corresponds to the highest maximum of the function. This component grows for levels $22 > \rho_0 > 21$ and a new independent component appears at the level of the second-highest maximum, $\rho_0 = 21$. Those two components remain independent while $\rho_0 > 20$ but merge when reaching $\rho_0 = 20$, the value of the first minimum. Basically, the minimum *destroyed* a component that was *created* by a maximum. By convention, we say that it destroys the most recently created one (i.e the maximum with the lowest density) and that the minimum and left maximum therefore form a persistence pair (as illustrated on the middle sketch) with the persistence $21 - 20 = 1$. The four sketches in the bottom part illustrate this pairing process for the four different functions. One should note that a given critical point may not always be paired in the process and that because the 1D case is very simple, a given type of critical point always creates or always destroys, but this is not the case, in general, for critical points that are not extrema.

A very common task when studying galaxy distributions or cosmological N-body simulations involves identifying galaxy clusters or dark matter haloes. This is often achieved using relatively simple

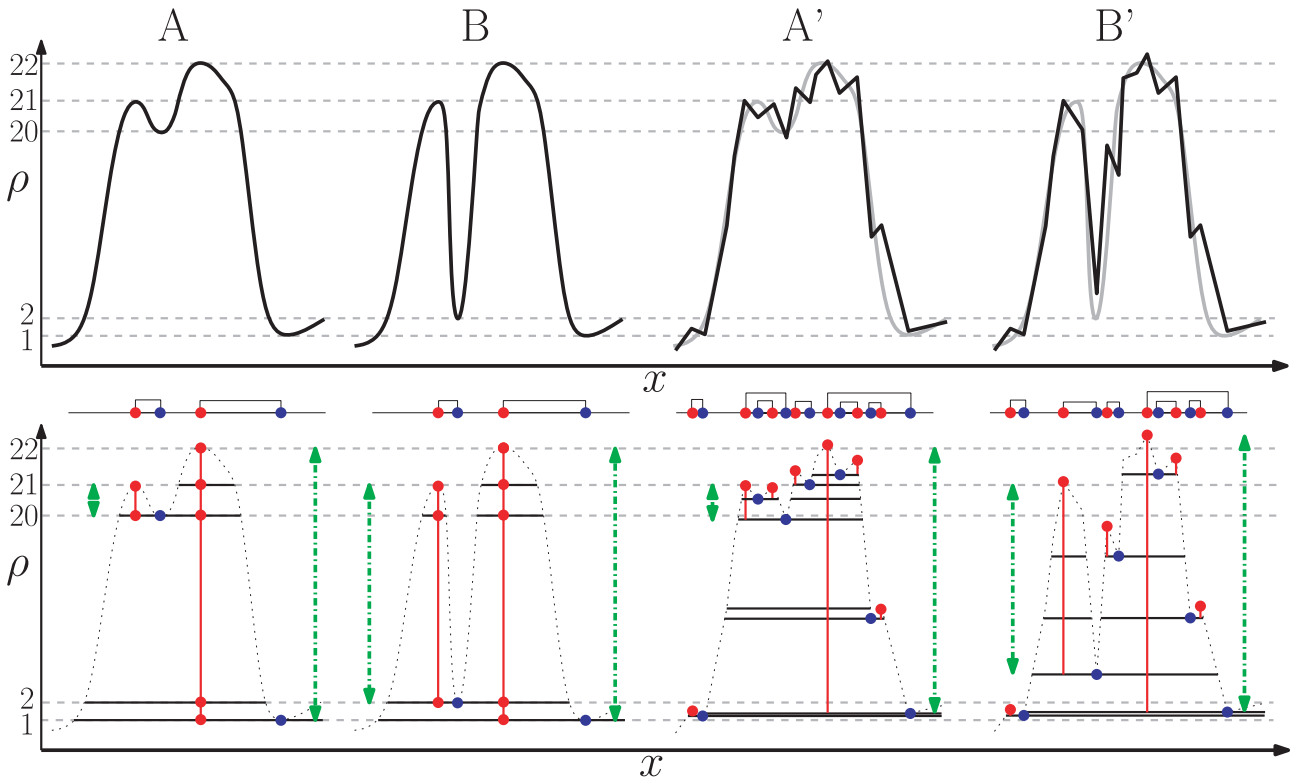

Figure 5. Illustration of the concept of the persistence over a 1D function. The upper panel shows two functions (left-hand panel) and their discretely sampled counterparts, with the noise added (right-hand panel). The lower panel displays the evolution of the excursion sets of these functions at the level of different critical points as the density threshold increases. The green dot–dashed vertical arrows emphasize the lifetime of components in the sublevel sets; the persistence pairs are displayed in the middle part over the function's Morse–Smale complex.

but robust methods, such as the FOF algorithm (Huchra & Geller 1982) that basically involves carefully selecting a global level ρ_c and considering each independent component in the excursion set ρ_c of the density field $\rho(\boldsymbol{x})$ as an independent cosmological structure. Applied to the functions A in Fig. 5, for example, such a method may detect one or two different peaks with $\rho_c = 19$ or 20.5, respectively, but it will not yield any information on whether those peaks are comparable or if one of them is more meaningful than the other. Persistence, on the other hand, can make such distinction, because it is built using information present in *all* the excursion sets: while function B contains two comparably persistent peaks, function A really contains only one (the peaks' persistence is symbolized by the length of the green arrows in the figure). The remarkable fact is that this stays true even if the sampling is poor and noise is present, as illustrated by functions A' and B'. Because of noise, many spurious peaks exist in these two functions, which may potentially lead to numerous fake identifications, but even in that case, where a density selection method would clearly fail to count the peaks correctly, persistence easily identifies the presence of only one persistent peak in A', and two in B', as in the case of functions A and B.

Although a very simple 1D case was illustrated here, the general idea remains the same in higher dimensional spaces. In general, one studies how components of sublevel or excursions sets are created and destroyed, but in higher dimensions, one also has to keep track of more complex structures than independent components, such as the formation of 2D holes or 3D shells in the structure (i.e. the 1-cycles and 2-cycles).

As mentioned earlier, persistence can equally be computed directly for discrete functions defined over simplicial complexes, given that one can define a concept similar to that of growing sublevel or excursion sets in such context. Note, however, that for practical reasons and because it is always defined in such a way in the literature, we will mainly use the sublevel set convention in the discrete case (i.e. the function is scanned from the bottom to top). A filtration, defined over a simplicial complex K, is a strictly growing set of subcomplexes K^i of K. Each K^i of a filtration contains a subset of the simplexes in K larger than K^{i-1} and smaller than K^{i+1}. More formally:

Definition 4.3. **(Filtration)** A filtration $\mathcal{F}$ of a finite simplicial complex K is a sequence of $N+1$ subcomplexes K^i of K such that

(1) $\emptyset = K^0 \subseteq K^1 \subseteq \ldots \subseteq K^{N-1} \subseteq K^N = K$,
(2) $K^{i+1} = K^i \cup \delta^i$,

where each δ_i is a different set of simplexes of K and $A \subseteq B$ means that A is included in or equal to B.

Basically, the size of a subcomplex in a filtration grows with its index, similarly to the sublevel sets of a smooth function which grow with the threshold value. So by defining a discrete function $\rho_D(\sigma_i)$, which associates a value to each and every simplex σ_i of K, one also defines an ordering over the simplexes in K (e.g. according to the ascending values of ρ_D). The discrete equivalent of a growing sublevel set for a smooth function ρ is therefore a filtration $\mathcal{F}_{\rho_D}$ within which each simplex σ_i enters at a time i such that $\rho_D(\sigma_{i-1}) \leq \rho_D(\sigma_i) \leq \rho_D(\sigma_{i+1})$. In that case, a subcomplex K^i contains all the simplexes of K with values lower than that of $\rho_D(\sigma_i)$ (see Fig. 6 for an example of such a filtration).

Similarly to the sublevel sets of the smooth function ρ, as the filtration $\mathcal{F}_{\rho_D}$ grows, new components, loops, shells, etc., appear, reflecting the topology of ρ_D. Those topological features are generally called k-cycles and we define them formally in the context of the discrete theory (this definition would conceptually be very close in the context of smooth functions though):

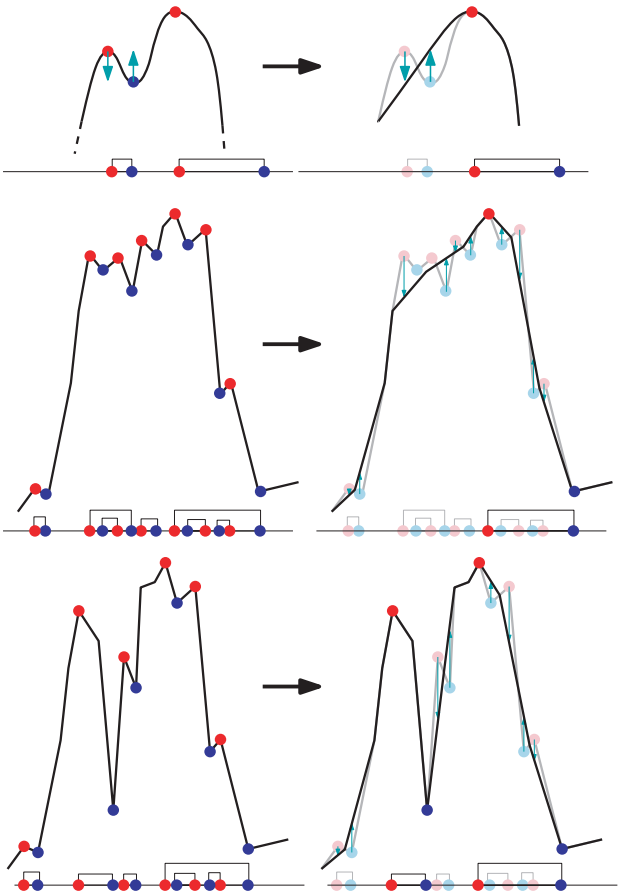

Figure 6. Illustration of the topological simplification process applied to functions A, A' and B' defined in Fig. 5 (see the top, middle and bottom panels). The diagram under each function represents its Morse–Smale complex and persistence pairs.

Definition 4.4. **(k-cycle)** A k-cycle in a simplicial complex K is a k-dimensional topological feature with $0 \leq k < D$, where D is the number of dimensions. When $D = 3$, for instance, a 0-cycle is an independent component (i.e. a set of simplexes non-linked to the rest of the complex), a 1-cycle is a loop (a set of simplexes that form a ring with a hole in the middle) and a 2-cycle is a shell (a set of simplexes bounding a 3D empty region).

As for a smooth function, one can therefore track the creation and destruction of k-cycles in $\mathcal{F}_{\rho_D}$ as simplexes enter the filtration, pairing critical simplexes into persistence pairs:

Definition 4.5. **(Persistence)** The persistence measures the 'lifetime' of topological features (i.e. k-cycles) in a filtration of a finite simplicial complex K induced by a discrete function ρ_D or equivalently in the growing sublevel sets of a smooth function ρ. The arrival of each critical simplex in the discrete case or critical points in the smooth case corresponds to the creation or destruction of a topological feature (k-cycle). The persistence pairs critical simplexes $\sigma_a - \sigma_b$ (or critical points $P_a - P_b$) that create and destroy a given feature, their corresponding persistence being defined by the difference of their 'arrival time', $\rho_D(\sigma_a) - \rho_D(\sigma_b)$ [or $\rho(P_a) - \rho(P_b)$]. It can also sometimes be useful to define a persistence ratio as the ratio of those values.

The computation of persistence pairs in a 2D filtration is illustrated in Appendix C and intuitively, the persistence describes how much a function would need to change to remove a topological feature.

The main interest of being able to identify persistence pairs of critical points (or simplexes) in a given function is that it yields an objective topological criterion to assess the significance of those critical points (or simplexes). Actually, one can go even further and show that it is actually always possible to *locally* modify the function to cancel non-persistent pairs out and therefore remove the topological noise. The process is illustrated in Fig. 6. In 1D, a persistence pair is always formed of a minimum and a maximum. If those two critical points are direct neighbours, one can in fact increase the value around the minimum and decrease the value around the maximum until the value at the maximum becomes smaller than that at the minimum. When this happens, both points are not critical anymore and none of the other critical points is affected. In the top panel, for instance, the process is applied to the less-persistent bump of function A. Note that the details of how the function is modified are not important, but rather the fact that it is possible to cancel a non-persistent pair and remove it from the Morse complex (see the diagrams below the functions). For instance, if one considers that structures whose persistence is lower or equal to the persistence of the smaller bump of function A are not significant (i.e. generated by noise with high probability), then one can remove the corresponding topological features so that function A becomes topologically equivalent to its simplified version (top right-hand panel) with the corresponding Morse complex. Applying the same process to A', the noisy version of A, one actually obtains a function with an identical topology and Morse complex (middle panels). This means that even in the presence of a relatively important noise, it is still possible using the persistence to recover the topology and Morse complex of the underlying function (see also the bottom panel to check how the topology of function B in Fig. 5 can be recovered from its noisy counterpart, B'). We detail in Section 6.2 a generic algorithm that implements symbolic topological simplification in order to recover the structure of the Morse complex of the matter distribution on large scale from a raw noisy version computed directly over a Delaunay tessellation.

5 DISCRETE MORSE COMPLEX

The basis of the necessary mathematical background being introduced in Sections 2–4, we now start detailing the corresponding algorithm and implementation used in DisPerSE. As previously mentioned, our purpose is to compute a *discrete* Morse complex and use its properties to identify and characterize the structure of the cosmic web. This approach has both advantages of being applicable to spaces with 3D or more and having a solid mathematical framework (Gyulassy 2008, see e.g. chapter 6). To summarize, a simplicial complex is computed from a discrete distribution (galaxy catalogue, N-body simulation, etc.) using the Delaunay tessellation and a density ρ is set to each galaxy using the DTFE (roughly speaking, the density at a vertex is proportional to the inverse volume of its dual Voronoi cell). A discrete Morse function is then defined by heuristically tagging a properly chosen value to each simplex in the complex (i.e. the segments, facets and tetrahedron of the tessellation). From this discrete function, we then compute the discrete gradient and deduce the corresponding discrete DMC (see Section 3; Forman 2002). The DMC is then used as the link between the topological and geometrical properties of the density field. Its critical points together with their ascending and descending manifolds are identified to the peaks, filaments, walls and voids of the density field (see Section 2). At this stage, the DMC is mainly defined by the Poisson sampling noise and measurement uncertainties and we filter it using the persistence theory (see Section 4 and Appendices B and C). For that purpose, we consider the filtration of the tessellation according to the values of the discrete Morse function and use it to compute persistence pairs of critical points. The DMC is finally simplified by cancelling the pairs that are likely to be generated by noise. This is achieved by computing the probability distribution function of the persistence ratio of all types of pairs in scale-invariant Gaussian random fields and cancelling the pairs with a persistence ratio whose probability is lower than a certain level.

5.1 Discrete gradient

As stated in Section 3, a discrete gradient field is derived from a proper discrete Morse function, which must satisfy Definition 3.4. Although those conditions are restrictive enough to make the deduction of a valid discrete Morse function difficult, they allow for a wide variety of such functions to exist; one has to keep in mind that the final discrete gradient field should be as similar as possible to its continuous counterpart $\nabla\rho$, the gradient of the density field ρ. An optimal method to define a discrete gradient has yet to be discovered, but Lewiner (2002) proposed a nice review on the topic and relatively advanced solutions. Unfortunately, these solutions involve the computation of relatively complex hypergraphs and are not easily applicable to large data sets. Instead, we implement here a modified version of the one presented in Gyulassy (2008), which presents the advantage of not depending on an arbitrary labelling of the simplexes.

The goal is to build a discrete Morse function $\rho_{\rm D}$ that complies with Definition 3.4 while remaining as similar as possible to its smooth counterpart, ρ. Conditions 3.4 put constraints on the relative values of facets and cofacets, but not directly on simplexes of the same dimension. As we use the DTFE to compute density, ρ is determined at the location of each vertex and we may therefore set $\rho_{\rm D}(\sigma_0) = \rho(\sigma_0)$ for any vertex $\sigma_0 \in K$. We then have to set values of $\rho_{\rm D}$ for higher dimensional simplexes (i.e. segments, triangles, etc.) in such a way that discrete Morse conditions (3.4) are ensured, while the topology of ρ is sufficiently preserved. In other words, arbitrary values of $\rho_{\rm D}$ may introduce spurious topological features only if they have a sufficiently low persistence. The simplest way to ensure discrete Morse conditions is to set all simplexes as critical: simplexes only have to be higher than their faces and lower than their cofacets. We therefore define a critical discrete Morse function whose spurious critical points (i.e. those not stemming from ρ) are not persistent.

Let σ_k be a k-simplex that belongs to K, Facet$[\sigma_k] \in S$, the facets of σ_k, and Vertex$[\sigma_k] \in S$, the facets of σ_k with dimension 0 (i.e. its vertices). We may build a critical discrete Morse function from ρ by setting

$$\begin{cases} k = 0: & \rho_{\rm D}(\sigma_0) = \rho(\sigma_0), \\ k > 0: & \rho_{\rm D}(\sigma_k) = \max\left(\rho_{\rm D}\left(\text{Facet}\left[\sigma_k\right]\right)\right) \\ & \qquad + \epsilon^k \sum \rho_{\rm D}\left(\text{Vertex}\left[\sigma_k\right]\right), \end{cases} \quad (2)$$

where max () stands for the maximal value of its arguments, d is the number of dimensions and ϵ is an infinitely small value. One can easily check that such a function does comply with Definition 3.4 of

a discrete Morse function. In fact, the value of a simplex is always slightly higher than the value of its highest facet, and thanks to the factor of ϵ^k, two simplexes sharing the same highest facet have different values if two vertices in K cannot have the same density. In practice, this is always the case when computing densities using the DTFE and in the following, we will therefore assume that we are in such a situation. For that reason, equation (2) defines the value of $\rho_{\rm D}$ uniquely from a given smooth function ρ and independently of any arbitrary labelling of the simplexes. Note that to compute the DMC, one only needs to be able to compare simplexes and it is therefore not necessary to give a particular value to ϵ, as only a comparison operator needs to be implemented. This definition of $\rho_{\rm D}$ allows for a unique ordering over the simplexes of K.

As explained in Section 3, a discrete gradient can be defined over K by grouping pairs of simplexes whose dimensions differ only by 1 (i.e. a vertex and a segment, a segment and a triangle or a triangle and a tetrahedron) and such that Conditions (3.6) are satisfied. A group of two paired simplexes form a gradient pair and the remaining unpaired simplexes are critical (the equivalent of the critical point for a smooth density field[8]). Looking at Conditions (3.6), one can see that for two simplexes to form a gradient pair, the simplex of a lower dimension should always have a value higher than the other. But because $\rho_{\rm D}$ has precisely been defined such that any simplex has a value higher than its facets, no pair may be formed, and all the simplexes in K are therefore initially critical. As a consequence, the Morse complex of $\rho_{\rm D}$ can be readily deduced: each k-simplex is a critical simplex of order k, and it is linked by an arc to each of its facets and cofacets, which are also critical. Many of those arcs actually link critical simplexes whose discrete Morse function $\rho_{\rm D}$ only differ by an infinitesimal amount $\Delta\rho_{\rm D} \propto \epsilon^p$ though, and we call such arcs ϵ-persistent. Because along those arcs the value of the function only changes infinitesimally, they can be cancelled while only modifying the value of $\rho_{\rm D}$ by an infinitely small amount. In fact, doing so one can basically exchange the values of $\rho_{\rm D}$ given to each critical simplex at the extremity of the ϵ-persistent arc and pair them within a gradient arrow. By repeating this process until no ϵ-persistent arcs exist anymore, one can therefore deduce a correct discrete gradient.

In practice, we proceed by considering the sets of the k-simplexes of K one by one, in ascending order of their dimension, and within each set, we iterate over the simplexes σ_k in ascending order of their value $\rho_{\rm D}(\sigma_k)$. For each of them, if it is not already in a gradient pair, we retrieve the lowest of its cofacets $\alpha_{k+1} \in \langle\sigma_k\rangle$ that is not already in a gradient pair and which value is only infinitesimally higher than $\rho_{\rm D}(\sigma_k)$. If it exists, we pair them; else, σ_k remains unpaired. Note once again that the value of $\rho_{\rm D}$ does not need to be explicitly modified in the actual implementation, as α_{k+1} and σ_k may only differ infinitesimally if σ_k is the highest facet of α_{k+1}. The algorithm ends when all the simplexes have been checked once. We show in Fig. 7 a practical example of how the algorithm runs on a simple smooth function and a 2D simplicial complex spanning over its domain of definition.

5.2 Discrete Morse complex computation

Once a proper discrete gradient has been defined over a simplicial complex, it becomes relatively straightforward to deduce its corresponding DMC. According to Definition 2.4, the ascending (descending) manifold of a critical point P_k of order k is the set of integral lines that end (start) at P_k. The discrete analogue of an integral line is a V-path (i.e. a sequence of simplexes linked by the discrete gradient, see Definition 3.7) and one can therefore identify ascending (descending) manifolds by following the V-paths that end (start) at a critical simplex C_k. The core of the algorithm consists in a simple 'breadth first search' where sequences of cofacets and gradient pairs are identified according to Definition 3.7. Each manifold is stored in a separate set-type data structure as one simplex may be reached by different V-paths within a manifold. Let $\mathcal{A}(C_k)$ be the set that stores the ascending manifold of the critical k-simplex C_k. The recursive algorithm starts by considering the set of the *cofacets* of C_k, stored in an array $A_{\rm cur}$ that will basically contain, at the nth step of the algorithm, the set of $(k+1)$-simplexes in the nth gradient pair of any V-path starting at C_k. At each step, the content of $A_{\rm cur}$ is scanned and for each $(k+1)$-simplex, there exist four possibilities:

(i) It is critical, in which case it is skipped as the V-path ends.

(ii) It is not critical, and is paired to a k-simplex in a gradient pair. In that case, the k-simplex is added to $\mathcal{A}(C_k)$ and stored in a temporary array $A_{\rm tmp}$.

(iii) It is not critical, but is paired by a discrete gradient to a k-simplex already in $\mathcal{A}(C_k)$. In that case, it is skipped.

(iv) It is not critical and is paired to a $k+2$-simplex in a gradient pair. In that case, it is skipped.

Once all simplexes in $A_{\rm cur}$ have been treated, the content of $A_{\rm cur}$ is replaced by the *cofacets* of the k-simplexes in $A_{\rm tmp}$ and the process is iterated until $A_{\rm cur}$ is empty at which stage all the simplexes in $\mathcal{A}(C_k)$ have been retrieved. The computation of the descending manifold $D(C_k)$ is achieved in exactly the same way, except that cofacets are replaced by facets. A pseudo-code implementation is presented in Algorithm 1 (see the non-tagged lines only). Note that in this implementation, only k-simplexes are stored to describe the manifold of a critical k-simplex, which reduces memory usage. It also implies that the algorithm does not compute the extended discrete manifolds of Definition 3.9, but rather those of Definition 3.8. This is indeed not a problem though as those manifolds can easily be extended at query time from the identified sets of k-simplexes. Practically, extending an ascending (descending) k-manifold consists in recursively adding the cofacets (facets) of any simplex in the manifold, as well as the ascending (descending) p-manifolds ($p > k$) of any of its critical p-simplexes.

Fig. 8 illustrates the result of applying this algorithm over the simple discrete gradient of Fig. 7 (note that the corresponding discrete function and gradient have been reproduced in Fig. 8a). The four diagrams displayed in Figs 8(c) and (d) show the result obtained while computing the discrete extended ascending (left-hand panel) and descending (right-hand panel) 1-manifolds of the three saddle points (pink-, yellow- and blue-dashed lines), and the discrete extended ascending (left-hand panel) and descending (right-hand panel) 2-manifolds of the two minima and two maxima (pink- and yellow-shaded regions), respectively.

As an example, let us detail first the process followed by our algorithm to measure the ascending 1-manifold $\mathcal{A}(C_1)$ of C_1, the critical 1-simplex (i.e. saddle point) with label d [see the red path in the left-hand panel of Fig. 8(c)]. We start by considering the cofacets of $C_1 = d$ and as there is only one, labelled B, we initially set $A_{\rm cur} = [B]$. The 2-simplex B is linked to segment j by a gradient arrow, j is therefore added to $\mathcal{A}(C_1)$ and $A_{\rm tmp} = j$. Segment j has two cofacets, the triangles B and D and we therefore set $A_{\rm cur} = [B, D]$. We then proceed by considering all triangles in $A_{\rm cur}$ one by one.

[8] Note that a critical point of type k from the smooth theory is equivalent to a critical k-simplex of the discrete theory. In 2D, minima are critical vertices, saddle points are critical segments and maxima are critical triangles.

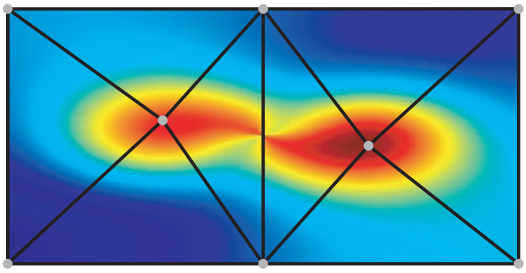

(a) Example of a smooth function and a simplicial tesselation of space

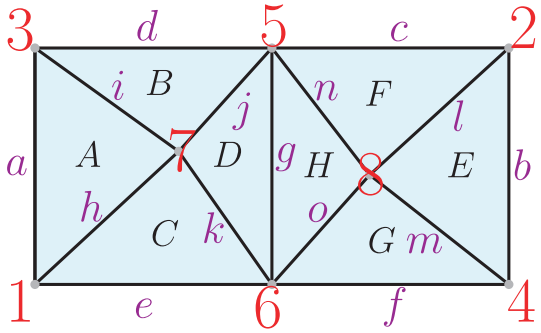

$$
\begin{array}{llll}
a = 3 + 4\epsilon & e = 6 + 7\epsilon & i = 7 + 10\epsilon & m = 8 + 12\epsilon \\
b = 4 + 6\epsilon & f = 6 + 10\epsilon & j = 7 + 12\epsilon & n = 8 + 13\epsilon \\
c = 5 + 7\epsilon & g = 6 + 11\epsilon & k = 7 + 13\epsilon & o = 8 + 14\epsilon \\
d = 5 + 8\epsilon & h = 7 + 8\epsilon & l = 8 + 10\epsilon &
\end{array}
$$

$$
\begin{array}{ll}
A = 7 + 10\epsilon + 11\epsilon^2 & E = 8 + 12\epsilon + 14\epsilon^2 \\
B = 7 + 12\epsilon + 15\epsilon^2 & F = 8 + 13\epsilon + 15\epsilon^2 \\
C = 7 + 13\epsilon + 14\epsilon^2 & G = 8 + 14\epsilon + 18\epsilon^2 \\
D = 7 + 13\epsilon + 18\epsilon^2 & H = 8 + 14\epsilon + 19\epsilon^2
\end{array}
$$

(b) The corresponding discrete Morse function defined over the simplicial complex (see equation 2)

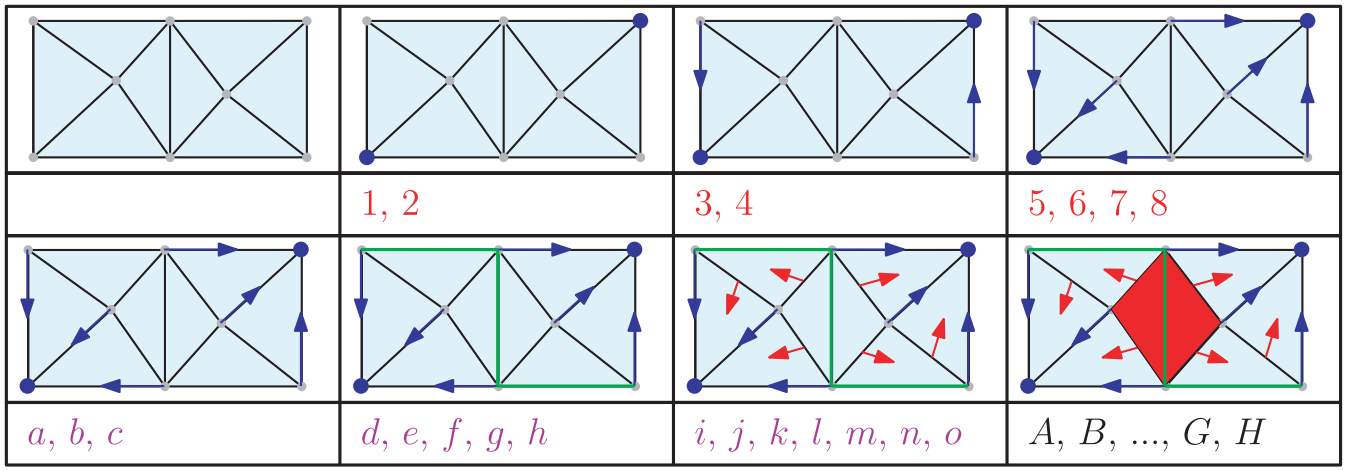

(c) Computation of the discrete gradient

Figure 7. Illustration of the computation of a discrete gradient from a simple smooth function and a simplicial complex spanning its domain of definition, as shown in panel (a). The corresponding discrete Morse function is represented in panel (b). Each vertex is labelled with the value of the corresponding smooth function, and the lower-case and upper-case letters correspond to the labels of the segments and triangles, respectively, for which the corresponding value of $\rho_{\rm D}$ is shown on the right-hand side of the panel (see equation 2). Note that sorting segment or triangle labels according to alphabetical order also sorts them in increasing order of their value. Panel (c) illustrates the computation of the discrete gradient according to the algorithm described in Section 5.1, which works by considering the vertices, segments and triangles one after the other, in increasing order of their value (from the left-hand to right-hand side and top to bottom in the figure). Starting with the first vertex, ${\rho_{\rm D}}^{-1}$ (1) (lower left-hand vertex), its cofacets are the segments labelled a, h and e with the values $3 + 4\epsilon$, $7 + 8\epsilon$ and $6 + 7\epsilon$, respectively. As none of those values differs from 1 by a factor of ϵ only, no pair can be formed and the vertex remains critical (i.e. unpaired, represented by a blue disc in the figure). The vertex with value 2 presents the same configuration and is therefore also critical, but the third one to enter, labelled 3, has one available cofacet labelled a with the value $3 + 4\epsilon$ that is only infinitesimally higher, which means the vertex and segment form a gradient pair (blue arrow between 3 and a in the figure). The case of vertex 4 is similar and it is paired to segment b. The next vertex, labelled 5, is problematic because it presents two cofacets with infinitesimally higher values, c and d, but the conflict is easily solved by pairing with one with the value closest to 5, segment c. We then proceed until no vertex is available anymore and start considering segments (left-most box of the second row in the figure). Segments a, b and c are skipped because they are already paired to vertices 3, 4 and 5 respectively. Segment d is free though but does not have an infinitesimally higher cofacet (i.e. triangle B); it is therefore a critical segment (i.e. the equivalent of a saddle point, represented in green). Segments e and h are paired while f and g are found to be critical. This leads to segments i whose cofacets are A and B, whose values differ from that of i by $11\epsilon^2$ and $15\epsilon^2$, respectively; i is therefore paired to the closest triangle in value, A (red arrow on the diagram). The remaining segments are processed the same way and one can then start reviewing the triangles. Only D and H are not paired, and as in 2D triangles have no cofacets, they are critical (coloured red in the figure). The final discrete gradient is shown in the bottom right-hand box in panel (c).

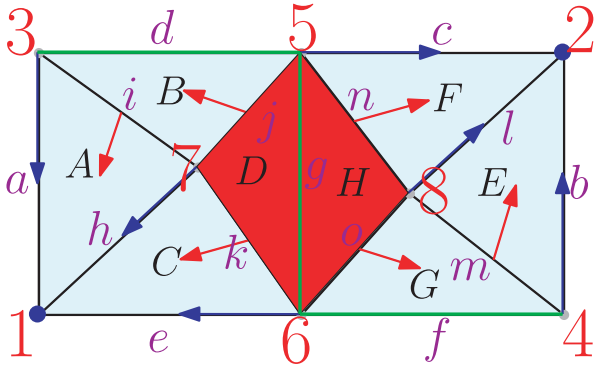

(a) Reproduction of the example discrete Morse function and its discrete gradient (see figure 7)

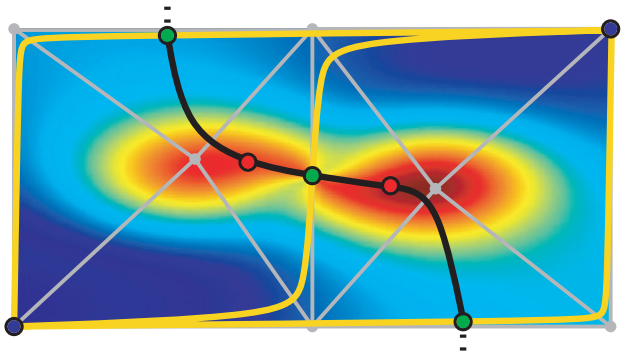

(b) Resulting discrete Morse-smale complex

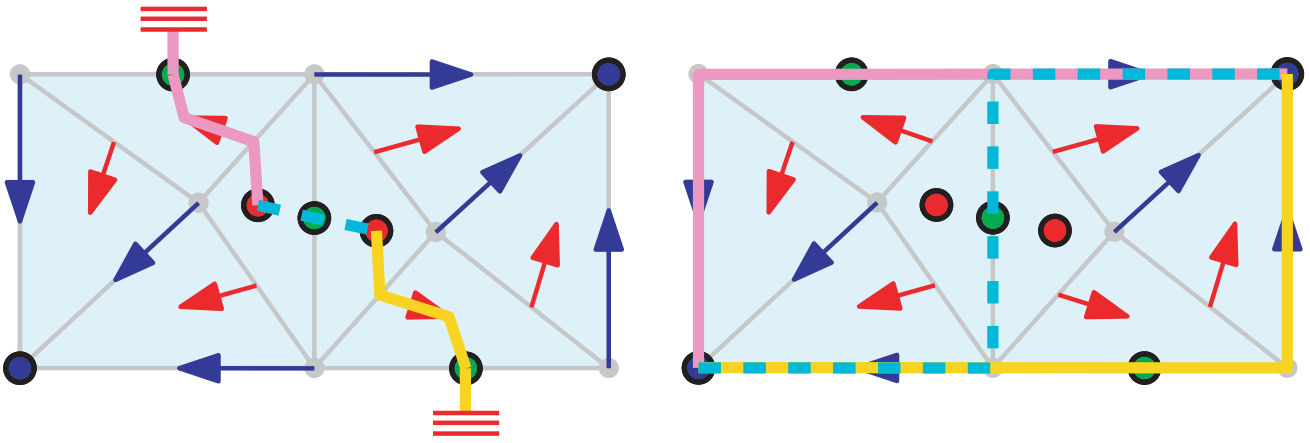

(c) Computation of the discrete extended ascending (left) and descending (right) 1-manifolds (see definition 3.9) of the three critical 1-simplexes (*i.e.* saddle points, the green disks, critical simplexes being represented by disks for clarity)

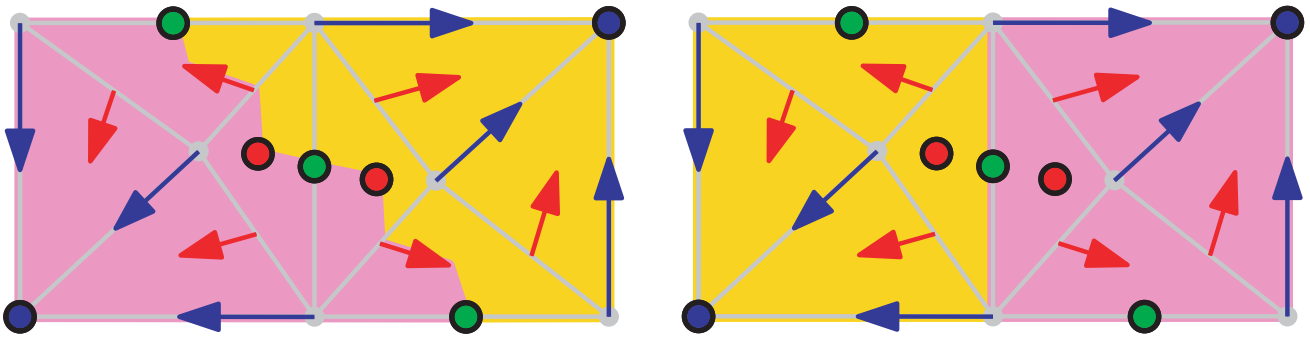

(d) Computation of the discrete extended ascending (left) and descending (right) 2-manifolds (see definition 3.9) of the two critical 0-simplexes (*i.e.* minima, the blue disks, critical simplexes being represented by disks for clarity)

Figure 8. Illustration of the computation of the discrete extended ascending and descending manifolds and corresponding Morse–Smale complexes from a discrete gradient. The application of the algorithm described in Section 5.2 over the simple discrete function and the gradient shown in panel (a) (see Fig. 7 for the labels' description) are illustrated in panels (c) and (d) for the ascending (left-hand panel) and descending (right-hand panel) 1-manifolds and 2-manifolds, respectively (critical simplexes are identified by coloured discs in their centre). In panel (c), the ascending (left-hand side) and descending (right-hand side) 1-manifolds of the three critical 1-simplexes (i.e. equivalent of saddle points, represented by green discs) are represented as pink plain, cyan-dashed and yellow plain broken lines, respectively. The 1-manifolds are represented as sets of segments joining the centres of simplexes according to Definition (3.7), a V-path is an alternating sequence of k- and $(k+1)$-simplexes linked by a facet–cofacet relation or belonging to a gradient pair. Note in the right-hand panel how it is possible for two descending 1-manifolds (blue dashed and plain yellow or plain pink) to share a portion of their path. In panel (d), the ascending (left-hand panel) and descending (right-hand panel) 2-manifolds of the two critical 0-simplexes (i.e. equivalent of minima, represented by blue discs) are coloured in pink and yellow, respectively. The Morse–Smale complex is a set of n-cells obtained by intersecting pairs of ascending and descending manifolds (see Definitions 2.7 and 2.8) and it is represented over the initial smooth function in panel (b). In this figure, the black and yellow curves represent the arcs (i.e. 1-cells) linking maxima–saddle points and minima–saddle points, respectively. It is very striking how the algorithm manages to correctly capture the essential features of the Morse–Smale complex, even though it was only applied over a very crude simplicial tessellation of space: not only the critical points where correctly identified as critical simplexes, but also the way they are connected by arcs is also correct (note that the arcs' geometry was smoothed for clarity reasons).

The 2-simplex B is not critical but is paired to segment j which already belongs to $\mathcal{A}(C_1)$; it is therefore skipped and we are left with considering triangle D which is critical and is therefore also skipped. Eventually, we obtain $\mathcal{A}(C_1) = [j]$. The pink path in the figure corresponds to the extended version of $\mathcal{A}(C_1)$, obtained by recursively including also the cofacets of the simplexes in $\mathcal{A}(C_1)$, namely triangles B and D.

Similarly, the algorithm can be applied to the critical vertex C_0 with value 1 to retrieve its ascending 2-manifolds displayed in pink on the left-hand panel of Fig. 8(d). The cofacets of vertex 1 are segments a, h and e and, as none of them is critical, the algorithm starts with $A_{\rm cur} = [a, h, e]$. The segments in $A_{\rm cur}$ are paired with vertices 3, 7 and 6, respectively, which are not critical vertices and do not yet belong to $\mathcal{A}(C_0)$; they are therefore added to $\mathcal{A}(C_0)$ so that $\mathcal{A}(C_0) = A_{\rm tmp} = [3, 7, 6]$. The content of $A_{\rm cur}$ is then replaced by all the segments that are cofacets of at least one vertex in $A_{\rm tmp}$ and we have $A_{\rm cur} = [a, i, d, h, j, k, e, g, f]$. Considering the segments in $A_{\rm cur}$ one by one, a, h and e are skipped because they are paired to vertices 3, 7 and 6, respectively, which belong to $\mathcal{A}(C_0)$, d, g and f are skipped because they are critical, and segments i, j and k are skipped because they are not paired to 1-simplexes, but to the 2-simplexes A, B and C, respectively. This leaves $A_{\rm tmp}$ empty and as a consequence $A_{\rm cur}$ becomes void which stops the algorithm with $\mathcal{A}(C_0) = A_{\rm tmp} = 3, 7$ and 6. The pink-shaded region in the figure corresponds to the extended version of $\mathcal{A}(C_0)$, obtained by adding also the cofacets of vertices 3, 7 and 6, which are segments a, h, e, d, i, j, g, k, o and f and triangles A, B, C, D, G and H, as well as the extended ascending 1-manifolds of critical 1-simplexes d, g and f.

The computation of the arcs in the Morse–Smale complex is slightly more involved. A Morse–Smale complex is formed by critical nodes and arcs linking them together. Those arcs are integral lines that start at a critical point of order $k + 1$ and end at a critical point of order k, so they always have dimension 1: they are represented by curves. Their discrete equivalents are V-paths linking critical (k + 1)-simplexes and critical k-simplexes. In 2D, they are simply described by the ascending and descending 1-manifolds (the blue-, pink- and yellow-dashed lines in the upper part of Fig. 8b), but this is not the case in higher dimensions where arcs are generally described by the 1D intersections of a descending and an ascending manifold. The bottom part of Fig. 8(b) shows the discrete Morse–Smale complex computed from the simple density field ρ represented by the background colour. It was obtained, thanks to a modification of the manifold algorithm: when computing an ascending (descending) manifold of a critical k-simplex, we store the list of critical (k + 1)-simplexes [(k−1)-simplexes] that are encountered and for each of them, trace the V-paths that led to them by storing in separated arrays all the simplexes in each path when the recursive procedure is returning. This way we obtain, for each pair of the critical k-simplex and (k + 1)-simplex that are linked by a V-path, the set of all simplexes in the V-path (i.e. the arcs of the Morse complex). Note that in Fig. 8(b), each ascending (descending) 1-manifold is actually made of two arcs, each linking the same saddle point to a maximum (minimum). Algorithm 1 presents the pseudo-code for a function that computes the ascending or descending arcs and manifolds of a critical k-simplex, the manifolds and arcs being returned in a global simplex array M and global list of simplex array *arcs*, respectively. In this code, the lines dedicated to identifying arcs are tagged to differentiate them from the simpler manifold identification algorithm. After this function is called on a critical simplex C_k, M will contain the index of all the k-simplexes in the ascending (descending) manifold of C_k (not including C_k) and *arcs* will contain a list of arrays, each containing the k-simplexes in a V-path between C_k and another critical simplex $C_{k+1}(C_{k-1})$, including $C_{k+1}(C_{k-1})$ and C_k.

We end this section with a comment on our implementation. The ascending $(d - k)$-manifold and descending k-manifold of a critical k-simplex are represented by lists of k-simplexes. This certainly makes sense for the descending k-manifold, as in 3D, for instance, volumes will be represented by lists of tetrahedrons, surfaces by lists of faces and lines by lists of segments. However, this is not the case for the ascending $(d - k)$-manifold, where, for instance, the ascending 3-manifold of a minimum is represented by a list of vertices. To solve this issue, one can choose to use extended manifolds instead of regular manifolds. This can be problematic though, for instance, for visualization purpose, not only because it considerably increases the number of simplexes within each manifold, but also because in that case two neighbouring k-manifolds will edge

Algorithm 1: Computes the ascending or descending manifolds and arcs of a critical simplex S_k. Variables *arcs* and M store the retrieved arcs and manifold. Triangular marks tag the lines dedicated to arc identification only.

```
1: function GetManifold(σ_k, ascending)
Require: σ_k is a critical k-simplex
Require: M is an empty list of simplexes
Require: arcs is an empty list of arrays of simplexes
2:    if ascending then
3:       A_cur ← getCofaces(σ_k)
4:    else
5:       A_cur ← getFaces(σ_k)
6:    end if
7:    A_tmp ← {}
8:    curArcs ← {}                                   ▷
9:    for all c ← A_cur do
10:      p ← getGradientPair(c)
11:      if getDimension(p) == k and p ∉ M then
12:         M → insert(p)
13:         if not isCritical(p) then
14:            A_tmp → insert(p)
15:         else                                     ▷
16:            newArc ← {c}                          ▷
17:            arcs → pushBack(&newArc)              ▷
18:            curArcs → insert(&newArc)             ▷
19:         end if                                   ▷
20:      end if
21:   end for
22:   for all c ← A_tmp do
23:      newArcs ← GetManifold(c, ascending)
24:      curArcs → insert(newArcs)                   ▷
25:   end for
26:   for all c ← curArcs do                         ▷
27:      c → pushBack(σ_k)                           ▷
28:   end for                                        ▷
29:   return curArcs                                 ▷
30: end function
```

k-simplexes. For instance, in Fig. 8(d), the extended ascending 2-manifolds should actually share 2-simplexes B, D, H and G if our algorithm was followed. It is not the case in the figure though because we actually used the dual tessellation for the representation of the extended ascending manifolds (i.e. the Voronoi tessellation in our case, where the complex is computed on a Delaunay tessellation). In fact, the dual tessellation associates a cell of dimension

$(d - k)$ to each k-simplex and one only has to interpret the list of simplexes in an ascending manifold in terms of its dual Voronoi cells, surfaces, lines or vertices, which does not necessitate any modification of the algorithm. Note that this point of view is also interesting as it enforces the fact that ascending and descending manifolds intersect transversely (i.e. they cannot be tangent at any point), an essential property of a Morse–Smale function (see Section 2). In practice, we always use the dual representation for the visualization of the descending manifolds, k-dimensional regions being best represented by lists of k-dimensional elements. Note nevertheless that k-manifolds remain stored in the memory as lists of k-simplexes as this is much more efficient.

6 DEALING WITH NOISE: PERSISTENCE AND TOPOLOGICAL SIMPLIFICATION

Using the algorithms introduced in the previous two sections, it is possible to compute efficiently the DMC of basically any discretely sampled function via the Delaunay tessellation of the sampling points. Applied directly to the Delaunay tessellation of a discrete galaxy catalogue or of a N-body dark matter simulation, the algorithm could therefore theoretically be used to identify the filaments, walls and voids. However, because it cannot discriminate between the spurious Poisson noise induced detections and the actual cosmic web features, it is of no practical interest as is. As an example, we applied it to the output of a $50\,h^{-1}$ Mpc large dark matter simulation downsampled to 64^3 particles. Running a simple FOF algorithm (Huchra & Geller 1982) with a linking length equal to one twentieth of the interparticular distance and a minimal number of particles of 20 leads to the identification of 800 bound structures (i.e. potential dark matter haloes). Computing the Morse complex of the same distribution leads to the identification of 12 771 maxima (i.e. potential haloes) and 32 457 type-1 saddle points (i.e. potential filaments). This suggests that only about ∼6 per cent of the detected structures are cosmologically significant and that most of the detected filaments actually link spurious noise induced maxima. In order to remedy this problem, we apply the concept of the persistence (Edelsbrunner et al. 2000), introduced in Section 4. Roughly speaking, the persistence defines a mathematically rigorous framework to assess the significance of topological features, while the Morse theory, by means of the Morse–Smale complex, establishes the link between the local geometry and topology. We describe in the following how, using those theories together, the Morse complex can be simplified in order to get rid of its unwanted features.

6.1 Pairing critical simplexes and persistence

Within the context of a smooth function, the persistence can be understood as a measure of the lifetime of a given topological feature (interpreted as the relative importance or significance of that feature) within the evolving sublevels sets at levels varying from one extreme of the function possible values to the other. Within a discrete context, a very similar concept and interpretation can be made for the filtration (see Definition 4.3) of a simplicial complex K: new simplexes entering the filtration create or destroy topological features, defining their persistence in terms of how many new simplexes had to enter the filtration before a given topological feature was destroyed. In that case, one therefore measures the importance of the different topological features induced by the function that defines the order of entrance of each simplex in the filtration. As we are interested in the topology and geometry of the density function ρ, it is natural to use its discrete counterpart $\rho_{\rm D}$ (see equation 2) to define the time each simplex enters the filtration, as it associates a distinct value to each simplex. We therefore consider the filtration $\mathcal{F}$ of K according to the ascending values[9] of $\rho_{\rm D}$, similarly to what was done in Section 5.2 to compute the Morse complex, and recast the persistence measure in terms of the difference in the values of $\rho_{\rm D}$ associated to the simplex that creates a feature and the simplex that destroys it.

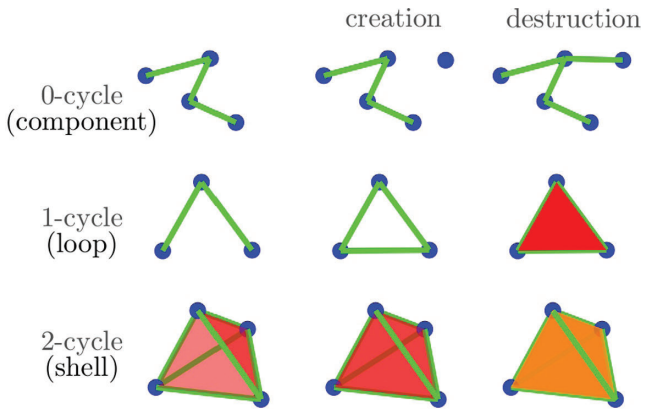

Figure 9. Creation and destruction of k-cycles in a filtration according to $\rho_{\rm D}$ (equation 2). An unlinked component creates a 0-cycle, a loop around a hole creates a 1-cycle and a shell around an empty volume creates a 2-cycle.

Because of the way $\rho_{\rm D}$ was defined, any simplex enters $\mathcal{F}$ before its cofacets. In the 3D case, for instance, this is illustrated inn Fig. 9. A vertex (0-simplex) is never linked to the rest of the subcomplex when it enters $\mathcal{F}$ and therefore we say that it will always *create* a new component (i.e. a 0-cycle) in the filtration. Similarly, when a segment enters, its two faces already belong to $\mathcal{F}$ while its cofacets do not yet: it forms a bridge between two 0-simplexes and may therefore either *destroy* one component if those two 0-simplexes belonged to distinct 'islands' or *create* a new 1-cycle (i.e. a loop, a torus-like structure) in the other case. The same way, a facet could *destroy* a 1-cycle by filling the hole in its centre or *create* a 2-cycle (i.e. a shell) and a tetrahedron may only destroy a 2-cycle (i.e. fill a shell). A consequence of the fact that all simplexes create or destroy something is that all simplexes in the complex are initially critical, as was already noted in Section 5.1, and our goal is to establish which critical simplexes create and destroy a given k-cycle of $\mathcal{F}$ (i.e. a component, a loop, a shell, etc.).

Actually, that is exactly what the algorithm that computes the discrete gradient does for the so-called ϵ-persistent arcs (i.e. arcs that link simplexes whose value $\rho_{\rm D}$ only differs by an infinitesimal amount ϵ, see Section 5.1). In fact, a simplex σ_k and its facet σ_{k-1} may belong to a gradient pair if their values differ only by ϵ (i.e. if they enter consecutively in the filtration). When this is the case, the value of $\rho_{\rm D}$ is symbolically modified by an infinitesimal amount so that σ_{k-1} actually enters just before σ_k and none of them may create or destroy a cycle anymore. While σ_k created a new k-cycle destroyed by σ_{k-1} in the initial filtration, this is not the case anymore after the modification, as both simplexes are not critical anymore and belong to the gradient pair instead. We therefore only need to pair the critical simplexes that survive to the discrete gradient computation (i.e. that belong to the DMC) into persistence pairs. Edelsbrunner et al. (2000) first introduced an

[9] Note that the choice of ordering according to the ascending or descending value is totally arbitrary and has no importance.

algorithm in 3D. Although more general and efficient approaches have been developed since (e.g. Cohen-Steiner, Edelsbrunner & Morozov 2006; Zomorodian 2009), we present here a variation of the original one, directly implemented over the Morse complex. Note that, given that only the critical simplexes identified in the DMC of K create or destroy cycles, one only needs to consider the Morse complex directly (i.e. as opposed to considering each and every simplex in K) to identify persistence pairs. From that point, it therefore does not matter anymore how the Morse–Smale complex was computed or whether it is discrete or not, as both have identical combinatorial properties anyway. Under the assumption that the discrete Morse function was computed with enough care to correctly inherit the topology of the underlying density field, we can therefore indifferently talk about the critical points of the smooth density field ρ or the critical k-simplexes σ_k of the simplicial complex K in the following. It is also equivalent to describe the persistence in terms of creation/destruction events in the level sets of ρ or in the filtration steps of the filtration induced by $\rho_{\rm D}$ (by convention, we choose to order the entrance time by ascending values of $\rho_{\rm D}$, making it similar to the level sets of ρ).

The algorithm starts by tagging each critical simplex σ_k as *positive* or *negative* depending on whether it creates or destroys a cycle. As was noted before, in 3D, the critical vertices and tetrahedrons (equivalent to minima and maxima) may only create a 0-cycle and destroy a 2-cycle, respectively. The critical 0-simplexes are therefore all tagged positive and the critical 3-simplexes are tagged negative. The sign of the rest of the critical simplexes is determined by following the growth and merging of each component in the filtration using a 'union-find' type data structure.[10] Depending on whether a segment entering the filtration links two previously independent components (i.e. destroys a 0-cycle) or creates a new bridge within one unique component (i.e. creates a 1-cycle), it will be tagged negative or positive as it destroys a component or creates a 1-cycle. Tracking the creation of 2-cycles (i.e. shells) or destruction of 1-cycles by the critical 2-simplexes in the filtration seems much more complex though, but it can actually be made easy by considering the filtration $\mathcal{F}'$ induced by $-\rho_{\rm D}$, where simplexes enter in the opposite order to $\mathcal{F}$. For symmetry reasons, a 2-simplex creating a 2-cycle in $\mathcal{F}$ actually destroys a component in $\mathcal{F}'$ and is therefore positive, while a simplex destroying a 1-cycle in $\mathcal{F}$ actually creates 1-cycle in $\mathcal{F}'$ and is therefore negative. Exactly the same algorithm and 'union-find' type data structure can therefore be used to track those events in $\mathcal{F}'$ and decide the sign of each critical 2-simplex in $\mathcal{F}$.

Practically, let us consider the filtration in the ascending order first. An entry is created in a 'union-find' structure for each critical simplex in the DMC, each of them is initially attributed a different group Id. Whenever a segment enters the filtration, the group Id of its two facets are retrieved and we check if they differ or are equal. In the first case, this means the segment created a bridge between two previously disjoint structures. It is therefore tagged negative and the groups of the two vertices and the segment are merged in the union-find structure. In the second case, both vertices already belonged to the same structure, which means that the introduction of the segment created a new 1-cycle (i.e. a loop that passes through the newly created bridge). The segment is therefore tagged positive and its group is merged with that of its facets. The sign of the 2-simplexes (triangles) is determined in the same way, but reversing the order of the filtration: a face is tagged positive, whenever it creates a bridge between two previously unlinked tetrahedrons and negative whenever it links two tetrahedrons that were already linked.

[10] A union-find data structure is particularly efficient at managing a large number of sets of elements. It implements fast set merging (the 'union' operation) and is able to recover efficiently to which set a given element belongs to ('find' operation).

Algorithm 2: Finds persistence cycles created by a negative critical simplex σ_k.

```
1: function CYCLESEARCH(σ_k)
Require: σ_k is a negative critical k-simplex (parameter)
Require: ppairs stores persistence pairs (global)
Require: cycles store all previously computed cycles, each associated to a negative simplex (global)
Require: CurSet is a Z_2-Set of simplexes (see text), empty when first called (local)
2:    α_nei ← GETMSCNEIGHBORS(σ_k)   ▷ α contains the simplexes that share an arc with σ_k in the DMC.
3:    for all β ← α_nei do
4:       if TYPEOF(β) == TYPEOF(σ_k) − 1 and not SIGNOF(β) == SIGNOF(σ_k) then
5:          CurSet → INSERT(β)
6:       end if
7:    end for
8:    while not ISEMPTY(CurSet) do
9:       σ_{k−1}^cur ← GETHIGHESTOF(CurSet)
10:      if ISEMPTY(cycles[σ_{k−1}^cur]) then
11:         cycles[σ_{k−1}^cur] ← CurSet
12:         cycles[σ_k] ← CurSet
13:         ppairs → INSERT(σ_{k−1}^cur, σ_k)
14:         break
15:      else
16:         for all β ← cycles[σ_{k−1}^cur] do
17:            CurSet → INSERT(β)   ▷ note that adding the cycle of σ_{k−1}^cur modulo 2 actually removes simplex σ_{k−1}^cur.
18:         end for
19:      end if
20:   end while
21: end function
```

Now that each critical simplex σ_k has been attributed a sign, we can reconsider the filtration $\mathcal{F}$ of the critical simplexes in ascending order and identify the persistence pairs using Algorithm 2. Instead of detailing how this, rather complex, algorithm works, let us first explain its application to a simple 2D example for the sake of clarity. Note that the method is very similar whatever be the number of dimensions, as long as the sign of each critical simplex has been previously determined and so deducing the 3D case from the 2D one should be straightforward. We first define a few variable names and types the algorithm uses. The purpose of the function CYCLESEARCH(σ_k) is to retrieve the $(k-1)$-cycle destroyed by the negative critical simplex σ_k. For each call, the result is stored in a variable *cycles* that will at the end contain the description of all cycles, each associated to its creating and destroying a critical k-simplex. Each cycle is stored as a list of critical (k − 1)-simplexes that form a (k − 1)-cycle within the Morse–Smale complex (for instance, a loop is stored as a list of critical segments). Another variable, labelled *ppairs*, stores pairs of critical

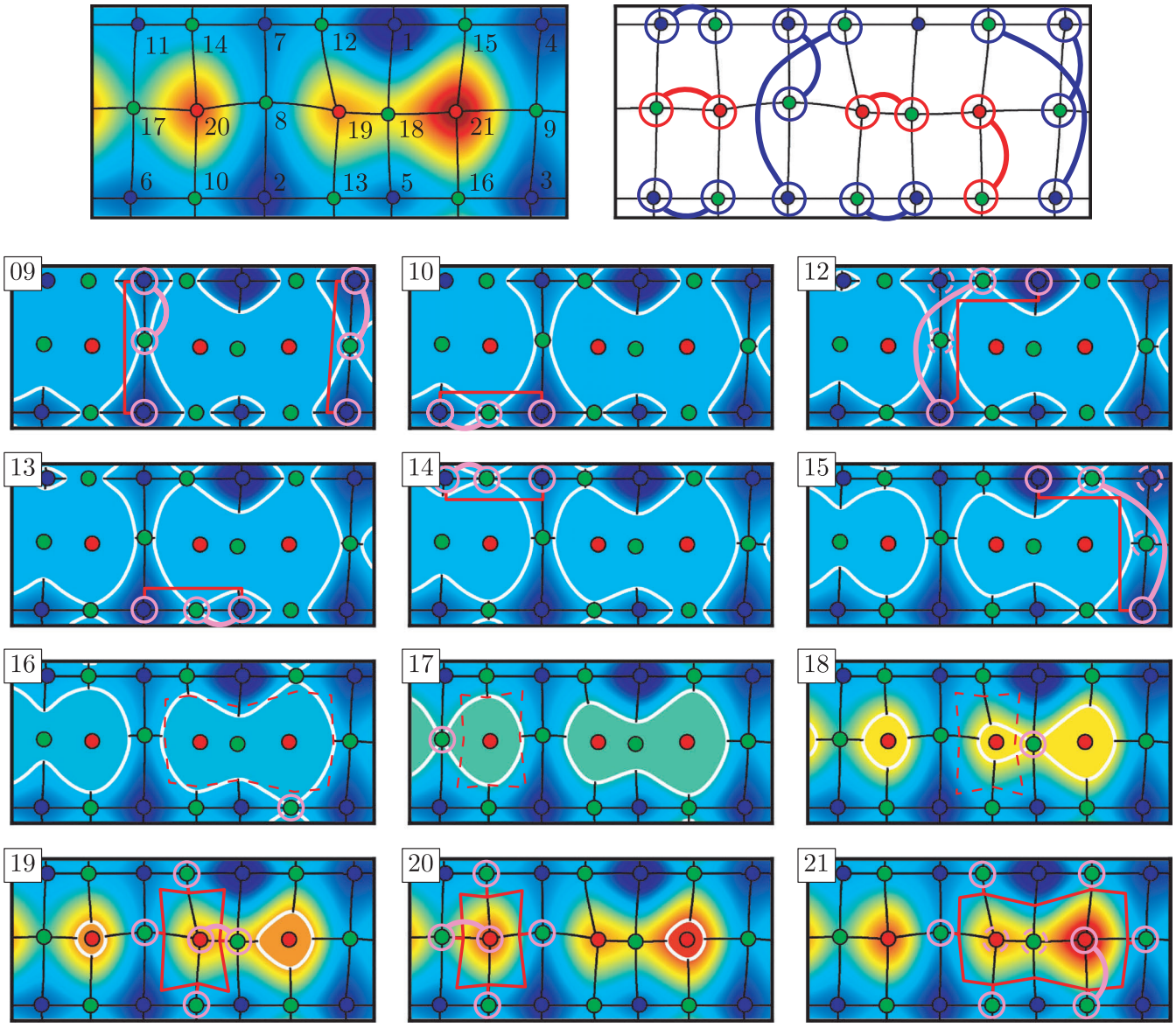

Figure 10. Illustration of the computation of persistence pairs using Algorithm 2 presented in Section 6.1. On the top left-hand panel, the Morse–Smale complex of the underlying smooth function ρ is represented with blue, green and red discs, standing for minima, saddle points and maxima, respectively. Note that the Morse complex is actually a DMC computed from a discrete morse function ρ_{D} (see equation 2) over a high-resolution tessellation (not represented), so the blue, green and red discs equally stand for critical vertices, segments and triangles, respectively (the two views are equivalent under the assumption that ρ_{D} correctly identifies the topology of ρ). The numbers n beside the disc correspond to the corresponding values of the density ρ. In the 12 panels in the bottom part, the evolution in the sublevel sets (i.e. the set of points where density ρ is smaller than a given threshold ρ_n) of the smooth density field is shown in the background, at levels $\rho_n = n$ corresponding to the value n in the upper left-hand corner of each panel. In each panel, the identification of a new persistence pair in the DMC is represented by a pink arc, while the corresponding cycle is symbolized by the red line. Note that cycles and pairs are identified at the moment they are destroyed, not created, and the red-dashed lines in panels 16–18 roughly indicate the shape of the 1-cycles (i.e. 1D loop) at the moment of their creation, for information. The pink plain and dashed circles indicate all nodes of the DMC that are concerned with the creation or destruction of a cycle at a given step. Finally, all the identified persistence pairs are represented in the top right-hand panel, in blue or red, depending on their type. A detailed description of the computation of the persistence pairs and k-cycles as shown in this figure is given in the main text (see the second half of Section 6.1).

simplexes that create or destroy each cycle $[\sigma_k, \sigma_{k-1}]$. Basically, the function CycleSearch(σ_k) is called once every time a negative critical simplex σ_k enters the filtration. Internally, the function uses a variable *CurSet*, of special type '$\mathbb{Z}_2$-Set', to store a temporary list of critical (k − 1)-simplexes considered at a given time. The type '$\mathbb{Z}_2$-Set' implements the k-chain group addition of Definition B.1 or, in other words, it behaves like a regular 'Set-type' structure that stores sets of elements, but contrary to a normal 'set', adding an element already contained in the $\mathbb{Z}_2$-Set results in its actual removal.[11]

We show in Fig. 10 the aforementioned practical example of persistence pairs and corresponding k-cycles computation over a

[11] Hence the name, as each element behaves as if it was counted modulo 2, with coefficients in $\mathbb{Z}_2$.

simple Morse–Smale complex. The upper left-hand panel shows a DMC computed from a high-resolution triangulation of the underlying density field ρ (note that only the smooth function is represented, not the simplicial complex). As mentioned earlier, only the structure of the Morse–Smale complex is necessary to identify the cycles, so in these figures, we represented in the background the sublevel sets of the density field ρ instead of steps in the filtration $\rho_{\rm D}$ to show how cycles are created and destroyed. We could identically have shown subsets of a simplicial complex and actually, at this stage, we could equally say that the coloured discs represent minima/critical points/maxima of the smooth field ρ or critical vertices/segments/triangles (i.e. 0/1/2-simplexes) of the discrete Morse function $\rho_{\rm D}$.

A selection of 12 steps corresponding to the entrance in the ascending filtration of 12 of the 21 critical simplexes are represented in the panels in the bottom part. The entrance of the first eight critical simplexes (blue discs) is not represented and the first-displayed step, step 9, corresponds to the entrance of the rightmost critical 1-simplex (green disc). Note, however, that before step 9, the critical vertices (i.e. minima) from 1 to 7 already entered creating each one component in the filtration, and critical segment 8 that also entered, destroying the 0-cycle created by critical vertex 7 which was merged with that of vertex 2 (this destruction is still represented at step 9 by the pink and red lines though). Considering critical segment $\sigma_1 = 9$, we first retrieve its two neighbouring critical 0-simplexes, labelled 4 and 3, and we therefore have $\mathit{CurSet} = \{3, 4\}$. We first consider the highest, $\sigma_0^{\rm cur} = 4$, and check if there is a cycle associated to it in $\mathit{cycles}[\sigma_0^{\rm cur}]$. As this is not the case, it means that we have found the cycle of σ_1 and therefore set $\mathit{cycles}[\sigma_1] = \mathit{cycles}[\sigma_0^{\rm cur}] = \mathit{CurSet} = \{3, 4\}$ and insert the pair $[\sigma_1, \sigma_0^{\rm cur}] = [9, 4]$. In panel 09 , all the critical simplexes involved in the cycle are circled in pink, the pink arc connects the critical simplexes in the identified pair and the red line represents the cycle. For instance, in that case, we identified that critical segment 9 destroys the component (0-cycle) created by critical vertex 4, which results in the components created by critical vertices 3 and 4 merging into each other (see the sublevel sets in the background).

Step 10 is very similar to step 9, with critical segment $\sigma_1 = 10$ entering, and we therefore add the persistence pair [10, 6] to *ppairs* and set $\mathit{cycles}[\sigma_1] = \mathit{cycles}[\sigma_0^{\rm cur} = 6] = \{6, 2\}$. Step 11 is skipped as it corresponds to the entrance of a positive critical vertex (i.e. the creation of a new component), but step 12 is more interesting. Critical segment 12 is negative and we therefore start the algorithm as previously by setting $\mathit{CurSet} = \{7, 1\}$, its neighbour critical vertex on the DMC. The highest critical vertex in *CurSet* is $\sigma_0^{\rm cur} = 7$, which was already paired at step 8 (represented in panel 09). We therefore add the cycle associated to it, $\mathit{cycles}[\sigma_0^{\rm cur} = 7] = \{2, 7\}$, to *CurSet*, which gives $\mathit{CurSet} = \{7, 1\} + \{2, 7\} = \{1, 2\}$, as the addition is performed modulo 2 (*CurSet* is of type $\mathbb{Z}_2$-Set). The new highest critical vertex in *CurSet* is therefore $\sigma_0^{\rm cur} = 2$, which is not paired yet. We therefore add the new pair [12, 2] to *ppairs* and set $\mathit{cycles}[\sigma_1 = 12] = \mathit{cycles}[\sigma_0^{\rm cur} = 2] = \mathit{CurSet} = \{1, 2\}$, which basically means that when critical segment 8 enters, the component created by vertex 2 merges into that of vertex 1. Steps 13 and 14 correspond to simple pairings (similar to step 9), and step 15 is similar to step 12, as critical vertex 4 is already paired, resulting in variables *ppairs* and *cycles* being updated according to panels 13–15.

The critical segment entering at step 16 is different though, as it creates a 1-cycle (symbolized by the red-dashed lines in panel 16). Indeed, its neighbours' critical vertices on the DMC are 3 and 5, which already belong to the same component at step 16 (as can be seen on the underlying sublevel set or on the DMC, by observing that the path [5, 13, 2, 8, 7, 12, 1, 15, 4, 9, 3] only has critical simplexes with values below 16). As this critical segment is therefore positive, we skip it for now, but we will see later how its cycle will be identified when it gets destroyed by a critical 2-simplex. The following steps 17 and 18 are similar, and the corresponding critical segments are skipped.

The first negative critical 2-simplex enters at step 19. Following Algorithm 2, we start with $\mathit{CurSet} = \{8, 12, 18, 13\}$, the four critical segment neighbours of critical triangle 19 on the DMC. The highest-valued critical vertex in *CurSet* is $\sigma_1^{\rm cur} = 18$, which is not yet paired, and we therefore add pair [19, 18] to *ppairs* and set $\mathit{cycles}[\sigma_2 = 19] = \mathit{cycles}[\sigma_1^{\rm cur} = 18] = \{8, 12, 18, 13\}$, represented by the red loop in panel 19 (see also the red-dashed loop in panel 18, when the cycle was created). This means that critical segment 18 created a new 1-cycle that was destroyed by critical triangle 19 and this cycle is represented by the closed path formed by critical segments {8, 12, 18, 13}, which are linked to each other through their neighbour critical vertices in the DMC, 1, 7, 2 and 5 (the 1-cycle is given by the sequence [18, 5, 13, 2, 8, 7, 12, 1, 18], which can be easily retrieved at query time from the information in *ccyles*). Critical triangle 20 also destroys a 1-cycle. The process is similar to the previous step and variables are updated accordingly. We finally proceed to step 21, where the last critical simplex enters. It is also negative (as all critical triangles are anyway) and we start with $\mathit{CurSet} = \{9, 15, 16, 18\}$. The highest critical segment is $\sigma_1^{\rm cur} = 18$, which is already paired to critical triangle 19, and its cycles are therefore added modulo 2 to *CurSet*, giving $\mathit{CurSet} = \{9, 15, 16, 18\} + \mathit{cycles}[\sigma_1^{\rm cur} = 18] = \{9, 15, 16, 18\} + \{8, 12, 18, 13\} = \{9, 15, 16, 8, 12, 13\}$. As critical segment 16, the highest in *CurSet*, is free, this means we are done with identifying the last cycle. We therefore update variables *ppairs* and *cycles* accordingly and the algorithm terminates.

The upper right-hand panel shows all of the persistence pairs over the DMC and one can convince himself/herself of the correctness of the cycles retrieved at steps 19–21 by comparing them to what they actually looked like in the sublevel sets when they were created, at steps 16–18 (see the dashed red cycles and newly created closed loops in the white isocontours in the background). Although we do not show examples here, the method is strictly similar in higher dimensions.

6.2 Simplification

The relative importance of topological features can be reliably assessed using the persistence theory and it was briefly shown in Section 4 how it is possible in the 1D case to locally modify a smooth function in order to cancel a low-persistence pair of critical points without affecting other critical points. Although it would also seem a viable option to directly modify ρ in order to cancel non-persistent pairs in the higher dimensions, this may not be the best thing to do. From a purely technical point of view, for large data sets, the computational cost of actually modifying ρ and recomputing the Morse–Smale complex every time would be excessive. From a theoretical point of view, one would need to arbitrarily define a more or less natural way to smoothly transform ρ so that the cancelling pairs would disappear without affecting the remaining critical points. Fortunately, such a transformation does not need to be explicitly conducted and it is enough to know that it exists and how it affects the Morse–Smale complex.

As a simple example, an arbitrary modification[12] of the smooth density field of Fig. 10 that cancels the low-persistence pair [18, 19 is presented in the top panels of Fig. 11. As expected, this modification of ρ leads to the removal of the saddle point and maximum, and a particular reorganization of the arcs in the Morse Complex. Before cancellation, saddle point 18 was linked to two minima (1 and 5) and two maxima (19 and 21). With its removal, the arcs emanating from the minima get rerouted to maximum 21 (as maximum 19 is also cancelled in the operation) and they are therefore not critical anymore: they are removed from the Morse complex. The situation is different for saddle points 8, 12 and 13 though, which were linked to maximum 19. During the cancellation, the gradient of ρ is reversed between the cancelled points (see the lower panels) and the arcs that led to maximum 19 are therefore free to continue their ascension up to the former position of the cancelled saddle point, and further along the arc [18, 21], to finally reach maximum 21. Those field lines still link saddle points to maxima, are critical and therefore belong to the new modified Morse complex.

The field line reorganization scheme during a cancellation can be intuitively understood in the general case by defining a similar minimalistic transformation of a discrete Morse function and its discrete gradient. Basically, the essential feature lies in the reversal of the gradient path between the cancelled critical points. Such an operation can easily be defined over a discrete gradient (Forman 2002). The corresponding modification is shown in the bottom panel of Fig. 11, in the case of a discrete Morse function similar to ρ and defined over a tessellation: by reversing the path of discrete gradient arrows between the critical points (purple shade), the two critical points are effectively removed, while the rest of the discrete gradient is left unmodified, and it is easy to predict the consequences of this modification on the discrete Morse complex. Let us call σ_k and σ_{k+1}, the critical k and $(\mathrm{k}+1)$-simplexes to cancel, and α^i_{k+1} and β^j_k, the critical $k+1$ and k-simplexes, respectively, linked to σ_k and σ_{k+1} by an arc in the DMC. By reversing the gradient path between σ_k and σ_{k+1}, one also reroutes all the arcs and manifolds that previously reached one of those critical simplexes. After cancellation, an ascending arc emanating from β^j_k still reaches the formerly critical simplex σ_{k+1}, and it can be extended through the reversed path, and continues to follow any previously ascending arc emanating from σ_k, leading to a critical $(\mathrm{k}+1)$-simplex α^i_{k+1}. Similarly, any descending $(\mathrm{k}+1)$-manifold of α^i_{k+1} now reaches σ_{k+1} and can therefore be extended by the descending $(\mathrm{k}+1)$-manifold of σ_{k+1}. For the same reason, the ascending $(d-k)$-manifolds of β^j_k can be extended by the ascending $(d-k)$ manifolds of σ_{k+1}. One therefore does not need to actually perform any gradient path reversal and the cancellation of the critical pair $[\sigma_k, \sigma_{k+1}]$ is achieved directly on the DMC using the following procedure:

(i) Let α^i_{k+1} and β^j_k be the N_α and N_β critical $k+1$ and k critical simplexes sharing an arc in the DMC with σ_k and σ_{k+1}, respectively.

(ii) Create a new arc between each of the N_α, N_β pair $[\alpha^i_{k+1}, \beta^j_k]$ by joining arcs $[\alpha^i_{k+1}, \sigma_k]$, $[\sigma_k, \sigma_{k+1}]$ and $[\sigma_{k+1}, \beta^j_k]$. The path $[\sigma_k, \sigma_{k+1}]$ must be reversed during the operation.

(iii) Extend the descending manifold of each α^i_{k+1} with the descending manifold of σ_{k+1}.

[12] Note that achieving the modification shown in this example was actually made easy by the fact that the function itself is analytically defined as a sum of Gaussian functions; it would have been much more challenging in the general case.

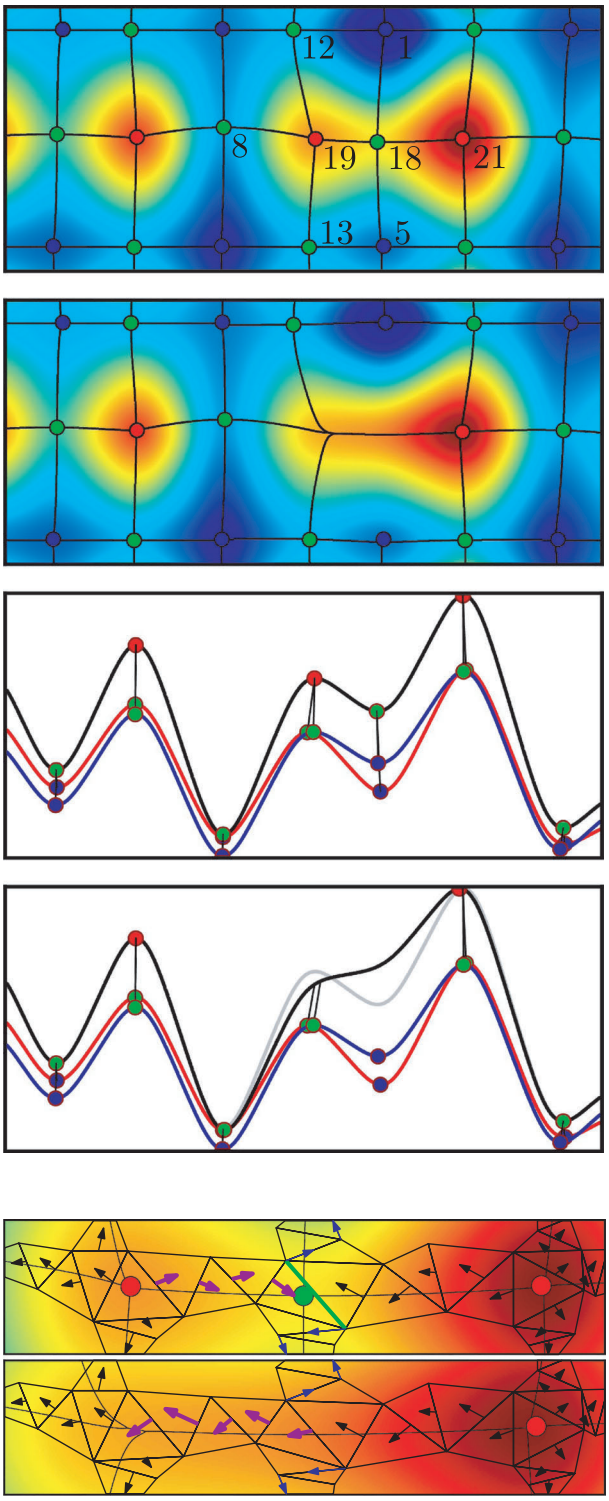

Figure 11. Topological simplification of a maximum and saddle point persistence pair in the smooth 2D field ρ of Fig. 10. In the upper part, from the top to bottom, the four panels display the Morse complex before and after simplification, and the corresponding density profiles along the three horizontal axes of the Morse complex (red, black and blue for the upper, middle and lower axes, respectively). The density profile before simplification is represented in grey. The lowest panel shows an equivalent cancellation of critical pairs in a discrete Morse complex by the discrete gradient reversal. Note that non-essential gradient pairs and simplexes have been omitted for clarity, as they are not affected by the path reversal.

(iv) Extend the ascending manifold of each β_k^j with the ascending manifold of σ_k.

(v) Delete the critical simplexes σ_k and σ_{k+1}, together with their four ascending and descending manifolds and all of the arcs leading to or emanating from them.

It is important to remark that, in general, the simplification of a pair may lead to an increase in the total number of arcs in the complex. This is particularly true when none of the cancelling simplex is a 1-saddle or a $D-1$-saddle, as in that case, the number of arcs is not bounded. Moreover, there exist two specific cases where a cancellation is impossible. The first is when critical simplexes do not share an arc in the DMC. The second is when they share more than one arc, as in that case, the gradient path reversal would lead to the creation of a looping path in the discrete gradient, which is forbidden (see Section 3). The detailed procedure to deal with this is explained in Section 7.

6.3 Filtering Poisson noise

As mentioned previously, mainly because of the Poisson noise, it is not possible to use the raw DMC to identify structures in the cosmic web. In fact, most of the critical points, arcs and manifolds are actually spurious artefacts created by the sampling noise. This is especially true in the present case, where we wish to use the DTFE density and a simplicial complex computed from the Delaunay tessellation of a discrete realization. As a matter of fact, the scale-free nature of the DTFE makes it locally very sensitive to the Poisson noise, as information is always locally extracted at the sample resolution limit. Our approach to remedy this problem consists in computing a significance level for each persistence pair and cancelling the persistence pairs whose significance is below a given threshold.

Let r be the persistence ratio of a persistence pair $q_k = [\sigma_k \sigma_{k+1}]$, then

$$r\left(q_k\right) = \rho_{\mathrm{D}}\left(\sigma_{k+1}\right) / \rho_{\mathrm{D}}\left(\sigma_k\right). \tag{3}$$

We note $P_k\left(r_0\right)$ is the cumulative probability that a persistence pair of critical simplexes of orders k and $k+1$ and with the persistence ratio $r \geq r_0$ exists in the Delaunay tessellation of a random discrete Poisson distribution. It is then convenient to denote the relative importance of a given critical pair q_k in terms of its significance, $S\left(q_k\right)$, expressed in units of 'σ' with an analogy to the Gaussian case:

$$S\left(q_k\right) = S_k\left(r\left(q_k\right)\right) = \mathrm{Erf}^{-1}\left(\frac{P_k\left(r\left(q_k\right)\right)+1}{2}\right), \tag{4}$$

where Erf is the error function. As a purely analytical derivation of $P_k\left(r\right)$ seems clearly out of reach, we use the Monte Carlo simulation to estimate it, measuring $P_k\left(r_0\right)$ as the fraction of persistence pairs of order k with the persistence ratio $r \geq r_0$ in a Poisson sample. The results are shown in Fig. 12. In that figure, the values of $P_k\left(r\right)$ are plotted as a function of r in green, blue and red for $k = 0$, 1 and 2, respectively, and the horizontal dashed lines represent different significance levels in units of 'σ', ranging from $S = 1\sigma$ (top panel) to $S = 5\sigma$ (bottom panel). From these results, the following fits can be extracted in the 3D case (represented as the black-dashed lines in Fig. 12):

$$\begin{aligned} P_0(r) &= \exp[-\alpha_0(r-1) - \alpha_1(r-1)^{\alpha_2}] \\ &\text{with}\, \alpha \approx [3.694, 0.441, 2.538], \end{aligned} \tag{5}$$

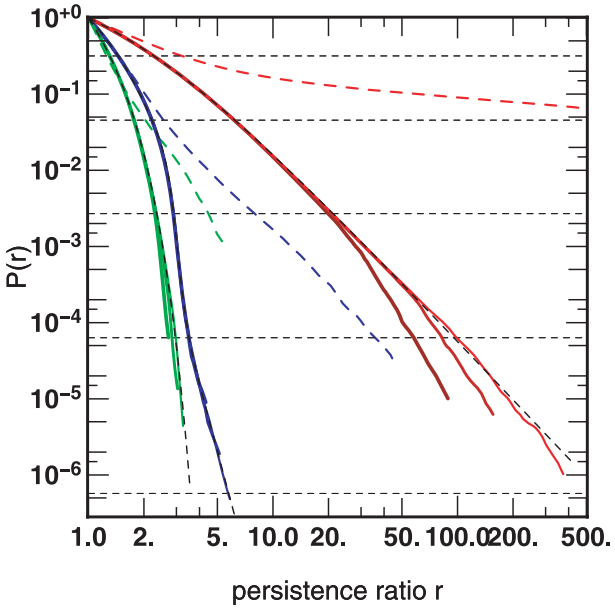

Figure 12. The cumulative probability $P_k\left(r\right)$ that a persistence pair of order k with the persistence ratio greater or equal to r exists in a 3D scale-free Gaussian random field (coloured plain curves) and in a 50 h^{-1} Mpc dark matter cosmological simulation (coloured dashed curves). The red, blue and green curves correspond to maxima–1-saddle, 1-saddle–2-saddle and 2-saddle–minima pairs, respectively. The different shades, from darker to lighter, correspond to 64^3-, 128^3- and 192^3-particle realizations, respectively. The black-dashed curves show fits to the Gaussian case, as presented in the main text, while the horizontal dashed lines correspond to different significance levels in units of 'σ', ranging from $S = 1\sigma$ (top panel) to $S = 5\sigma$ (bottom panel).

$$\begin{aligned} P_1\left(r\right) &= f_1(1-t) + f_2 t \\ &\text{with}\, f_1 = \exp\left[-\beta_0\left(r-1\right)\right], \quad f_2 = \beta_1 r^{-\beta_2}, \\ &t = (1+\beta_3/u^{\beta_4})^{-1}, \\ &\beta \approx [2.554, 4.000, 9.000, 1.785, 14.000], \end{aligned} \tag{6}$$

$$\begin{aligned} P_2\left(r\right) &= [1+\gamma_0\left(r-1\right)]^{-\gamma_1} \\ &\text{with}\, \gamma \approx [0.449, 2.563], \end{aligned} \tag{7}$$

and in the 2D case we obtain

$$\begin{aligned} S_0^{\mathrm{2D}}\left(r\right) &= \exp\left[-\alpha_0\left(r-1\right) - \alpha_1\left(r-1\right)^{\alpha_2}\right] \\ &\text{with}\, \alpha \approx [2.00, 0.01, 3.50], \end{aligned} \tag{8}$$

$$\begin{aligned} S_1^{\mathrm{2D}}\left(r\right) &= (r-1)^{-\beta_0\left[1+\beta_1 \log(r-1)\right]} \\ &\text{with}\, \beta \approx [0.75, 0.20]. \end{aligned} \tag{9}$$

A relatively similar approach was undertaken in a code named ZOBOV (Neyrinck 2008) to measure the significance of cosmological voids. The approach developed in this paper nevertheless differs from ours in that it is limited to voids and that they do not use persistence pairs. Instead, they pair minima of the density field to the lowest 1-saddle point on the surface of their ascending 3-manifolds (i.e. the voids themselves) that is not already paired to another minimum with higher density. This explains why our fit of $P_0\left(r\right)$ differs from theirs.

The fact that the expression of the fits for $k = 0$ and 2 is relatively simple compared to the one for $k = 1$ may seem intriguing

at first sight. However, if the fit for function $P_1(r)$ actually requires more coefficients, then it is mainly because it undergoes some sort of transition around $r = 4$, which roughly corresponds to a significance level of 3.5σ. We believe that this only reflects the nature of the DTFE itself, whose probability distribution function is clearly biased towards high densities as the number of minima is limited by the comparatively larger volume of the Voronoi cells they occupy (see Schaap & van de Weygaert 2000; van de Weygaert & Schaap 2009). The size of our Monte Carlo sample being limited results in an increase in the number of $k = 1$ type pairs when fewer and fewer comparatively lower density minima become available to form pairs. We also note that this tendency is present in the cumulative probabilities of the persistence pair ratio measured in cosmological simulations as well (coloured dashed curves). Nevertheless, those probabilities are significantly higher than that in the Poisson sample for any value of k and it therefore seems that it should be reasonably easy to filter spurious persistence pairs without affecting too much those storing precious information on the cosmic web topology.

6.4 Illustration in 2D

Fig. 13 shows the DMC of a 2D discrete distribution of ∼350 000 particles with periodic boundary conditions computed at different levels of significance. The discrete distribution (upper left-hand panel) was obtained by projecting a subsampled $10\,h^{-1}$ Mpc slice of a $50\,h^{-1}$ Mpc large dark matter N-body simulation at redshift $z = 0$. The resulting Delaunay tessellation, composed of ∼1000 000 1-facets and 670 000 2-facets, and the corresponding DTFE density field are shown in the upper middle and upper right-hand panels. Note that identifying the filamentary structure in such a distribution is particularly challenging because of its very high dynamic range and also because many filaments simply disappear into low-density regions as they leave the slice in the original 3D distribution. The filamentary structure captured by the DMC is depicted in red in the middle and bottom rows through the representation of its ascending 1-manifolds, after cancellation of the persistence pairs at a significance level of 0σ (left-hand panel, no simplification), 2σ (middle panel) and 4σ (right-hand panel). The middle left-hand panel nicely illustrates the strong influence of the Poisson noise, as without simplification, filaments are basically detected almost everywhere in the distribution. This is particularly obvious when zooming in what was a dark matter halo in the former 3D distribution: whereas one can identify by eye a few obvious filaments connecting to the central clump, the algorithm (correctly) detects a swarm of local peaks and filaments locally created by random fluctuations in the distribution.

It is quite striking though how much applying the above-described persistence-based simplification procedure succeeds at selecting what one would intuitively define as a filament. Already, at a 2σ level (middle panels of the middle and bottom rows), it is clear that the large-scale network of filaments is correctly identified as well as the valley resulting from the projected cosmic voids of the non-projected distribution (the ascending 2-manifolds associated to the minima, symbolized by the white discs). At a level of 2σ, the probability that a topological feature such as an arc in the DMC is the result of the Poisson noise is ∼5 per cent. At 4σ, this probability goes down to ∼0.006 per cent and any arc in the DMC can therefore safely be considered a feature of the underlying distribution. The lower right-hand panel shows the arcs of the DMC that link maxima (purple crosses) and saddle points (green triangles) at a significance level of 4σ around the projection of a large dark matter halo. At that level, the intricate initial network is reduced to a very neat set of filaments branching on a central clump. Note that while the network itself is simplified, the resolution is preserved, which, for instance, allows for the correct identification of the merger of two relatively noisy filaments in the top right-hand corner while preserving a very clean network on large scale (middle right-hand panel).

The application to the 3D distribution and in particular galaxy catalogues and large-scale N-body simulations is presented in the companion paper, Paper II.

7 BOUNDARY CONDITIONS AND TECHNICALITIES

7.1 Boundary conditions

Whereas boundary conditions are not a concern in the Morse theory, as it is defined over infinite or borderless spaces, things are clearly different when one tries to apply it to real data sets. The easiest case corresponds to periodic boundary condition data, such as those encountered in the N-body simulation of the matter distribution on large scales in the Universe. Because it is impossible to simulate the whole Universe and the gravity has an infinite outreach, periodic boundary conditions are often used as a trick to obtain a smooth gravitational potential and emulate the isotropy of space within a restricted volume usually shaped as a box. Enforcing periodic boundary conditions over a cube basically amounts to assimilating opposite faces, any object leaving the cube through one face immediately enters the opposite one. Mathematically speaking, such a space is called a torus $\mathbb{T}^d$, where d is the number of dimensions, and the Morse theory readily applies to such spaces. From a practical point of view, we use the periodic exact 3D periodic boundary conditions Delaunay tessellation (Caroli & Teillaud 2010) implemented in CGAL[13] when the distribution is 3D. We also implemented our own periodic boundary conditions within CGAL for the $d \neq 3$ case using a simpler, though less-rigorous and optimized, technique. This method basically consists in building a larger distribution by replicating a fraction of the box to extend each boundary, computing the Delaunay tessellation over this extended domain and then identifying the identical k-facets crossing the opposite faces of the initial box (the Delaunay tessellation of Fig. 13 was obtained using such method).

Of course, periodic boundary conditions only apply to periodic data sets, which is usually not the case for observational data, and one therefore needs to treat the boundaries of the distribution with special care. The simplest way to do so consists in transforming the definition domain of the data set into a boundaryless domain, a procedure called compactification. Usual compactification techniques consist in transforming the definition domain into a sphere by adding a point at infinity and attaching it to each boundary cell of the Delaunay tessellation or transforming it into a torus, practically making it periodic by replicating a mirror image of the distribution through its boundaries. Both of these methods have pros and cons. Whereas sphere compactification is easy to build, whatever be the geometry of the initial data set, it tends to pollute measurements around the boundaries by affecting the discrete gradient computation, therefore creating numerous fake manifolds and arcs that have to be ignored. This is not the case with the torus compactification, which creates relatively smooth conditions close to the boundaries, but it may only be easily implemented on cubic boxes and requires

[13] CGAL is the c++ Computational Geometry Algorithm Library, see http://www.cgal.org

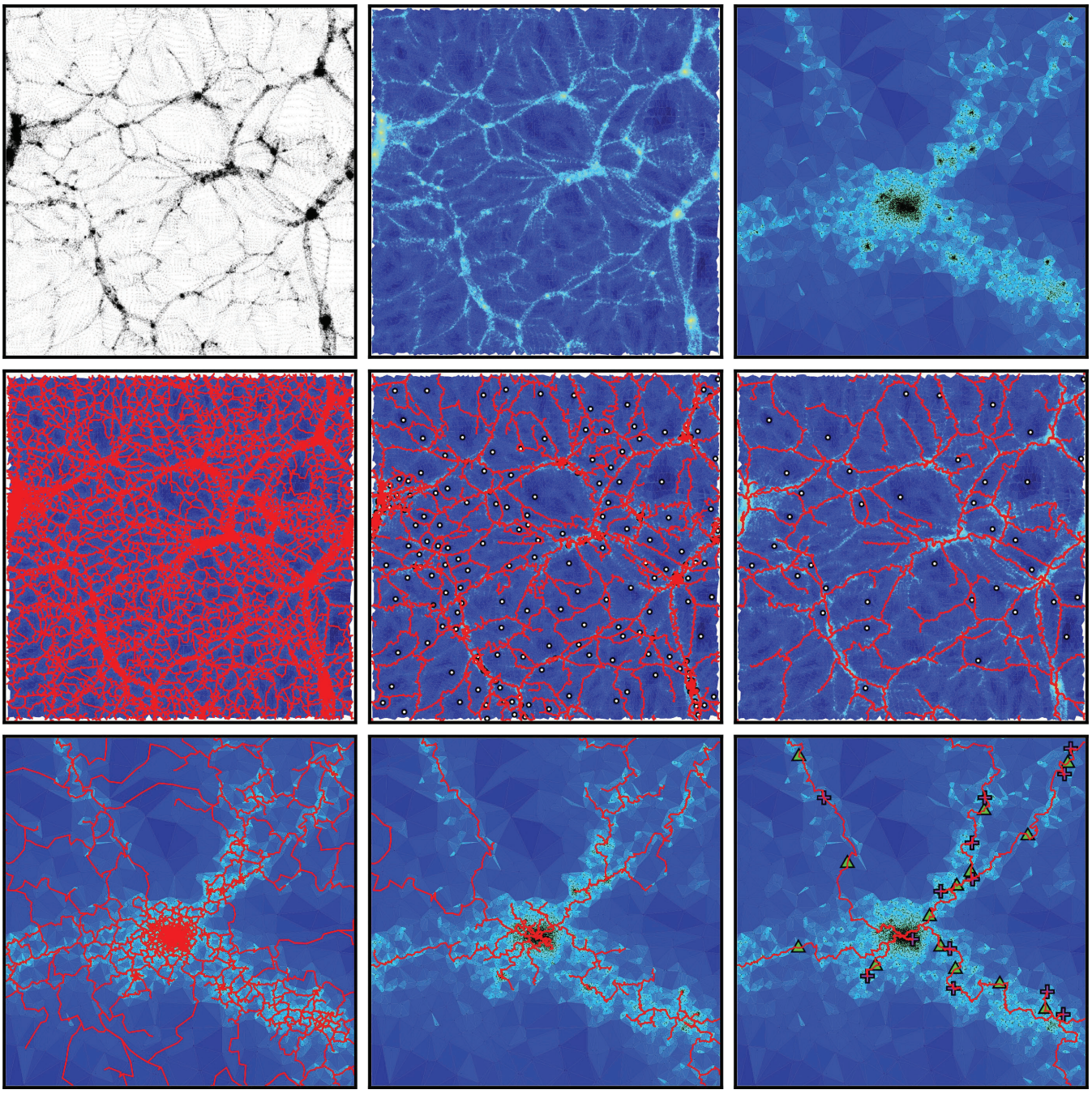

Figure 13. The filaments measured in a 2D distribution obtained by projecting the particles from a slice of an N-body cosmological simulation. The initial discrete distribution, its Delaunay tessellation and a zoom in a halo (from the upper middle part of the distribution) are displayed in the top row, with colours corresponding to the DTFE density. The filamentary structure is traced in red in the middle row, as the geometry of the arcs remaining after cancellation of persistence pairs with the significance less than 0σ (middle left-hand panel), 2σ (middle) and 4σ (middle right-hand panel). A zoom around a projected halo is shown on the bottom row. The white discs, green triangles and purple crosses stand for the minima, saddle points and maxima, respectively. (Note that they are only represented on some panels for clarity.)

replicating the data set a large number of times (27 times in 3D), significantly increasing the necessary computational time and resources accordingly.

Our implementation of the boundary conditions is a hybrid between the sphere and torus compactification that tries to preserve the advantages of both while getting rid of their limitations. The idea is that the torus compactification is efficient because of the relatively natural extrapolation of the density field it allows, which, as a result, does not affect the computation of the discrete gradient at a large distance from the boundary. We therefore allow the user to choose what fraction of the distribution should be mirrored on each boundary (a value around $10 \sim 15$ per cent of the initial distribution size seems to work fine) and then apply a sphere compactification on the new distribution by adding a point at infinity, with minus infinite density, that forms simplexes with the new boundary of the enlarged distribution. We then proceed with tagging as 'boundary'

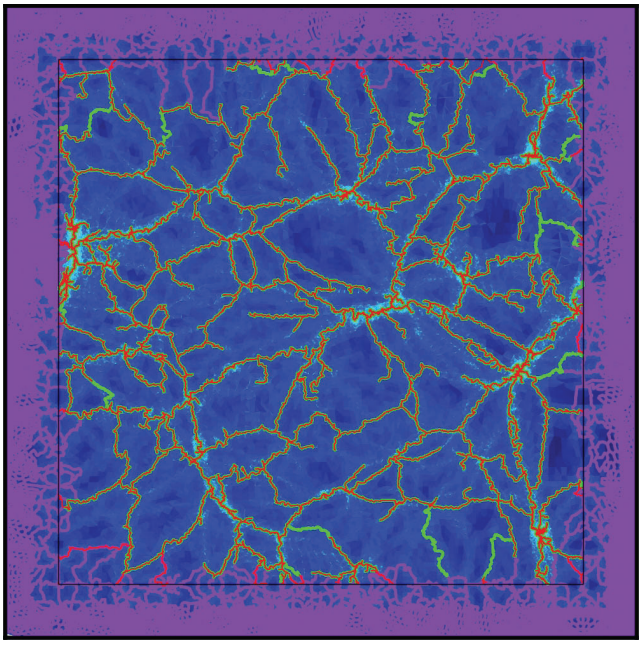

Figure 14. Illustration of the computation of the DMC with non-periodic boundary conditions. The boundary of the initial 2D distribution is delimited by the thin black square and any particle in the distribution within a distance of 10 per cent the initial domain size is mirrored (see also Fig. 13). The thick green and purple network shows the 3σ filaments measured in the non-periodic distribution, the purple part being discarded after topological simplification as belonging to the boundary. The filaments obtained in the periodic boundary situation are displayed in red for comparison.

any k-simplex of the Delaunay tessellation that contains a replicated vertex, the infinite vertex or whose DTFE density may have been affected by the distribution outside the definition domain. This last condition in fact prevents the boundary simplexes, whose DTFE density may be wrong, to affect the resulting DMC and we determine which simplexes may be affected by checking whether the circumsphere of each highest-dimensional d-simplex intersects the boundary, in which case it is, with all its facets and vertices, tagged as 'boundary'.

Note that one has to pay particular attention to the boundaries during the topological simplification process as the persistence of critical pairs formed with a boundary simplex has spurious persistence ratios. The point at infinity is special; it has a minus infinite density and is allowed to form persistence pairs with as many vertices as necessary, any of those persistence pairs having infinite persistence. The persistence pairs formed between the non-infinite boundary simplexes and those within the valid part of the distribution are treated normally during the simplification process, but the topological features they form are nevertheless spurious and any persistence pair with at least one critical simplex on the boundary is therefore deleted[14] after topological simplification. The whole process is illustrated in Fig. 14 in the 2D case, using the same distribution as that of Fig. 13. In that figure, the filamentary structure detected at 3σ is represented for the same distribution as when it is considered periodic (thin red network) and non-periodic (thick green network), and it is clear that both mostly agree. One can see none the less that, as should be expected, the small portions of the (red) periodic network crossing the boundaries cannot be detected in the non-periodic case and that a few portions of (green) filaments lying slightly farther away are detected only in the non-periodic case. This results from the fact that persistence pairs of distant critical simplexes may be different in the non-periodic distribution, because the k-cycles coupling them are not allowed to cross the boundaries. As a result, the persistence ratios of certain critical points may differ in both cases and they may therefore still exist at the 3σ level in the non-periodic case, while they were cancelled at the 2.5σ level in the periodic one.

[14] We really mean *deleted* in that case and not cancelled as a regular pair would be.

7.2 Smoothing the manifolds

Because the scale resolution of practical samples is always limited, so is the resolution of the ascending and descending manifolds of the DMC. When identifying the filaments, voids or walls in cosmological distributions, their precise shape therefore becomes arbitrary at scales lower than the initial sampling resolution. Within our implementation, the DMC features are subsets of the initial Delaunay tessellation or of its dual Voronoi tessellation and the identified structures therefore naturally tend to adapt to the measured sample much better than they would if one was using a regular sampling grid, for instance. The DMC is nevertheless always computed at the sampling resolution limit and its geometry is mainly dictated by the Poisson noise on that scale. It may therefore be desirable to have a way to enforce some continuity and differentiability even at the cost of the loss in resolution (e.g. for representation purposes). The smoothing method that we use is pretty much the same as that presented in Sousbie et al. (2009) as it presents the advantages of being simple, robust and fast. The idea involves smoothing the filaments individually by fixing the critical points and averaging the position of each non-fixed segment's endpoint with the position of its closest neighbouring endpoints a given number of times. Within our implementation, a filament is defined as a sequence of N linked vertices, the vertices corresponding to the centre of mass of simplexes in the Delaunay tessellation. Let x^i_j be the jth coordinate of the ith vertex. Then, after smoothing, its new coordinates, y^i_j, are computed as

$$y^i_k = A^{ij} x^j_k, \tag{10}$$

with

$$A^{ij} = \begin{cases} 3/4 & \text{if} \quad i = j = 0 \quad \text{or} \quad i = j = N, \\ 1/2 & \text{if} \quad i = j, \\ 1/4 & \text{if} \quad i = j + 1 \quad \text{or} \quad i = j - 1, \\ 0 & \text{elsewhere}, \end{cases} \tag{11}$$

where equation (10) is applied s times in order to smooth over s simplexes in the simplicial complex. The corresponding smoothing length is naturally adaptive and such a smoothing ensures the continuity of the filaments' location over s Delaunay simplexes. Note that it is very easy to adapt this method to the ascending and descending manifolds of the DMC (i.e. the voids, walls, etc.) as any of them is defined as a simplicial complex within our implementation. The position of each vertex in a manifold can therefore similarly be averaged with that of its neighbours s times to obtain sufficient smoothness.

7.3 Essential implementation issues

Finally, we close this section by presenting two technical issues that are essential for the practical implementation of the algorithm.

7.3.1 Cancellation order

When cancelling persistence pairs, the order in which the pairs are cancelled has a crucial importance, both in terms of computational time and in terms of memory consumption. This is especially true in 3D. In fact, where the number of arcs linking a given 1-saddle (2-saddle) and a maximum (minimum) is always 2, there is no bound on the number of arcs between two saddle points of different types. Following the arc redirection algorithm described in Section 6.2, the cancellation of two saddle points of different types may therefore lead to a dramatic increase in the total number of arcs in the complex. Let P and Q be the 1-saddle and 2-saddle, respectively. Then P is linked to $P_\uparrow$ = 2-maxima and $P_\downarrow$ = 2-saddles, while Q is linked to $Q_\uparrow$ = 1-saddles and $Q_\downarrow$ = 2-minima. The cancellation therefore creates $N_\mathrm{c} = (P_\downarrow - 1)(Q_\uparrow - 1)$ arcs and destroys $N_\mathrm{d} = 2 + 2 + P_\downarrow + Q_\uparrow - 1$ arcs, and the number of additional arcs after cancellation is $N = N_\mathrm{c} - N_\mathrm{d} \propto P_\downarrow\, Q_\uparrow$ for large values of $P_\downarrow$ and $Q_\uparrow$. This means that the number of arcs in the complex may temporarily increase quadratically and it is not uncommon to obtain saddle points with hundreds of thousands of arcs at a given moment.[15] Within our implementation, we therefore always cancel the pair $\{P, Q\}$, with P the critical point of highest type, that minimize the number N of created arcs first, with $N = N_\mathrm{c} - N_\mathrm{d} = (P_\downarrow - 1)(Q_\uparrow - 1) - P_\downarrow - P_\uparrow - Q_\downarrow - Q_\uparrow + 1$.

7.3.2 Impossible cancellations

There exist special configurations where two critical points are linked by two or more different arcs (think, for instance, of the circular crest around the crater of a volcano). Those particular configurations cannot be cancelled, as applying a discrete gradient reversal (see Section 6.2) would result in the formation a V-path (i.e. discrete integral line) that loops on to itself; this is impossible as a V-path is a strictly decreasing alternating sequence of k-simplexes (see Definition 3.7). This is not a problem though for the cancellation of the maximum–1-saddle and minimum–2-saddle persistence pairs, as such persistence pairs cannot be formed if the critical points are linked by more than one arc [taking the example of the volcano, the highest point on its crest is a maximum, which is always positive (creating) and this is also the case with the lowest point on the crest which is a positive saddle point, as it creates the ring formed by the crest around the volcano]. Yet the 3D case of a 1-saddle–2-saddle persistence pair is different, as nothing prevents such configurations to occur. In practice, such configurations do not arise naturally and we noted that using the order for cancelling pairs defined previously drastically reduces the number of occurrences of such non-cancellable configurations (of order $\sim$10 for a 128^3-particle simulation cut at 4σ). For those few remaining pairs, we offer the possibility in our implementation to skip them or force their removal after keeping only one of the arcs between the critical points within the persistence pair. This last option is the preferred one and although it seems difficult to justify from a theoretical point of view, the fact that the occurrence of non-cancellable pairs depends on the precise cancellation order suggests that it is acceptable to do so (note that the consequences on the resulting Morse–Smale complex are quite minimal anyway).

[15] This does not mean that hundreds of thousands of arcs will be present in the simplified complex, as a single maximum–1-saddle or a minimum–2-saddle persistence pair may later cancel all those arcs leading to a dramatic decrease in the total number.

8 CONCLUSION

We presented a method that allows for the scale-free and parameter-free coherent identification of all types of 3D astrophysical structures in potentially sparse discretely sampled density fields, such as N-body simulations or observational galaxy catalogues. The method is based on the Morse theory (Section 2), *discrete* Morse theory (Section 3) and persistence theory (Section 4), and the implementation of the corresponding algorithm was detailed in Sections 5–7. In particular, our specific algorithm was designed with astrophysical applications in mind, as it directly applies to the Delaunay tessellation of point set samples,[16] and we paid a particular attention to the computation of the discrete Morse function so that it correctly represents the underlying DTFE density. From this discrete Morse function, DisPerSE basically computes the discrete Morse–Smale complex of the density function and uses it to identify structures: the ascending 3-, 2-, 1- and 0-manifolds of the theory being identified to the voids, walls, filaments and clusters, respectively. The implementation was designed so that each component of the cosmic web and its geometry can be easily identified and studied as individual objects or as a group of objects so that their relationship can be easily recovered: one can, for instance, identify the voids bordering a given wall or the clusters at the extremities of a given filament. Moreover, as the persistence criteria were recast in terms of the confidence level with respect to noise, it makes DisPerSE very easy to use, as it is the only parameter required to identify structures at optimal resolution. It shows a great deal of potential for astrophysical applications for the following reasons that distinguish it from traditional methods:

(i) It applies directly to discrete data sets via their Delaunay tessellation, which makes it scale free and allows the identified structures to always be defined down to the resolution limit of the sample.

(ii) It is based on the *discrete* Morse theory, which means that, as opposed to methods based on the *smooth* Morse theory, the mathematical formalism does apply rigorously to the type of data sets one usually has to deal with in astrophysics. This implies that the well-studied formalism of the Morse theory readily applies to the numerically identified structures (which is not the case with watershed-based methods, for instance, see Appendix A).

(iii) All the different types of structures are defined coherently: triangulated space can basically be divided into sets of volumes, surfaces, curves and points that correspond to voids, walls, filaments and clusters, respectively. Each structure is identified *individually* and the cosmic web can therefore be rigorously divided into individual filaments, each corresponding to a given saddle point.

(iv) It readily takes into account the sampling and Poisson noise via the persistence theory, allowing the user to define a detection confidence level in term of 'number of σ' and provides the corresponding simplification of the DMC. As shown in Paper II, this fact actually produces results obtained in highly sampled simulations and sparse galaxy catalogues which are qualitatively very similar, opening the way to a direct comparison of the properties of the cosmic web in simulations and observational catalogues.

(v) Because the foundation of the method is based on topology and uses the persistence theory, it also allows for a very robust computation of topological invariants such as Betti numbers or the Euler characteristics (see e.g. van de Weygaert et al. 2010); this is

[16] In fact, the algorithm can also be used directly over structured regular meshes and we implemented a version that works directly on a regular grid.

possible even in the presence of an important shot noise and without having to define any smoothing scale; it therefore takes into account the multiscale nature of the cosmic web (see Paper II).

Its application to 3D cosmic simulated and observed data sets is presented in the companion paper, Paper II. Let us emphasize, however, that even if there is a wide range of application in astrophysics already, the domain of the application of DisPerSE is undoubtedly wider.

ACKNOWLEDGMENTS

The author gratefully acknowledges support from Japan Society for the Promotion of Science (JSPS) Postdoctoral Fellowhip for Foreign Researchers Award P08324.

The author thanks the anonymous referee for his/her careful reading of this manuscript and very interesting comments which helped to improve its content.

The author thanks C. Pichon for a careful reading and commenting on the manuscript, H. Kawahara for his fruitful comments and Y. Suto for his constant help and support.

This work was made possible through an extensive usage of the YORICK programming language by D. Munro (available at http://yorick.sourceforge.net/) and also CGAL, the Computational Geometry Algorithms Library (http://www.cgal.org), which was used to compute the Delaunay tessellations.

REFERENCES

Abazajian K. N. et al., 2009, ApJS, 182, 543
Aragón-Calvo M. A., van de Weygaert R., Araya-Melo P. A., Platen E., Szalay A. S., 2010a, MNRAS, 404, L89
Aragón-Calvo M. A., Platen E., van de Weygaert R., Szalay A. S., 2010b, ApJ, 723, 364
Aragón-Calvo M. A., van de Weygaert R., Jones B. J. T., 2010c, MNRAS, 408, 2163
Aubert D., Pichon C., Colombi S., 2004, MNRAS, 352, 376
Bardeen J. M., Bond J. R., Kaiser N., Szalay A. S., 1986, ApJ, 304, 15
Bertschinger E., 1985, ApJS, 58, 1
Beucher S., Lantujoul C., 1979, in Proc. Int. Workshop on Image Processing: Real-Time Edge and Motion Detection/Estimation. CCETT/INSA/IRISA, IRISA Report 132, Rennes, p. 17
Bond J. R., Kofman L., Pogosyan D., 1996, Nat, 380, 603
Caroli M., Teillaud M., 2010, CGAL User and Reference Manual, 3.6 edn. CGAL Editorial Board. INRIA, Sophia Antipolis, Méditerranée
Cohen-Steiner D., Edelsbrunner H., Morozov D., 2006, Computational Geometry (SCG'06). ACM, New York, p. 119
Colberg J. M. et al., 2008, MNRAS, 387, 933
Colless M. et al., 2003, preprint (astro-ph/0306581)
de Lapparent V., Geller M. J., Huchra J. P., 1986, ApJ, 302, L1
Delfinado C. J. A., Edelsbrunner H., 1995, Comput.-Aided Geom. Des., 12, 771
Edelsbrunner H., Letscher D., Zomorodian A., 2000, in, 41st Ann. Symp. Foundations of Computer Science, Topological Persistence and Simplification. IEEE Comput. Soc. Press, Los Alamitos, CA, p. 454
Edelsbrunner H., Letscher D., Zomorodian A., 2002, Discrete Comput. Geom., 28, 511
Edelsbrunner H., Harer J., Natarajan V., Pascucci V., 2003, Proc. Nineteenth Ann. Symp. Comput. Geom. ACM, New York, p. 361
Edelsbrunner H., Harer J., Zomorodian A., 2003, Discrete Comput. Geom., 30, 87
Forero-Romero J. E., Hoffman Y., Gottlöber S., Klypin A., Yepes G., 2009, MNRAS, 396, 1815
Forman R., 1998a, Math. Z., 228, 629
Forman R., 1998b, Adv. Math., 134, 90
Forman R., 2002, Sém. Lothar. Combin., 48, Art. B48c, 35 pp. (electronic) 2, 7, 10, 13, 23
Gay C., Pichon C., Le Borgne D., Teyssier R., Sousbie T., Devriendt J., 2010, MNRAS, 404, 1801
Gottloeber S., 1998, in Mueller V., Gottloeber S., Muecket J. P., Wambsganss J., eds, Large Scale Structure: Tracks and Traces Galaxy Tracers in Cosmological N-Body Simulations. p. 43
Gyulassy A., 2008, PhD thesis, Univ. California, Berkeley
Hahn O., Porciani C., Carollo C. M., Dekel A., 2007, MNRAS, 375, 489
Hatcher A., 2002, Algebraic Topology. Cambridge Univ. Press, Cambridge
Hoffman Y., Shaham J., 1982, ApJ, 262, L23
Huchra J. P., Geller M. J., 1982, ApJ, 257, 423
Icke V., 1984, MNRAS, 206, 1P
Jost J., 2008, Riemannian Geometry and Geometric Analysis, 5th edn. Universitext, Springer-Verlag, Berlin
Kirshner R. P., Oemler A., Jr, Schechter P. L., Shectman S. A., 1981, ApJ, 248, L57
Lewiner T., 2002, Master's thesis, PUC-Rio, Rio de Janeiro
Milnor J., 1963, Morse Theory. Princeton Univ. Press, Princeton, NJ
Neyrinck M. C., 2008, MNRAS, 386, 2101
Neyrinck M. C., Gnedin N. Y., Hamilton A. J. S., 2005, MNRAS, 356, 1222
Novikov D., Colombi S., Doré O., 2006, MNRAS, 366, 1201
Okabe A., 2000, Spatial Tessellations: Concepts and Applications of Voronoi Diagrams. Wiley, Toronto
Platen E., van de Weygaert R., Jones B. J. T., 2007, MNRAS, 380, 551
Platen E., van de Weygaert R., Jones B. J. T., 2008, MNRAS, 387, 128
Pogosyan D., Bond J. R., Kofman L., Wadsley J., 1996, BAAS, 28, 1289
Pogosyan D., Pichon C., Gay C., Prunet S., Cardoso J. F., Sousbie T., Colombi S., 2009, MNRAS, 396, 635
Robins V., 2000, PhD thesis, Univ. Colorado
Roerdink J. B. T. M., Meijster A., 2000, Fundam. Inform., 41, 187
Schaap W. E., van de Weygaert R., 2000, A&A, 363, L29
Sousbie T., Pichon C., Courtois H., Colombi S., Novikov D., 2008a, ApJ, 672, L1
Sousbie T., Pichon C., Colombi S., Novikov D., Pogosyan D., 2008b, MNRAS, 383, 1655
Sousbie T., Colombi S., Pichon C., 2009, MNRAS, 393, 457
Sousbie T., Pichon C., Kawahara H., 2011, MNRAS, in press (doi:10.1111/j.1365-2966.2011.18395.x) (Paper II, this issue)
Springel V., White S. D. M., Tormen G., Kauffmann G., 2001, MNRAS, 328, 726
Stoica R. S., Martínez V. J., Mateu J., Saar E., 2005, A&A, 434, 423
Stoica R. S., Martínez V. J., Saar E., 2010, A&A, 510, A38
Tweed D., Devriendt J., Blaizot J., Colombi S., Slyz A., 2009, A&A, 506, 647
van de Weygaert R., Schaap W., 2009, in Martinez V. J., Saar E., Gonzales E. M., Pons-Borderia M. J., eds, The Cosmic Web: Geometric Analysis. Springer-Verlag, Berlin, p. 291
van de Weygaert R., Aragon-Calvo M. A., Jones B. J. T., Platen E., 2009, preprint (arXiv:0912.3448)
van de Weygaert R., Platen E., Vegter G., Eldering B., Kruithof N., 2010, Int. Symp. Voronoi Diagrams Sci. Eng., 0, 224
Zomorodian A. J., 2009, Topology for Computing. Cambridge Univ. Press, Cambridge

APPENDIX A: APPLICABILITY OF THE MORSE THEORY TO PRACTICAL DATA SETS

There exist a large number of methods to reconstruct a smooth density field from a discrete sample of galaxies in a catalogue or a dark matter particle distribution in a cosmological simulation. Whether one uses a simple constant-resolution uniform grid to sample the original distribution or a more sophisticated scale-free method, such as the DTFE (Schaap & van de Weygaert 2000; van

de Weygaert & Schaap 2009), that is able to reconstruct the unbiased density field over the full dynamic range of the sample; the initial sampling always defines some lower scale resolution below which one is free to infer the behaviour of the distribution. As the constraints undergone by a Morse function (Definition 2.2) are essentially local (continuity, differentiability and non-degeneracy of the critical points), one could imagine designing some sophisticated interpolation scheme that would enforce Morse properties on the distribution. In practice, designing such an interpolation scheme seems extremely difficult though and to our knowledge, this kind of solution has never been implemented. Another solution consists in relaxing Morse conditions by computing the manifolds and the Morse complex of a non-Morse function, and later correcting for this omission by enforcing the correct combinatorial properties on the pseudo-Morse complex (see Definition 2.8.1). The approach has been successfully developed by Edelsbrunner, Harer & Zomorodian (2003) and Edelsbrunner et al. (2003) for the 2D and 3D cases, respectively, but at the cost of a very high algorithmic complexity. The method has been implemented and tested for the 2D case, but there exists no implementation to date in the case of a 3D function, although the method has been mathematically proved to be correct. Another more radical approach simply consists in abandoning the idea of rigorously computing the Morse complex and rather relying directly on a pseudo-Morse complex. A pseudo-Morse complex is an approximation of a Morse complex and its combinatorial properties are not guaranteed by the Morse theory anymore. This is mainly the result of a fundamental property of the paths defined by following the gradient arrows, the so-called integral lines, being violated: they are not guaranteed not to cross anymore, as they should with a Morse function (see Definitions 2.3 and 2.3.1). The second approach recently became relatively popular in astrophysics as a way to identify cosmologically significant structures, mainly using the watershed transform. The watershed technique (see Beucher & Lantujoul 1979; Roerdink & Meijster 2000) was first applied to this kind of problem by Platen et al. (2007) as a means of identifying voids in large-scale structures (see also Platen, van de Weygaert & Jones 2008; Colberg et al. 2008; Aragón-Calvo et al. 2010a); it was later extended to the identification of walls and filaments through a pseudo-Morse complex by Sousbie et al. (2009) and it is also used by Aragón-Calvo et al. (2010b). However, although promising, these techniques seem to be doomed by the lack of a consistent theory and therefore of a good understanding of the properties of the pseudo-Morse complex, as illustrated in the following.

The watershed transform segments a field into isolated regions called basins, the analogues of the ascending manifolds of the minima (or equivalently 0-manifolds, see the top left-hand panel of Fig. A1). The boundary of those basins delineates the walls (see the bottom left-hand panel) and the regions at the boundary of three basins describe the filaments as an approximation of the ascending manifolds of the first-kind saddle points. We show in Fig. A1 how the fact that only a pseudo-Morse complex is computed can lead to subtle but significant errors in the identification of the filaments in the galaxy distribution. Fig. A1(a) illustrates the problem in 2D, using a similar implementation to the one presented in Sousbie et al. (2009). A density field is sampled on a high-resolution Cartesian grid and a watershed transform is applied, generating basins (labelled by letters). The filaments are therefore identified as the basins' boundary (black curves) and form a pseudo-Morse complex: a network that links the critical points together (the red, green and blue discs, standing for the maxima, saddle points and minima, respectively). One can see that the filaments seem to be correctly identified but according to the Morse theory, if the watershed transform yielded a correct Morse complex, then field lines would only cross at critical points and the bifurcation points, located at the intersection of at least three basins (for instance, A, B and D or B, C and D), would therefore be maxima. This is not the case in Fig. A1(a) because the function is not a Morse function and its gradient lines may therefore intersect where the filaments seem to bifurcate (the gradient direction along critical lines is represented by the grey arrows). If the function complies with the Morse criteria, then these bifurcation points would actually look like the blue-dashed line in the framed zoom in the upper right-hand corner of the figure. This is not a significant problem for the identification of filaments in 2D, as it can theoretically be corrected for through some post-treatment, but as shown in Fig. A1(b), the consequences are more dramatic in the 3D case.

In order to assess the extent of this problem, a 3D multiscale version of the probabilistic watershed transform presented in Sousbie et al. (2009) was implemented directly over a Delaunay tessellation computed from a discrete point sample (see also van de Weygaert et al. 2009, chapter 7.E). Each vertex of the tessellation is attributed a density using the DTFE method (van de Weygaert & Schaap 2009) and the probabilistic watershed transform is applied using the natural neighbourhood defined by the dual Voronoi cells to propagate the probabilities. Basically, the minima and maxima are identified as those vertices with only higher or lower density neighbours, respectively, and the probability that each vertex belongs to the integral line of a given extremum is computed according to Sousbie et al. (2009). This defines the watershed basins attached to minima and maxima [i.e. the void patches and peak patches according to the terminology of Sousbie et al. (2009) or the pseudo-ascending and pseudo-descending 3-manifolds according to the Morse theory terminology]. Fig. A1(b) shows the triangulated interface between void patches (i.e. the boundary of the cosmological voids), computed over the Delaunay tessellation of a subsampled 512^3-particle dark matter cosmological simulation in a $50\,h^{-1}$ Mpc box. This surface represents the density 'walls' of the cosmic web, shaded according to the locally interpolated density. The surface is seen from the point of view of the minimum inside the void patch and one can identify a dark matter halo on the middle right-hand part of the image. Following Sousbie et al. (2009) (see also Aragón-Calvo et al. 2010b), the filaments are identified as those segments located at the 1D interface of at least three different void patches and are represented by the non-dashed red and yellow lines. It is clear from the figure that the yellow shaded lines are spurious as they do not correspond to any filament visible in the overdensity field projected on to the surface. One can also remark that the network does not pass through the local maximum located at the centre of the halo, which should obviously be the case for a cosmological filament. Actually, a more reasonable network could be obtained by displacing the red lines to match the blue-dashed ones and removing the yellow-shaded spurious identifications. The cause of those errors is actually similar to the one described in the previous paragraph for the 2D case: the density function does not comply with the Morse criterion and its field lines may therefore cross. The sketch in the lower left-hand panel illustrates what happens along the dashed black line, in the plane perpendicular to the surface: the void patches A and B are sandwiched between C and D, resulting in the identification of critical lines at the spurious intersection of ADC and BCD, symbolized by two red dots in the sketch, and the intersection of the dashed black line and the red and yellow critical lines in the 3D image. Actually, the only real critical line is at the true intersection of the four patches, symbolized by the blue dot in

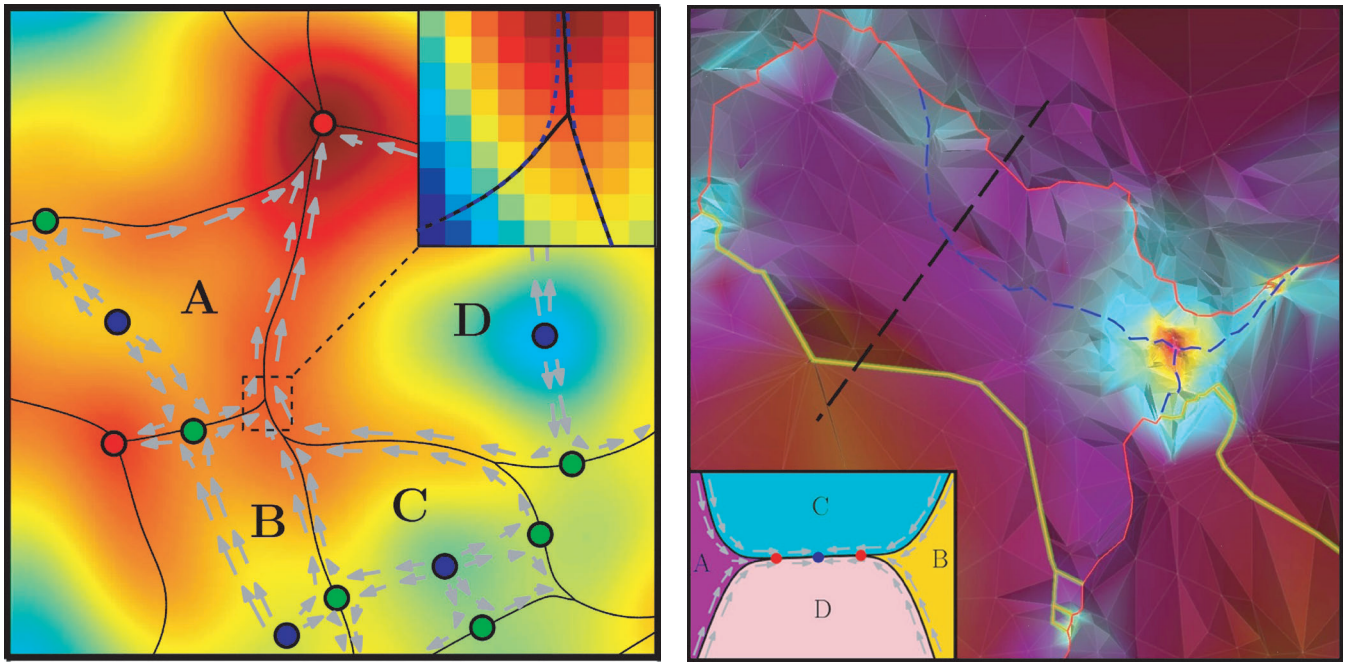

(a) 2D case (b) 3D case

Figure A1. Illustration of a problem in the identification of the filaments when using the watershed technique to recover the Morse complex directly from a non-Morse function. Panel (a): filaments (black curves) of a 2D field sampled at discrete locations over a high-resolution grid, with grey arrows showing the gradient direction along those filaments. The maxima/saddle points/minima are represented as red/green/blue discs, respectively, and the letters designate regions delimited by filaments. Panel (b): filaments identified on a 3D Delaunay tessellation of a 50 h^{-1} Mpc large dark matter simulation with the density computed using the DTFE. The surface represents the boundary of a void, shaded according to the logarithm of the density and viewed from its corresponding minimum. The red and yellow curves show the filaments detected by a multiscale watershed method. See the main text for more explanations.

the sketch and blue-dashed line in the figure (i.e. where the field lines really end, as represented by the grey arrows).

This tendency of the void and peak patches to get sandwiched between each other is perfectly natural and understood in the Morse theory, and it is not a simple consequence of the particular selected sampling method, but rather of the fact that the sampling is used at all. Moreover, it seems to be particularly the case in the large-scale cosmological dark matter density fields, probably as a consequence of the nature of the initial Gaussian random field from which tiny perturbations evolve to form the cosmic web (see the discussion on bifurcation points in Pogosyan et al. 2009). In short, this shows that the simple approach that consists in requiring filaments to be at the intersection of walls, which are at the intersection of voids, is a bit naive, as in practice, when the field is sampled and/or noisy, these boundaries do not have the right properties and do not trace the cosmic network correctly. These problems, among others, severely limit the domain of the application of the watershed-based method (for instance, it renders practically impossible their usage to count the number of filaments attached to a given halo or the measurement of the physical properties of individual filaments) and demonstrate the necessity to adopt a different, mathematically more consistent approach.

APPENDIX B: SIMPLICIAL HOMOLOGY

The homology theory studies the topological properties of spaces (intuitively, its number of components, how they are connected or if holes exist, etc.). Roughly speaking, it does so by studying the properties of deformable chains and loops over these spaces and giving a method to relate them to sequences of Abelian groups, the so-called homology groups. The goal of this section is only to give the reader enough intuitive understanding of its restriction to simplicial complexes – the weaker simplicial homology – to grasp the concept of the topological persistence as introduced by Edelsbrunner et al. (2002). For that reason, although we give a few necessary mathematical definitions, we always try to explain them in a less-formal and more intuitive manner. One could always refer to Zomorodian (2009, chapter 4) for a very interesting and somewhat more rigorous introduction or Hatcher (2002) for a thorough reference.

In order to understand the simplicial homology, one should first define the k-chain group over a simplicial complex K that contains p simplexes.

Definition B.1. **(k-chain group)** Let $k \in \{0, \ldots, d\}$ be the dimension of the k-chain, then $\{\sigma_1, \ldots, \sigma_p\}$ is the set of all the k-simplexes in K. Any k-chain c_k can be written as

$$c_k = \sum_{i=1}^{p} n_i \sigma_i, \; n_i \in \mathbb{Z}/2\mathbb{Z} = \{0, 1\}.$$

The k-chain group, $C_k(K)$, is the group with element c_k and addition defined as

$$c_k + c'_k = \sum_{i=1}^{p} (n_i + n'_i)\sigma_i.$$

In other words, a k-chain is a subset of the simplexes in K with dimension k. For a 3D simplical complex, such as the Delaunay tessellation of a galaxy catalogue, it would be a set of vertices, segments, facets or tetrahedrons. Note that in this definition, although the more general case could be considered, the coefficients n_i are chosen to be positive integers modulo 2 which, as we will see, is

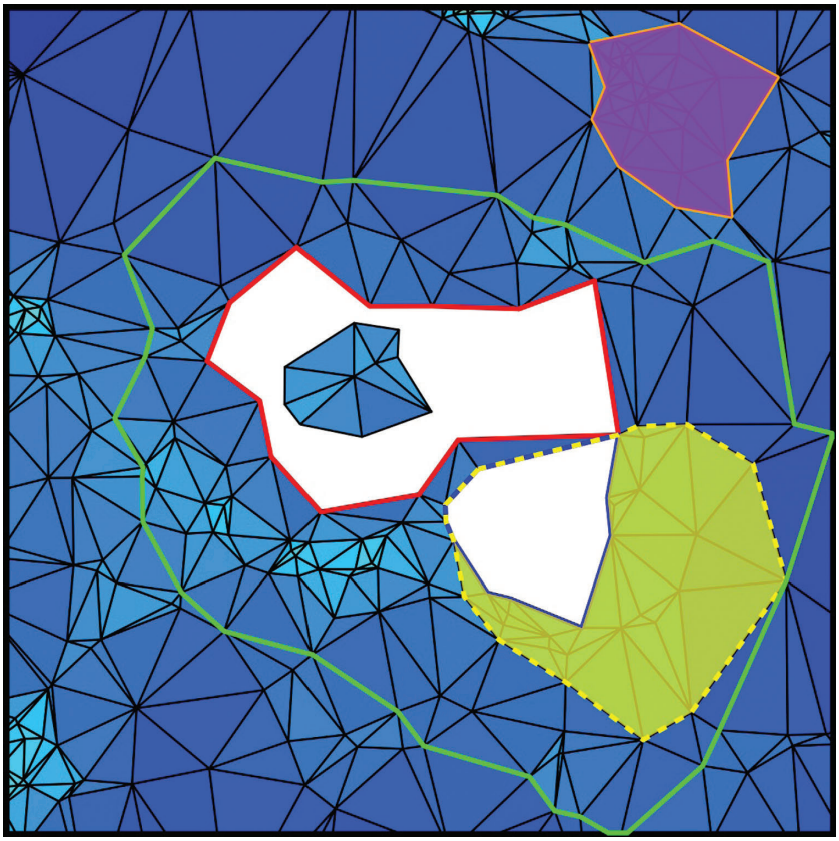

Figure B1. Illustration of 1-boudaries and 1-cycles of a 2D simplicial complex extracted from a filtration of a Delaunay tessellation. The facets present in the filtration are coloured with different shades of blue, depending on the local density, and there are two holes at this stage (white parts). See the main text for explanations.

sufficient to capture interesting topological properties. This means that a given simplex can only be absent or present once in a k-chain. Adding a simplex to a k-chain of $C_k(K)$ that already contains it therefore results in its actual removal (the addition being performed modulo 2). This definition alone only relates simplexes of identical dimensions, but for different values of k, $C_k(K)$ are independent. The notion of the topology (i.e. the connectivity of the simplexes in K) can be introduced through the definition of a boundary operator. Intuitively, the boundary of a simplex is a set of its facets:

Definition B.2. (Boundary operator) Let v_i be $k+1$ vertices of K and $\sigma = [v_0, v_1, \ldots, v_k] \in C_k(K)$ a k-simplex, then the boundary of σ is

$$\partial_k(\sigma) = \sum_{i=0}^{k} [v_0, \ldots, \hat{v}_i, \ldots, v_k],$$

where $\hat{v}_i$ means that vertex v_i is removed from the list. By extension, the boundary of a k-chain is defined as

$$\partial : C_k(K) \mapsto C_{k-1}(K)$$
$$c \mapsto \partial c = \sum_{\sigma \in C_k(K)} \partial\sigma.$$

Following this definition, the boundary of a k-chain only contains the (k−1)-simplexes that are facets of exactly one k-simplex in the chain. In Fig. B1, for instance, the segments in the orange contour (upper right-hand corner) are the boundary of the facets within the purple-shaded area; all other purple-shaded segments being faces of two facets, they cancel each other because of the addition modulo 2 in Definition B.1. A very important property of the boundary operator is that $\partial_{k-1}\partial_k = 0$: the boundary of a boundary is void. This is intuitively easy to understand as a boundary is a cycle and cycles do not have boundaries. The orange boundary of Fig. B1, for instance, forms a chain c_1 that does not have a boundary, as its segments all share the vertices at their extremity with exactly one other segment in c_k, and therefore appears twice when applying ∂_1 to c_1. The subgroup of $C_k(K)$ formed by the chains which are the boundary of a chain in $C_{k+1}(K)$ is called the image of ∂_{k+1}.

Definition B.3. (k**th boundary group** B_k) Let $B_k = \mathrm{im}\,\partial_{k+1}$ be the image of $C_{k+1}(K)$ under the boundary operator. Then B_k is a subgroup of $C_{k+1}(K)$ called the kth boundary group. Its elements form cycles called bounding cycles and therefore do not have a boundary.

In Fig. B1, a 1-chain of segments belongs to B_1 if it is the boundary of a 2-chain of 2D facets, which is the case for the orange contour (boundary of the purple-shaded facets) or the boundary of the yellow-shaded area. This is nevertheless not the case for the green-, red-, blue- and yellow-dashed contours as no set of facets can have these contours as a boundary due to the presence of the two holes. At best, the boundary of a 2-chain formed by a ring around a hole could include them, but it would necessarily contain additional cycles (the boundary of the hole). These contours are

nevertheless cycles and therefore neither do they have boundaries. They all belong to the wider kth cycle group:

Definition B.4. (**kth cycle group** Z_k) Let $Z_k = \ker \partial_k$ be the subset of $C_k(K)$ whose image under ∂_k is the null (k−1)-chain. Then, Z_k forms a subgroup of C_k called the kth cycle group and the kth boundary group B_k is included in Z_k.

The elements of Z_k are any chain that forms a cycle (or equivalently that have no boundary), and the green-, red-, blue- and yellow-dashed contours of Fig. B1 do belong to Z_1.

These elements are enough to get an idea of how the simplicial homology works. It involves trying to count how many different types of cycles it is possible to define for each dimension. To achieve this, one first needs to define what one means by 'different types of cycles', and to do so, the homology defines an equivalence relation over the k-chains:

Definition B.5. **(Simplicial homology)** Two cycles c and c' in the kth cycle group Z_k are said to be homologous if there exists a bounding cycle $b \in B_k$ such that

$$c + b = c'.$$

This equivalence relation can be used to define the class of equivalence of $z \in Z_k$, $[z]$, which contains all the elements of Z_k that are homologous to z (i.e. all $z' \in Z_k$ that can be written as $z + b = z'$ with $b \in B_k$).

In a nutshell, Definition B.5 formalizes, for simplicial complexes, the intuitive idea that two cycles are equivalent if they can be continuously deformed into each other. This definition is at the core of the regular homology theory. For instance, the 1-chains represented by the blue- and yellow-dashed contours of Fig. B1 are homologous, as one can obtain the yellow one by adding the boundary of the yellow-shaded 2-chain to the blue 1-chain. On the contrary, the red- and yellow-dashed 1-chains are clearly not homologous as it is impossible to find a chain that is both a boundary of a 2-chain and a transform one into the other through addition. This impossibility clearly comes from the fact that there exist holes in the simplicial complex and the homology shows that the presence of these holes directly affects the maximum number of non-homologous cycles one can create. This link can be established through the so-called kth homology group, which elements are the sets of homologous k-chains:

Definition B.6. (**kth homology group**) The kth homology group is the group which elements are the sets of homologous k-chains. It is defined as the quotient group of the kth cycle group Z_k by the kth boundary group B_k:

$$H_k = Z_k / B_k = \ker \partial_k / \mathrm{im}\, \partial_{k+1}.$$

An element h of H_k is represented by the class of equivalence [z] of all chains homologous to $z \in Z_k$.

In other words, in Fig. B1, an element of H_1 could be represented by the blue 1-chains around the smaller hole, as well as chains homologous to it such as the yellow-dashed one. Another element is the red 1-chain and its homologous chains, and yet another one is the class of equivalence of the green contour. But there is something different with the green 1-chains: it may not be homologous to the blue and red ones, but it could be obtained by adding to cycles homologous to the red and blue ones, respectively. This leads us to the definition of the Betti numbers, by means of which the homology describes the topology of a space:

Definition B.7. (**kth Betti number**) The kth Betti number β_k is the rank of the free[17] part of H_k:

$$\beta_k = \mathrm{rank} H_k = \mathrm{rank} Z_k - \mathrm{rank} B_k.$$

To put it simply, the kth Betti number, actually, is the minimal number of k-cycles equivalence classes (i.e. sets of homologous k-cycles) that one needs to generate any possible cycle through homology. Betti numbers are interesting because they are characteristics of the topological properties of a given space and in that sense allow quantification and comparison of the topologies of different spaces.

APPENDIX C: PERSISTENCE AND BETTI NUMBERS IN A SIMPLICIAL COMPLEX

In order to explain the computation of the persistence pair over a simplicial complex, we use Fig. 6, a figure inspired from fig. 3 of (Edelsbrunner et al. 2002). Although the reader can always refer to Appendix D for an explanation of the terminology, it is advisable to refer to Appendix B for a quick introduction to the simplicial homology. The initial discovery of persistence was triggered by the design of a simple algorithm to compute the Betti numbers over a filtration of a simplicial complex, first presented in Delfinado & Edelsbrunner (1995). A filtration of a simplicial complex (Definition 4.3) is a concept related to the one of the sublevel set (Definition 4.1). Basically, it consists in a set of subcomplexes which are given a particular order. Fig. C1 shows the subcomplexes K^i in a filtration $\mathcal{F}$ of a simplicial complex K, the index i being represented in the bottom left-hand part of each box. It is the counterpart of a sublevel set in the sense that the arrival order of each simplex in the filtration can be defined by a function that affects a value to each simplex, in which case each subcomplex K^i in the filtration can be defined as a set of simplexes with values higher or lower than a given threshold v_i. Note that the complex K is always the last to enter the filtration and is therefore represented in box number 17. In this particular filtration, the simplexes of K enter one at a time (we skipped a few steps for the sake of conciseness, as symbolized by the grey hatched box). This does not have to be the case in general though, but because each subcomplex in the filtration is a simplicial complex, a particular simplex may never enter a filtration before any of its facets. In each frame, the newly entering simplex is coloured in red or blue and the two numbers following the index are the Betti numbers $\beta^i = (\beta^i_0, \beta^i_1)$ of K^i. As detailed in Appendix B, β_0 represents the number of components in a complex (i.e. how many separated 'islands' exist), while β_1 is the number of holes or, equivalently, the number of independent non-homologous 1-cycles one can create in K^i in the more sophisticated language of homology.

Let us see how Betti numbers can be computed using this particular algorithm. K^0 is always the empty set and so the algorithm starts with $\beta^0 = (0, 0)$. A vertex first enters $\mathcal{F}$ to form K^1; this adds one new component in the filtration, but no one cycle can still be created, so $\beta^1 = (1, 0)$. As the entering vertex *created* a new component,

[17] The term 'free' in the definition actually excludes some specific cycles that may exist when the space has torsion (think about a möbius strip, for instance).

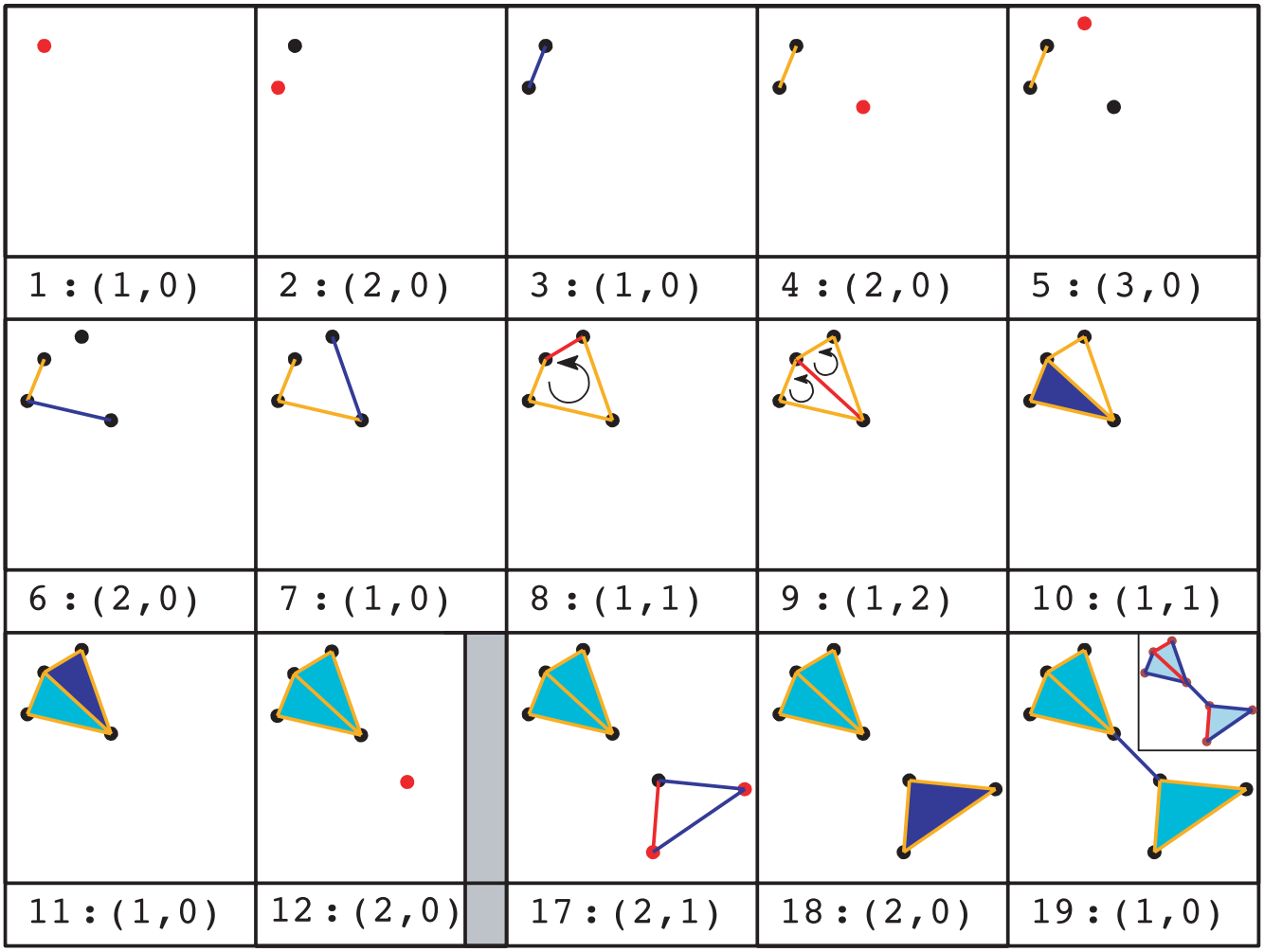

Figure C1. Illustration of the filtration of a 2D simplicial complex. Each box represents one step of the filtration, with index i (lower left-hand corner) and Betti numbers (β_0, β_1). The grey hatched box symbolizes the fact that a few steps are not represented.

it is represented in red and is labelled 'positive'. Step 2 is essentially the same and therefore $\beta^2 = (2, 0)$. In K^3 though, the first segment enters $\mathcal{F}$. Although we had two distinct components in K^2, the segment creates a link between them and only one component remains. As one component was *destroyed*, the entering segment is represented in blue and labelled 'negative', and β_0 decreases, leading to $\beta^3 = (1, 0)$ again. Nothing special happens up to K^8; every entering vertex creates a new component, thereby increasing β_1, while each new segment destroys a component, thereby decreasing the value of β_0, leading to $\beta^7 = (1, 0)$. The segment entering K^8 is different though, as it does not destroy any component: all the simplexes in K^7 were already linked and the new segment only links two vertices that already belonged to the same component. Actually, it *creates* a new class of 1-cycles (black rounded arrow) as it is now possible to draw a segment path that starts and ends at the same segment while passing through each other segment in the path only once (equivalently, it creates a hole within the cycle). The value of β_1 is therefore increased and $\beta^8 = (1, 1)$. The entering segment is labelled 'positive' and represented in red. The new segment in K^9 is of the same kind: it creates a second hole or equivalently a second class of cycles (black circular arrows) that is not homologous to the previous one. In fact, one cannot transform one into the other by adding the boundary of a set of facets, as there is no facet in the complex yet anyway. The entrance of a facet in K^{10} changes this fact, as this facet does fill one of the previously created hole: by adding the edges of this facet to the cycle created in K^8 one obtains a cycle created in K^9, the two classes therefore becoming homologous (remember that by adding a simplex to a complex already containing it, one actually removes it). This leads to β_1 being decreased and therefore $\beta^{10} = (1, 1)$. The filtration then goes on until all simplexes in K have entered and $\beta^{19} = (1, 0)$.

Although we only presented a 2D example here, the procedure works for any number of dimensions and one can in general think of a k-cycle as the shell of a deformed $(k+1)$-dimensional sphere triangulated with k-simplexes, the simplest k-cycle being the facets of a $(k+1)$-simplex. The algorithm therefore consists in labelling each k-simplex of K as 'positive' if it creates a k-cycle and 'negative' if it destroys one when entering the filtration.[18] Going a bit farther, one can see that actually any cycle destroyed by an entering simplex

[18] The question of how to decide whether a newly entered simplex actually belongs to a cycle or not is addressed in Edelsbrunner et al. (2002), but we do not present the method here as it is not essential to understand the concept of persistence. The implementation of such an algorithm is detailed in Section 6.2.

was created earlier in the filtration. For instance, the segment that enters in K^3 destroys the component created by the entering vertex in K^1 or K^2. By convention, we will say that it destroys the most recently created, the vertex entering K^2. Identically, the new segment in K^6 destroys the new component created in K^4 and the loop created in K^9 is destroyed by the facet entering K^{10}, while the facet entering K^{11} destroys the cycle created by the segment entering K^8. This defines pairs of negative and positive simplexes that create and destroy cycles, the partner of a positive (negative) k-simplex being a negative (k−1)-simplex (positive (k−1)-simplex). All the cycles can therefore be attributed some sort of 'lifetime' in the filtration, equal to the index difference of their creating and destroying simplexes. This lifetime is called their persistence. In the case of Fig. 6, for example, the most persistent topological feature of K would be that K has two main components, joined by a central bridge: the segment entering K^{19} destroys the component created by the vertex entering K^{12}, the persistence of this topological feature therefore is $19-12 = 7$, which is larger than any other in the filtration. Of course, for a given complex, the persistence of each cycle (and actually the cycles themselves) depends on their precise order of arrival and what the persistence really assesses is the topological properties of a function defined on the simplicial complex (i.e. the function that defines the order of arrival of the simplexes in the filtration).

APPENDIX D: TERMINOLOGY

Arc. An arc is a 1-cell: an integral line (or a V-path in the discrete theory) whose origin and destinations are critical points. The arcs of a Morse–Smale complex comply with Conditions 2.8.1; in particular, an arc always connects two critical points of order difference 1 (i.e. in 2D, a minimum and a saddle point or a maximum and a saddle point).

n-cell. A n-cell is a region of space of dimension n such that all the integral lines in the n-cell have a common origin and destination. The n-cells basically partition space into regions of uniform gradient flow (see Definition 2.7).

Coface. A coface of a k-simplex α_k is any p-simplex β_p, with $p \geq q$, such that α_k is a face of β_p. In 3D, the cofaces of a segment (i.e. a 1-simplex) are any triangle or tetrahedron (i.e. 2- or 3-simplex) whose set of summits (i.e. vertices) contains the two vertices at the extremities of the segment, as well as the segment itself (see Definition 3.2).

Cofacet. A cofacet of a k-simplex α_k is a coface β_{k+1} of α_k with dimension $k+1$. Equivalently, α_k is a facet of β_{k+1} (see Definition 3.2).

Critical point of order k. For a smooth function f, a critical point of order k is a point such that the gradient of f is null and the Hessian (matrix of second derivatives) has exactly k negative eigenvalues. In 2D, a minimum, saddle point and maximum are critical points of order 0, 1 and 3, respectively (see Definition 2.1).

Critical k-simplex. A critical k-simplex is the equivalent in the discrete Morse theory of the critical point of order k in its smooth counterpart. Note that in 2D, the equivalent of a minimum is a critical vertex (0-simplex), a saddle point is a critical segment (1-simplex) and a maximum is a critical triangle (2-simplex) (see Definition 3.5).

Crystal. A crystal is a 3-cell: a 3D region typically delimited by sixquads and 12 arcs, within which all the integral lines (or V-paths in the discrete case) have identical origin and destinations.

k-cycle. A k-cycle in a simplicial complex corresponds to a k-dimensional topological feature. In 3D, 0-cycles correspond to independent components, 1-cycles to loops and 2-cycles to shells (see Definition 4.4 and Appendix B).

Discrete gradient. A discrete gradient of a discrete Morse–Smale function f defined over a simplicial complex K pairs simplexes of K according to the rules of Definition 3.6. Within a gradient pair, the simplex with a lower value is called the tail and the other the head, and any unpaired simplex is critical (see Definition 3.6).

DMC. The DMC is the equivalent of the Morse–Smale complex applied to simplicial complexes (see discrete Morse theory as introduced in Section 3) (see Definition 2.5).

Discrete Morse–Smale function. A discrete Morse–Smale function f defined over a simplicial complex K associates a real value $f(\sigma_k)$ to each simplex $\sigma_k \in K$ and that obeys the condition described in Definition 3.4.

Excursion set. An excursion set of a function $\rho(x)$ is the set of points for which $\rho(x) \geq \rho_0$ (see also sublevel set).

Face. A face of a k-simplex α_k is any p-simplex β_p with $p \leq q$, such that all vertices of β_p are also vertices of α_k. In 3D, the faces of a 3-simplex (i.e. a tetrahedron) are the tetrahedron itself, the four triangles that form its boundaries, the six segments that form its edges and its four summits (i.e. vertices) (see Definition 3.2).

Facet. A facet of a k-simplex α_k is a face β_{k-1} of α_k with dimension $k-1$. The facets of a 3-simplex (i.e. a tetrahedron) are the four triangles (i.e. 2-simplexes) that form its boundaries (see Definition 3.2).

Filtration. A filtration of a simplicial complex K is a *growing* sequence of subcomplexes K^i of K, such that each K^i is also a simplicial complex. If the different K^i are defined by a discrete function $\rho_{\rm D}$ as a set of simplexes of K with value $\rho_{\rm D}(\sigma)$ less than or equal to a given threshold, a filtration can be thought of as the discrete equivalent of a sequence of growing sublevel sets of a smooth function (see Definition 4.3).

Gradient pair/arrow. A gradient pair or arrow is a set of two simplexes, one being the facet of the other, such that they are paired within a discrete gradient. Within a gradient pair, the simplex with a lower value is called the tail and the other the head.

Integral line. An integral line of a scalar function $\rho(\boldsymbol{x})$ is a curve whose tangent vector agrees with the gradient of $\rho(\boldsymbol{x})$. An integral line obeys Properties 2.3 (see Definition 2.3).

Level set/sublevel set. A level set, also called an isocontour, of a function $\rho(\boldsymbol{x})$ at level ρ_0 is the set of points such that $\rho(\boldsymbol{x}) = \rho_0$. The corresponding sublevel set is the set of points such that $\rho(\boldsymbol{x}) \leq \rho_0$ (see Definition 4.1).

Ascending/descending p-manifold. Within a space of dimension d, an ascending p-manifold is the set of points from which, following minus the gradient, one reaches a given critical point of order $d-p$. A descending p-manifold is the set of points from which, following the gradient, one reaches a given critical point of order p. For instance, ascending 1-manifolds in 3D can be associated to the filaments and ascending 3-manifolds describe the voids (see Definition 2.4).

Morse function. A Morse function is a continuous, twice-differentiable smooth function whose critical points are non-degenerate. In particular, the eigenvalues of the Hessian matrix (i.e. the matrix of the second derivatives) must be non-null (see Definition 2.2).

Morse complex. The Morse complex of a Morse function is the set of its its ascending (or descending) manifolds (see Definition 2.5).

Morse–Smale function. A Morse–Smale function is a Morse function whose ascending and descending manifolds intersect *transversely*. This means that there exists no point where an ascending

and a descending manifold may be tangent (see Definition 2.6 or 3.8 for the discrete case).

Morse–Smale complex. The Morse–Smale complex is the intersection of the ascending and descending manifolds of a Morse–Smale function. One can think of the Morse–Smale complex as a network of critical points connected by n-cells, defining a notion of hierarchy and neighbourhood among them. In particular, the geometry of the arcs (i.e. 1-cells) is determined by the critical integral lines (i.e. integral lines that join critical points) and the orders of two critical points connected by an arc may only differ by 1.

Peak/void patch. In 3D, a peak patch is a descending 3-manifold (i.e. the region of space from which, following the gradient, one reaches a given maximum) and a void patch an ascending 3-manifold (i.e. the region of space from which, following minus the gradient, one reaches a given minimum).

Persistence. The persistence of a persistence pair (or equivalently of the corresponding k-cycle it creates and destroys) is defined as the difference between the values of the two critical points (or critical simplexes in the discrete case) in the pair. It basically represents its lifetime within the evolving sublevel sets or filtration in the discrete case (see Section 4 and Definition 4.5).

Persistence pair. In the smooth context of a function ρ, the persistence pairs critical points P_a and P_b of ρ that, respectively, create and destroy a topological feature (or k-cycle) in the sublevel sets of ρ, at levels $\rho(P_a)$ and $\rho(P_b)$. In the discrete case of a simplicial complex K, a persistence pair is a pair of critical simplexes σ_a and σ_b of a given discrete function $\rho_{\rm D}(\sigma)$, such that σ_a creates a k-cycle (i.e. topological feature) when it enters the filtration of K according to $\rho_{\rm D}$ and σ_b destroys it when it enters (see Section 4 or Appendix C for more details).

Persistence ratio. The persistence ratio of a persistence pair (or equivalently of the corresponding k-cycle it creates and destroys) is the ratio of the values of the two critical points (or critical simplexes in the discrete case) in the pair. The persistence ratio is preferred to regular persistence in the case of strictly positive functions such as the density field of matter on large scales in the universe (see also the definition of persistence).

Quad. A quad is a 2-cell: a 2D region delimited by four arcs within which all the integral lines (or V-paths in the discrete case) have identical origin and destinations.

k-simplex. A k-simplex is basically the k-dimensional analogue of a triangle: the simplest geometrical object with $k + 1$ summits, called vertices. It is the building block of simplicial complexes (see Definition 3.1).

Simplicial complex. A simplicial complex K is a set of simplexes such that if a k-simplex α_k belongs to K, then all its faces also belong to K. Moreover, the intersection of two simplexes in K must be a simplex that also belongs to K (see Definition 3.3).

Vertex. A vertex is a 0-simplex or simply a point.

V-path. A V-path is the discrete equivalent of an integral line: it is a set of simplexes linked by discrete gradient arrows and the facet–cofacet relation. Tracing a V-path basically consists in intuitively following the direction of the gradient pairs of a discrete gradient from a critical simplex to another (see Definition 3.7).

This paper has been typeset from a TEX/LATEX file prepared by the author.